NON-LINEAR OPTICAL INTERACTIONS IN DYE DOPED GLASSES

by

ALOK SHARAN

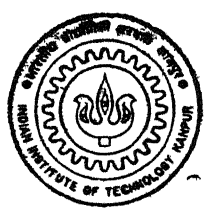

DEPARTMENT OF PHYSICS

INDIAN INSTITUTE OF TECHNOLOGY KANPUR

AUGUST, 1999

NON-LINEAR OPTICAL INTERACTIONS IN DYE DOPED GLASSES

A Thesis Submitted
in Partial Fulfillment of the Requirements
for the Degree of
Doctor of Philosophy

by

ALOK SHARAN

to the

DEPARTMENT OF PHYSICS
INDIAN INSTITUTE OF TECHNOLOGY KANPUR
AUGUST, 1999

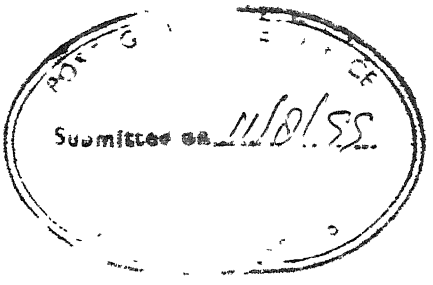

CERTIFICATE

It is certified that the work contained in this thesis entitled *"Non-linear Optical Interactions in Dye Doped Glasses"*, by *Alok Sharan*, has been carried out under my supervision and that this work has not been submitted elsewhere for a degree.

KK Sharma

Dr. K.K.Sharma
Professor
Department of Physics
Indian Institute of Technology
Kanpur

August, 1999

To,

My Parents

&

Sisters

SYNOPSIS

Nonlinear optical interactions have been studied in various material like atomic /molecular vapours, liquid crystals, photorefractive materials, semiconductor glasses, polymers and organics. This has been possible because of the availability of a wide range of laser wavelengths with equally wide range of powers. For our investigations we have chosen organic dye molecules doped in boric acid glass films. Strong absorption of organic dyes make them particularly suitable for nonlinear optical investigations in the visible region. The saturation of the $S_0 \rightarrow S_1$ transition is the dominant mechanism for the nonlinearity in these systems. However nanosecond lifetime of the excited state S_1 transition requires high power pulsed lasers with peak powers domain in the MW range to saturate the $S_0 \rightarrow S_1$ transition. The radiative lifetime of the lowest triplet state is quiet long but quenching mechanisms in liquid environment lead to considerable shortening of its lifetime. Thus the triplet state is not effective in reducing the saturation power levels in the liquid solutions of dyes. In a rigid environment, the triplet state regains its radiative lifetime ranging from few milliseconds to seconds. Correspondingly, the power requirements for saturation of the $S_0 \rightarrow S_1$ transition in a solid matrix are considerably reduced. This allows the observation of large (resonant) non-linear optical effects at incredibly low power levels available from continuous wave (CW) gas lasers. We have used 4-15 Watts CW Argon ion lasers to investigate non-linear optical properties of Rhodamine 6G, Fluorescein and Porphyrin derivatives doped in boric acid glass film of nominal thickness in the range of 30-50 μm.

The samples were in the form of thin films sandwiched between glass slides. Most of the Argon ion laser wavelengths are resonant with the $S_0 \rightarrow S_1$ transition of these dye-host systems. In this thesis, we have investigated saturation behaviour of these systems within the framework of rate equations. We have also studied two beam coupling and nearly degenerate four wave mixing in these systems. The effect of structural modifications in porphyrin derivatives on their non-linear optical properties has been attempted.

Chapter 1 : Introduction

The basics of the nonlinear optics are developed in this chapter. A brief description of different nonlinear processes and their origin in various materials are also discussed. The chapter ends with the setting up the aims of the present thesis.

Chapter 2 : Saturable Absorbers

In this chapter we present theoretical considerations for the origin of the optical nonlinearities in saturable absorbers to which the dye doped solids (the system investigated in this thesis) belong. Mathematical modeling of saturable absorbers are done in this chapter in the context

of three levels and four level systems using the rate equations approximation.

Chapter 3 : Sample Preparation and Characterization

The samples used for these studies are in the form of sandwiched films with nominal thickness in the range of 30-50 μm. Method of their preparation is discussed in these chapter. Ordinary methods for the measurement of thickness of films are not applicable to the sandwiched film used in the present work. A special method exploiting nonlinear behavior of these films has been used to measure film thickness. The absorption and emission spectra of Rhodamine 6G and Fluorescein doped in boric acid glass films are presented in this chapter. The saturation characteristics of R6G doped in BAG film at different wavelengths of the Argon ion laser are examined in the light of the discussions in **chapter 2**

Chapter 4 : Two Beam Coupling in R6G doped BAG Films

In this chapter the results of our investigations on the energy transfer between two beams of slightly different optical frequency propagating in R6G doped in BAG film are presented. A theoretical framework for these studies is first presented. This is based on the work of Zilio *et.al.* for two beam coupling in saturable absorbers. For saturable absorbers, it is necessary to introduce a frequency difference in the beams to be coupled. This is achieved by reflecting one of the beams off a peizomirror driven by a triangular voltage waveform. Frequency shifts upto 50 Hz, were achieved for our system. The two beam coupling signal disappears in the absence of the frequency shift. Experimental results on two beam coupling were interpreted in terms of the theoretical models developed.

Chapter 5 : Nearly Degenerate Four Wave Mixing in Dye Doped Solids

Nearly Degenerate Four wave mixing technique has been used in this part to study the ground state relaxation at room temperatures in various crystals. It has also been used to study the hyperfine levels in atomic systems. We use this technique to study the triplet lifetime of the dye doped glasses. Experimental techniques used for two beam coupling are discussed in **chapter 4** were used for these studies. The ground state relaxation in this systems primarily takes place in the form of repopulation of the ground state via the $T_1 \rightarrow S_0$ phosphorescent transition. These frequency domain experiments can provide accurate information on the phosphorescent lifetime. The results of our investigations on Rhodamine 6G and Fluorescein doped boric acid glass are presented in this chapter. We have used the optical phase conjugate wave to extract information on ground sate relaxation in these studies.

Chapter 6 : Effect of structural modification on the third order nonlinearity in

Tetraphenylporphyrin doped in boric acid glass

Structural changes in organic systems could lead to change in the speeds and strengths of the optical nonlinearities. In an attempt to study the effect of structural changes on third order nonlinearity we chose the planar molecule Tetraphenylporphyrin as a base molecule on which various structural modifications were carried out. Various chemically substituted porphyrin molecule were S_2TPP, $TPP(NO_2)_4$ and BrTPP we chose the first order diffracted signal in self-diffraction geometry to characterise the optical nonlinearity of these systems. The results are interpreted qualitatively in terms of the effect of structural changes on the π delocalisation.

Chapter 7 : Summary and Conclusions

We present the summary of the work done in this thesis and end with outlining some further studies which can be carried out on these systems.

Acknowledgements

With the writing of this thesis, I reach the beginning of the end of my Ph.D programme. I wish to record my deep sense of gratitude to the numerous people, both known and unknown, for their help and support, which helped in making "light" of my long (quasi-cw) stay at I.I T., Kanpur.

First and foremost, I thank my thesis supervisor Prof K.K. Sharma for constant support (both academic and non-academic) and encouragement to carry on my work with absolute freedom. I benefitted immensely from his incisive and probing questions. Each meeting with him was a revelation to me. Personally also, he has been very kind towards me.

I wish to thank Dr R. K. Thareja, Dr V. A. Singh, Dr Asima Pradhan, who were my peer review committee members, for their advice and support. I also wish to thank Dr Satyendra Kumar, Dr V. Ravishankar, Dr Bansi Lal for their interest in my work, progress and general well being.

I was fortunate to enjoy the company of my seniors – Bipin, Ravi, Divakar, Gurjar and Sandhya; together they provided me with a very friendly, encouraging and healthy atmosphere. It was in their company that I spent several glorious moments both inside as well as outside the lab. Each moment with them was a rewarding experience.

Outside the lab it was Jawed, Bogada, G.K. Singh, Pandeyji, Dada, Raghu, Rahul, Ajay, Salim, Himanshu, Sujoy and Shanti who provided the friendly support and all the help I needed whether it was related to software/hardware or just by engaging me in illuminating discussions on many a topic. It was Gautum, GDM, Subroto, Swapan, Khulbe, Alok Sri, and Harish who helped me with some of the instruments required during the course of the experiments. I also thank them for the emotional support they extended to me when everything looked bleak. It was their company which saw me through the dark tunnel. I will forever be grateful to them.

I also thank Gaurav, Saurabh, Sayan, Abir, Vivek, Prashanta and Prasenjit alongwith Rajan and other members of the graduate seminar group, and also the members of the Light Talk group for providing several opportunities to discuss and understand the various interesting phenomena and the latest in physics through seminars and informal talks.

Kuldeepjee, Upkarjee, Ramnath, Maharaj Singh, Om Prakash provided me with excellent technical support which saw many a dead instrument coming back to life. They were always ready to help - even when I required their help in the middle of the night - without any complaints and without expecting anything in return. My thanks to all of them.

I also wish to thank the staff of the CELT office, CELT workshop, Physics Electronics shop, ACES Electronics store for the support they extended to me.

During the writing of my thesis, when I was going through health problems which affected

my work it was Raghu, Mama, Gaurav, Aloksri, GDM, S.Ravi, Kushal and Rahul who saw me through. My heartfelt thanks to them once again.

I thank Aunty (Mrs. Sharma) for her general concern and several piece of advice which made my stay at I.I.T. Kanpur quite homely. I will always cherish those moments.

Finally I thank my parents and sisters, Jijajee, Rishav and Guddu, for providing me the emotional support and encouragement. Words desert me in expressing my gratitude towards my parents and sisters Ela and Sheeladi who have had to make immense sacrifices to help my programme come through The completion of my programme is itself a reward for all the hardships they endured I dedicate this thesis to them - for they also sacrificed their dreams so that I could realise mine. I really feel proud to be a part of them and tears roll my eyes as I write this. I hope not to let them down in future too.

My apologies to all those whom I have forgotten to mention here. I will always be thankful for the timely help they provided. I also wish to thank all the physicists of the world, who with their own unquenching thirst for knowledge have opened the door for others like me to follow.

Alok Sharma

Contents

List of Figures

List of Tables

Chapter 1

INTRODUCTION

In non-linear optics, unlike in linear optics, the optical properties of a medium such as its refractive index and the absorption coefficient get modified in the presence of the light field. Transparent optical materials were assumed to be essentially passive, unaffected by light traveling through them. High powers of laser beams made it possible for the first time to observe changes in the optical properties of such media. Intense light field can change the refractive index and/or the absorption coefficient of an optical material. When this happens, the light itself is affected by the change it has produced, in a variety of ways. The nonlinear response of the medium may then generate light with new colours, harmonics of the input light frequency, and when the input field contains multiple frequencies, the sum and the difference frequencies may be generated in the process. Further, the materials which are strongly absorbing at low incident light power may turn wholly or substantially transparent at high input powers. These are some of the manifestations of non-linear optics - a field which has seen a phenomenal growth with the advent of lasers.

The second harmonic generation experiment of Franken *et.al.*[1] marked the beginning of the applications of lasers to the field of nonlinear optics. They sent the beam from a ruby laser at 6942Å into a ruby crystal and observed 3471Å radiation, in addition to the red line of the ruby laser. Harmonic generation of electromagnetic waves at low frequencies has been known for a long time. It should also be possible to observe harmonics of optical waves. Yet an ordinary light source is too weak for such an experiment. Only after the lasers, intensities sufficient to observe second harmonic generation and other nonlinear effects were realisable. In a second harmonic generation experiment a coherent input beam generates another coherent beam. Nonlinear optics deals with nonlinear interaction of light with matter. Second harmonic generation is not the first nonlinear optical effect to be observed. Optical pumping-a nonlinear phenomenon was exhaustively studied by Kastler *et.al.*[2] before the advent of lasers. Resonant

excitation in the optical pumping experiments induces a redistribution of level populations and changes the properties of the medium Because of resonance with the atomic transition, light from conventional sources is able to perturb the material system to the extent that the optical pumping can be detected. CW atomic lamps were used in the early experiments on optical pumping Optical pumping is also one of the effective ways to create inverted populations. In general, however observation of nonlinear optical effects requires the application of lasers In comparison to blackbody radiation and radiation from other sources such as isotope lamps, laser light possesses high degree of brightness and coherence. As a result it is easier to induce a nonlinear effect in the medium with laser light. Numerous nonlinear optical phenomena have been since discovered. They have not only greatly enhanced our knowledge about the interaction of light with matter, but also brought a revolutionary change in optical technology[3–13]

In this chapter we give a brief introduction to nonlinear optics, mentioning some of the commonly observed nonlinear phenomena and the physical mechanisms responsible for their occurrence. The origin of the nonlinear optical interactions at the microscopic level will be discussed in the context of two-level system. In the concluding section, we set the aim of the investigations carried out in the thesis.

1.1 Formulation of Nonlinear Optics

All optical phenomena (linear and nonlinear) deal with the propagation of light waves in a medium. For linear optical phenomena, the medium simply changes the phase and the amplitude of the input light waves propagating through it to the extent determined by the real and imaginary parts of its refractive index which remains unchanged by the presence of light. In non-linear optics, the refractive index of the medium its real and/or the imaginary parts are changed by the presence of the light fields. These changes in the refractive index can lead to the appearance of new fields which are not present in the input light but are somehow related to them. All these effects, at least in principle are described by the wave equation,

$$\nabla^2\vec{E} + \epsilon_0 \frac{\partial^2\vec{E}}{\partial t^2} = \frac{\partial^2}{\partial t^2}(\vec{P}^L + \vec{P}^{NL}) \tag{1.1}$$

or

$$\nabla^2\vec{E} + \epsilon \frac{\partial^2\vec{E}}{\partial t^2} = \frac{\partial^2}{\partial t^2}(\vec{P}^{NL}) \tag{1.2}$$

where ϵ is the permittivity of medium and $\vec{E}$ is the total electric field present in the medium, $\vec{P}^L$ is the linear polarization, $\vec{P}^{NL}$ is the non-linear polarization produced in the medium by the input fields. The medium polarization is quiet difficult to handle because the polarization

at a given point in the medium at a certain instant of time may depend on the electric field not only present at that point and at that instant but may depend on the fields at points in its neighbourhood and at earlier times as well. The later effect arises because the growth and decay of the medium polarization are not instantaneous but have characteristics relaxation times Further, the induced polarization can be in the form of the distribution of the electric dipoles and higher moments induced in the medium by the light fields Higher moments in most situations can be neglected.

For input fields which are not too strong, it is possible to expand the induced polarization as power series,

$$\vec{P}(\vec{r},t) = \vec{P}^{L}(\vec{r},t) + \vec{P}^{NL}(\vec{r},t) \tag{1.3}$$

$$\vec{P}(\vec{r},t) = \vec{P}^{(1)}(\vec{r},t) + \vec{P}^{(2)}(\vec{r},t) + ... + \vec{P}^{(n)}(\vec{r},t) \tag{1.4}$$

The first term in this expansion is the linear polarization because it is linearly related to the electric field. This term alongwith the static polarization, if present, completely describe linear optics. The higher terms in the above expansion grouped together constitute the non-linear polarization and are responsible for the phenomena observed in non-linear optics. The relationship among the polarization terms and the electric fields can be expressed as,

$$\vec{P}^{(1)}(r,t) = \epsilon_0 \int_{-\infty}^{\infty} \int \chi^{(1)}(r,t;r_1,t_1).\vec{E}(r_1,t_1)dr_1dt_1 \tag{1.5}$$

and

$$\vec{P}^{(n)}(r,t) = \epsilon_0 \int_{-\infty}^{\infty} \int .. \int \chi^{(n)}(r,t;r_1,t_1..r_n,t_n).\vec{E}(r_1,t_1)..\vec{E}(r_n,t_n)dr_1dt_1..dr_ndt_n \tag{1.6}$$

Here, ϵ_0 is the permittivity of vacuum and $\chi^{(n)}$ are the tensors. Since the atomic size is much smaller than the wavelength of light, the local field in the neighbourhood of a point in the medium can be taken as homogeneous, making the susceptibility tensor space invariant. This is the electric dipole approximation. In general, one may have to solve the integro-differential wave equations which is obtained by substituting the above expression for the medium polarization in the wave equation (1.2) At times the Fourier transform representation for the electric fields and the polarization may be preferred. Defining,

$$E(\vec{r},t) = \frac{1}{\sqrt{2\pi}} \int_{-\infty}^{\infty} d\omega d\vec{k} \vec{E}(\omega,\vec{k}) e^{-\imath(\omega t - \vec{k}.\vec{r})} \tag{1.7}$$

$$P(\vec{r},t) = \frac{1}{\sqrt{2\pi}} \int_{-\infty}^{\infty} d\omega d\vec{k} \vec{P}(\omega,\vec{k}) e^{-i(\omega t - \vec{k}.\vec{r})} \tag{1.8}$$

$$E(\vec{k},\omega) = \frac{1}{\sqrt{2\pi}}\int_{-\infty}^{\infty} dtd\vec{r}\vec{E}(t,\vec{r})e^{i(\omega t-\vec{k}\,\vec{r})} \tag{1.9}$$

$$P(\vec{k},\omega) = \frac{1}{\sqrt{2\pi}}\int_{-\infty}^{\infty} dtd\vec{r}\vec{P}(t,\vec{r})e^{i(\omega t-\vec{k}\,\vec{r})} \tag{1.10}$$

It is possible to write,

$$\vec{P}(\vec{k},\omega) = \vec{P}^{(1)}(\vec{k},\omega) + \vec{P}^{(2)}(\vec{k},\omega) + \vec{P}^{(3)}(\vec{k},\omega) + ... \tag{1.11}$$

where

$$\begin{aligned}
\vec{P}^{(1)}(\vec{k},\omega) &= \chi^{(1)}(\vec{k},\omega).\vec{E}(\vec{k},\omega), \\
\vec{P}^{(2)}(\vec{k},\omega) &= \chi^{(2)}(\vec{k}=\vec{k_i}+\vec{k_j},\omega=\omega_i+\omega_j) : \vec{E}(\vec{k_i},\omega_i)\vec{E}(\vec{k_j},\omega_j) \\
\vec{P}^{(3)}(\vec{k},\omega) &= \chi^{(3)}(\vec{k}=\vec{k_i}+\vec{k_j}+\vec{k_k},\omega=\omega_i+\omega_j+\omega_k) \\
&\quad \vec{E}(\vec{k_i},\omega_i)\vec{E}(\vec{k_j},\omega_j)\vec{E}(\vec{k_k},\omega_k)
\end{aligned} \tag{1.12}$$

Hence χ^n are the crucial material parameters which determine the strength of the nonlinearity. They are intimately related to the microscopic structure of the medium and can be evaluated only with a full quantum-mechanical treatment. It is usually not possible to get direct experimental values for these quantities. However a number of techniques exist to extract information on them.

The electric field $\vec{E}$ propagating in the medium in z the direction can be expressed in terms of the plane waves,

$$\vec{E} = \frac{1}{2}\left[\sum_n A_n(r,t)e^{-i(\omega_n t-k_n z)} + c.c\right], \tag{1.13}$$

similarly the polarization $\vec{P}$ can be written as,

$$\vec{P} = \frac{1}{2}\left[\sum_j P_n(r,t)e^{-i(\omega_j t-k_j^p z)} + c.c\right] \tag{1.14}$$

Making the slowly varying envelope approximation (SVEA),

$$|\frac{\partial^2 A_j}{\partial z^2}| \ll |k_j\frac{\partial A_j}{\partial z}| \tag{1.15}$$

$$|\frac{\partial^2 A_j}{\partial t^2}| \ll |\omega_j\frac{\partial A_j}{\partial t}| \tag{1.16}$$

the wave equations(1.2) leads to a set of coupled equations for the field amplitudes

$$\nabla_{\perp}^{2} A_j + 2ik_j \frac{\partial A_j}{\partial z} = -4\pi \frac{\omega^2}{c^2} P_j^{NL} e^{-i\Delta k_j z} \tag{1.17}$$

where $\nabla_{\perp}^{2}$ is the transverse part of the Laplace operator, $\Delta k_j = (k_j - k_j^p)$ is the wave vector (phase)mismatch between the field and the polarization for the j^{th} frequency. The right hand side in of Eqn.1.16 is the source term for the new waves. An n^{th} order non-linear process will be characterised by the susceptibility tensor $\chi^{(n)}$. Even second and third order nonlinear processes generate a host of new phenomena. Physical processes taking place in different phenomena can be quiet different. We shall discuss some of these processes in this chapter. Before we do that we briefly describe another interpretation of nonlinear optical interactions which can be better appreciated in physical terms. It is possible to conceptualize the non-linear optical interactions in terms of the so called grating picture described below.

1.2 Grating Picture

Two coherent input fields interfering in a medium set up an interference pattern which will be stationary if the interfering fields are at the same frequency. If on the other hand the two fields have somewhat different frequencies, the interference pattern changes with time. Such an interference pattern is called a moving interference pattern. If the presence of the electric field can result in a change in the medium properties in some way, the extent of the change will vary from point to point depending upon the nature of the light interference pattern. The change can be in the density of the medium or in the distribution of the number of excited species in the medium. This modulation of the optical properties of the medium in the form of density changes or the changes in the excited state population or in any other from is akin to a diffraction grating and is referred to as 'Laser-Induced Grating'[11]. The modulation in any form changes the refractive index and/or the absorption coefficient of the medium. Modulation in refractive index alone gives rise to a 'phase grating' and modulation in the absorption coefficient alone is interpreted as an 'amplitude grating'. In general, however phase and amplitude gratings are present simultaneously. These gratings too, will be nonstationary if the interfering fields have somewhat different frequencies[14]. More than two coherent fields in the medium will give rise to more complex gratings. Density changes give rise to a thermal grating whereas population changes induce a population grating.

The beams producing the Laser Induced Grating (LIG) subsequently get diffracted from these gratings resulting in what is known as 'self-diffraction'. These gratings are called dynamic gratings as these are created only in the presence of external light fields. One can also use these gratings just like the usual gratings to study diffraction of any other light beam. The

diffracted beams will appear in phase-matched directions. The gratings formed in isotropic materials are scalar gratings whereas in anisotropic materials we have tensorial gratings because of the existence of preferred directions for the induced polarization.

1.3 Nonlinear Phenomena and mechanisms

Within the scope of the perturbation approach (Eq. 1.4), one may talk of nonlinear optical processes of different orders. The n^{th} order non-linear process is characterised by the polarization of n^{th} order $P^{(n)}$ (Eq. 1.12) which involves a product of 'n' field components.

The second and third order nonlinear effects are among the most commonly observed non-linear effects, although at times, fairly high order non-linearities can be observed. The second order is the lowest order nonlinearity. But it can be observed in media lacking inversion symmetry, hence it is not a universally observed nonlinear process. There is no such restriction on the third order non-linear process. Therefore the third order nonlinearity is the universally observed lowest order nonlinearity. The second order processes include sum-difference generation, second-harmonic generation, linear electro-optical effect (Pockels effect), optical rectification, three wave parametric fluorescence, etc. The third order processes include third harmonic generation, degenerate and non-degenerate Four wave mixing, DC Kerr effect, DC-induced second harmonic generation, non-degenerate two-photon absorption, stimulated Raman scattering, stimulated Brillouin Scattering etc. Optical phase conjugation is a four wave mixing process, where the third order polarization radiates a wave whose spatial part is the complex conjugate of one of the three input waves.

The physical origin of the nonlinear optical phenomena can be traced to various factors like structural modifications produced by light fields, orientational changes of the molecules in the presence of the light fields, thermally induced modulation of permittivity produced by light fields, etc. Light-induced structural changes may manifest through a change in the electronic density, in the average inter-atomic distance, in molecular orientation, in phase transition, etc. Further, they can be categorised as passive and active nonlinearities. In the first category are those phenomena in which the optical frequencies are far from resonances of the medium (known as 'nonresonant', 'nondissipative' or 'passive' nonlinearities), and in that case the exchange of energy between the field and the medium is through virtual excitations. Examples of this category are second- and third- harmonic generation. In the second category are those phenomena which are dissipative (active or dynamic nonlinearities) in this case the flow of energy from and to the optical field is through real energy transitions of the medium by processes of absorption and emission. Examples of nonlinear-optical phenomena in this category include Stimulated Raman scattering, two-photon absorption saturated absorption, etc. An important practical distinction

between various nonlinear processes is in their widely differing response times The response time is a vital limiting factor for some important applications, such as optical switching and signal processing. In the case of nonresonant or passive nonlinearities the response of the medium can be extremely fast - a few femtoseconds in some cases. Resonant non-linearities involve real transitions and are much slower but stronger and the important parameters in this case are the material relaxation times which are orders of magnitudes slower For gaseous media these typically fall in the nanosecond or microsecond range whereas in case of photorefractive material where there is displacement of charge carriers the response time is usually in milliseconds.

All nonlinear phenomena having different forms of manifestation have microscopic origin. The macroscopic polarization discussed earlier in this chapter is somehow to be connected to changes taking place at the microscopic level. We take a simple two level atom to develop this relationship

1.4 Two level atom

In section 1.1, our treatment of nonlinear optical processes has made use of power series expansion in terms of the incident electric fields to relate the response of the material system to the strength of the applied optical field In simpler situations, it is possible to express this relationship in this form,

$$\tilde{P}(t) = \epsilon_0 \left[\chi^{(1)}\tilde{E}(t) + \chi^{(2)}\tilde{E}(t)\tilde{E}(t) + \chi^{(3)}\tilde{E}(t)\tilde{E}(t)\tilde{E}(t) + ..\right] \tag{1.18}$$

However there are circumstances when the power series expansion does not converge. Alternate approaches must be found under these circumstances to describe the nonlinear optical effects. Under conditions of resonant excitation of a medium, the perturbative techniques fail to an adequately describe the response of the system to an applied optical field. However under these circumstances, it is usually possible to deal with only these atomic levels which are resonantly connected by the optical field. The contributions from other levels can usually be ignored. The increased complexity entailed in describing the system in a non-perturbative manner is thus partially compensated by concentrating on a small number of levels. This description may ignore many of the features in the real atomic systems. Still a great deal can be learnt about the non-linear processes in terms of two, three or four level models of atoms and molecules.

Most of the time we are interested in knowing the macroscopic polarization in a given ensemble of the atoms or molecules. Density matrix formalism is one such formalism for which the expectation value of the desired quantity can be formed after statistical averaging over th ensemble. As we shall see, this approach can describe the non-linear interactions non-

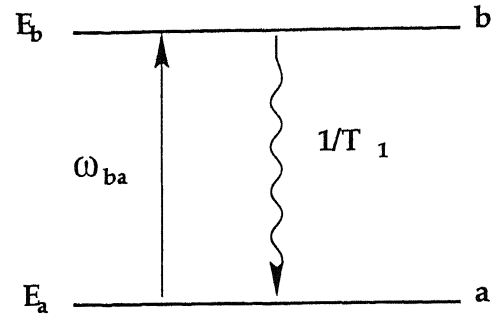

Figure 1.1: Two level atom (Upper level is 'b', and lower level is 'a').

perturbatively[9].

We denote the lower atomic level as 'a' and the upper level 'b' in Fig.1.1. For the moment we do not consider any kind of relaxation process and consider a closed two level system. Thus there is no loss of population. Such a two level system can be described by the Hamiltonian

$$\hat{H} = \hat{H}_0 + \hat{V(t)} \tag{1.19}$$

where H_0 is the atomic Hamiltonian and the interaction Hamiltonian $\hat{V(t)} = \hat{\mu}.\vec{E}$ describes the interaction of the atom with the electromagnetic field $\vec{E}$. We denote the energy eigen values of the state 'a' and 'b' as $E_a = \hbar\omega_a$ and $E_b = \hbar\omega_b$ respectively in the dipole approximation. The Hamiltonian $\hat{H}$ can be represented by the diagonal matrix whose elements are given by

$$H_{o,nm} = E_n\delta_{nm} \tag{1.20}$$

We also assume that the atomic wave functions have definite parity so that the diagonal matrix elements of $\hat{V(t)}$ vanish. We describe this system in terms of a density matrix $\hat{\rho}$

$$\hat{\rho} = \begin{bmatrix} \rho_{aa} & \rho_{ab} \\ \rho_{ba} & \rho_{bb} \end{bmatrix} \tag{1.21}$$

where $\rho_{ba} = \rho^*_{ab}$. The time evolution of the elements of the density matrix is given by

$$\begin{aligned} \dot{\rho}_{nm} &= \frac{-i}{\hbar}[\hat{H}, \hat{\rho}]_{nm} \\ &= \frac{-i}{\hbar}\sum_{\nu}(H_{n\nu}\rho_{\nu m} - \rho_{n\nu}H_{\nu m}) \end{aligned} \tag{1.22}$$

Decomposing the Hamiltonian into atomic and interaction parts,

$$\dot{\rho}_{nm} = i\omega_{nm}\rho_{nm} - \frac{i}{\hbar}\sum_{\nu}(V_{n\nu}\rho_{\nu m} - \rho_{n\nu}V_{\nu m}) \tag{1.23}$$

where $\omega_{nm} = ((E_n - E_m)/\hbar)$ is the transition frequency and n,m and ν correspond to any of the two states (a, b) of the atomic systems. The above equations constitute the density matrix equations of motion for a two-level atom in the absence of relaxation processes.

Further in this closed system let us assume that the 'on diagonal' terms relax with a rate $\Gamma_{ba}(= 1/T_1)$ from upper level b to lower level a and the 'off diagonal' terms with a rate $\gamma_{ba}(= 1/T_2)$. Then the equations of motion of the density matrix elements get modified. The diagonal elements of the density matrix ρ represent the probability of occupancy of levels, so that

$$\rho_{bb} + \rho_{aa} = 1 \tag{1.24}$$

Let us assume that at thermal equilibrium the population difference between the levels a and b equilibrate to $(\rho_{bb} - \rho_{aa})^{eq}$. Away from equilibrium, the rate of change of population difference $(\rho_{bb} - \rho_{aa})$, takes the form

$$\frac{d}{dt}(\rho_{bb} - \rho_{aa}) = -\frac{(\rho_{bb} - \rho_{aa}) - (\rho_{bb} - \rho_{aa})^{eq}}{T_1} - \frac{2i}{\hbar}(V_{ba}\rho_{ab} - \rho_{ba}V_{ab}) \tag{1.25}$$

$$\frac{d}{dt}(\rho_{ba} - \rho_{aa}) = -(i\omega_{ba} + \frac{1}{T_2})\rho_{ba} + \frac{i}{\hbar}V_{ba}(\rho_{bb} - \rho_{aa}) \tag{1.26}$$

Thus the density matrix equations of motion are reduced to the coupled equations which need to be solved. Let us briefly digress on the physical interpretation of the on-diagonal and off-diagonal relaxation terms. By setting $V_{ba} = 0$ in Eq. 1.25, we see that in the absence of the external field the initial population difference of levels relaxes to its equilibrium value with a characteristic time T_1. Consequently the relaxation time T_1 represents the population relaxation time. Similarly in the absence of the field, the off diagonal terms evolve as

$$\rho_{ba}(t) = \rho_{ba}(0)\exp^{-(\omega_{ba}+1/T_2)t} \tag{1.27}$$

This can be more physically interpreted by considering the expectation value of the induced dipole moment which can be calculated from the trace of the matrix $\langle\mu\rho\rangle$ and is given by

$$\langle\tilde{\mu(t)}\rangle = [\mu_{ab}\rho_{ba}(0)e^{-i\omega_{ba}t} + c.c]e^{-t/T_2} \tag{1.28}$$

This results shows that for an undriven atom the dipole moment oscillates at the frequency (ω_{ba}) and decays to zero in a characteristic time T_2 which is known as the dipole dephasing time T_2. In the presence of the monochromatic field of frequency ω

$$\tilde{E(t)} = \frac{1}{2}(Ee^{-i\omega t} + E^* e^{\imath\omega t}) \tag{1.29}$$

the matrix element of the interaction Hamiltonian are given as

$$V_{ba} = -\mu_{ba}(Ee^{-i\omega t} + E^* e^{\imath\omega t}). \tag{1.30}$$

From Eq. 1.27 we see that ρ_{ba} tends to evolve in time as $\exp(-i\omega_{ba}t)$. Hence when $\omega \approx \omega_{ba}$, the part of V_{ba} that oscillates as $e^{-\imath\omega t}$ would be better driving term than the part that oscillates as $e^{+\imath\omega t}$. This is the rotating wave approximation (RWA) which we shall make use of to solve the density matrix equation. Rewriting

$$\rho_{ba} = \sigma_{ba} e^{-\imath\omega t}, \tag{1.31}$$

the steady state solutions of the two coupled equations can be obtained as

$$\rho_{bb} - \rho_{aa} = \frac{(\rho_{bb} - \rho_{aa})^{eq}[1 + (\omega - \omega_{ba})^2 T_2^2]}{1 + (\omega - \omega_{ba})^2 T_2^2 + (\frac{4}{\hbar^2})|\mu_{ba}|^2 |E|^2 T_1 T_2} \tag{1.32}$$

$$\rho_{ba} = \sigma_{ba} e^{-i\omega t} = \frac{\mu_{ba} E e^{-\imath\omega t}(\rho_{bb} - \rho_{aa})}{\hbar(\omega - \omega_{ba} + \frac{1}{T_2})} \tag{1.33}$$

These expressions can be used to calculate the macroscopic polarization which is given in terms of off diagonal elements of the density matrix by

$$\tilde{P}(t) = N\langle\tilde{\mu(t)}\rangle = N\mathrm{Tr}(\hat{\tilde{\rho}}\hat{\tilde{\mu}}) \tag{1.34}$$

$$= N(\mu_{ab}\rho_{ba} + \mu_{ba}\rho_{ab}) \tag{1.35}$$

where N is the number density of atoms. The susceptibility χ is given as P/E where P is the complex amplitude of the polarization.

$$\chi = \frac{N(\rho_{bb} - \rho_{aa})^{eq}|\mu_{ba}|^2(\omega - \omega_{ba} - \frac{\imath}{T_2})T_2^2/\hbar}{1 + (\omega - \omega_{ba})^2 T_2^2 + (\frac{4}{\hbar^2})|\mu_{ba}|^2|E|^2 T_1 T_2} \tag{1.36}$$

The above expression gives total susceptibility of two level atoms including the linear and non-linear contributions. Introducing

$$\alpha_0(0) = \frac{4\pi\omega_b a}{c}[N(\rho_{bb} - \rho_{aa})^{eq}|\mu_{ba}|^2\frac{T_2}{\hbar}] \quad (1.37)$$

$$\Omega = \frac{2|\mu_{ba}||E|}{\hbar} \quad (1.38)$$

$$\Delta = \omega - \omega_{ba} \quad (1.39)$$

where $\alpha_0(0)$ is the unsaturated absorption coefficient at the linecenter. Eq. 1.36 then becomes

$$\chi = \frac{-\alpha_0(0)}{4\pi\frac{\omega_{ba}}{c}}\frac{\Delta T_2 - \imath}{1 + \Delta^2 T_2^2 + \Omega^2 T_1 T_2} \quad (1.40)$$

where Δ is the detuning of the input field from atomic resonance. As seen from this expression, χ is complex and can be expressed as $\chi = \chi' + \imath\chi''$. where

$$\chi' = \frac{-\alpha_0(0)}{4\pi\omega_{ba}/c}\frac{1}{\sqrt{1 + \Omega^2 T_1 T_2}}\frac{\Delta T_2/\sqrt{1 + \Omega^2 T_1 T_2}}{1 + \Delta^2 T_2^2/(1 + \Omega^2 T_1 T_2)} \quad (1.41)$$

$$\chi'' = \frac{-\alpha_0(0)}{4\pi\omega_{ba}/c}\left(\frac{1}{1 + \Omega^2 T_1 T_2}\right)\frac{1}{1 + \Delta^2 T_2^2/(1 + \Omega^2 T_1 T_2)} \quad (1.42)$$

We see from these expressions that in the presence of intense laser field χ' has standard dispersive lineshape and χ'' has a Lorentzian lineshape. And each of these line profiles have been broadened by the factor $1/\sqrt{1 + \Omega^2 T_1 T_2}$. The broadening of spectral lines because of the intense optical fields is known as 'power broadening'. The line center value of χ'' also has decreased with respect to its weak field value by the factor $1/\sqrt{1 + \Omega^2 T_1 T_2}$.

Fig1.2 shows the variation of the real and imaginary parts of χ, as a function of detuning for various values of the excitation parameters $\Omega^2 T_1 T_2$. The imaginary part which is proportional to intensity dependent absorption, decreases as the intensity is increased and leads to 'saturation' of the absorption coefficient. The real part of χ also decreases with increasing intensity, leading to saturation in dispersion. At higher intensities, the spectral lines become broad showing 'power broadening'.

In this formalism we have not made any assumption about the strength of the field, hence it is a non-perturbative approach. We can however perform power series expansion of χ in terms of $\Omega^2 T_1 T_2$ for low field strengths and compare term by term the results with those obtained through the perturbation approach.

Thus with a simplified two-level model, we can describe various non-linear phenomena. As evident, from the assumptions made in treating this model appropriate modifications would be necessary to deal with real atomic /molecular systems where the energy level schemes involve large number of levels which may be radiatively or nonradiatively coupled to the selected two

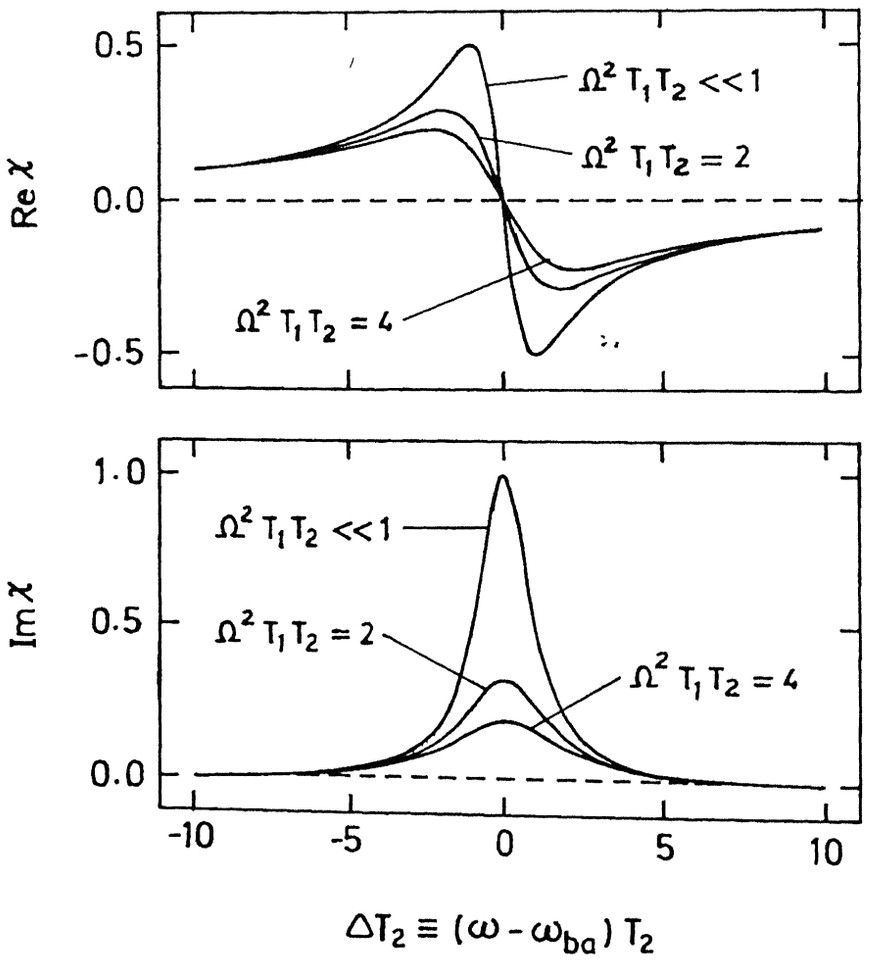

Figure 1.2: Variation of real and imaginary parts of the χ (in units of $\alpha_0 c/4\pi\omega_{ba}$) as a function of the optical frequencies ω for several values of the saturable parameters $\Omega^2 T_1 T_2$.

levels

1.5 Aim of the Thesis:

We have seen in the preceding section how a simple two-level model is able to provide a framework to describe nonlinear effects. However the actual physical systems of atomics and molecules are too complex to be understood by the simplified two level model. In this thesis, we concentrate on organic dye molecules doped in boric acid glass. Such systems constitute saturable absorbers as the absorption of these system can be reduced (saturated) by the optical field. The dye-molecules have band-like structure of vibrational and rotational modes, definitely far away from the idealized structure of sharp energy levels of the two level system. The fast relaxation rates in the intra-band transitions allow us nevertheless, to assume the energy level structure to be sharp in a certain sense. The $S_0 \rightarrow S_1$ band of the organic dyes lies in the visible range overlapping with the emission lines of an Argon ion Laser. Hosting the dye in the glassy medium enhances its triplet lifetime thereby reducing the lightpower required to observe the nonlinearity in the medium. We model this kind of saturable absorber in Chapter 2 as a 3 level system consisting of S_0, S_1 and T_1 or a 4 level system consisting of S_0, S_1, T_1 and T_2 states, interacting with visible radiation and bringing about the saturation in absorption.

Sample preparation and characterisation of dye doped thin films of boric acid glass will be discussed in chapter 3 Also in this chapter we will discuss mathematical modeling of saturable absorbers. Energy transfer between beams of slightly different optical frequencies will be the subject of study in the 4th chapter.

Nearly Degenerate Four wave mixing technique has been used in chapter 5 to study the ground state relaxation in Rhodamine6G and Fluorescein doped boric acid glass films at room temperatures.

Structural changes in organic systems can lead to changes in the speeds and strengths of the nonlinearities. In an attempt to study the effect of structure on third order nonlinearity we chose Tetraphenyl Porphyrin as the base molecule on which various structural modifications were carried out. The study on the structurally modified derivatives of tetraphenyl porphyrin are $\mathrm{S_2TPP}$, $\mathrm{TPP(NO_2)_4}$ and BrTPP are described in Chapter 6.

We conclude by summarising the results of various studies undertaken in this thesis in chapter7, where we also discuss the future scope of these investigations

References

[1] P.A. Franken *et. al. Phy. Rev. Lett.*, 7, (1961), 118.

[2] Kastler. A. J. *J. Phys. Paris*, **11**, (1956), 255.

[3] M. Schubert and B. Wilhelmi *Nonlinear Optics and Quantum Electronics ,John Wiley, New York* , (1986).

[4] N. Bloembergen *Nonlinear Optics, Benjamin, New York*, (1965).

[5] P.N. Butcher, *Nonlinear Optical Phenomena, Bull. No. 200, Eng.Exp. Stn, Ohio State Univ., Columbus*, (1965).

[6] Y. R. Shen, *The Principles of Nonlinear Optics, John Wiley, New York*,(1984).

[7] J.F.Reintjes, *Nonlinear Parametric processes in Liquids and Gases, Academic, Orlando*,(1984).

[8] D.L.Mills, *Nonlinear Optics, Springer Verlag, Berlin*,(1991).

[9] R.W.Boyd, *Nonlinear Optics, Academic, San Deigo*,(1992).

[10] V. S. Butylkin, A. E. Kaplan, Yu. G. Khronopulo and E. J. Yakubovich, *Resonant Nonlinear Optical Interactions of Light with Matter, Springer Verlag*, (1989).

[11] H. J. Eichler *et. al* , *Laser Induced Dynamic Gratings,Springer Verlag, Berlin*, (1986).

[12] R. A. Fisher(Eds), *Optical phase Conjugation, Academic, New York*,(1983).

[13] P. Gunter, J.P. Huignard(Eds) *Photorefractive Materials and their Applications I & II, Springer Verlag, Berlin* ,(1988).

[14] R.Trebino *et. al. IEEE J. Quant Elect*, **QE-22**, (1986), 1413.

Chapter 2

Saturable Absorbers

In the previous chapter we used a two level model to describe optical nonlinearities. However, the two-level model, as we shall see shortly , is inadequate to describe real atomic and molecular systems. In this chapter, we discuss the origin of non-linearities in materials which come under the category of saturable absorbers. As the name suggests the absorption in these materials decreases and eventually saturates at a low value (which may or may not be zero) as the intensity of the resonant or nearly-resonant light is increased. The discussion in this chapter will be confined to saturable absorbers of the kind we have investigated in this work. These are sandwiched films of xanthene dyes doped in boric acid glass. The dye molecules possesses large absorption cross-section in the spectral region covered by CW gas lasers. On excitation of the $S_0 \rightarrow S_1$ transition, a substantial number of molecules go over from the singlet S_1 to the triplet T_1 state as a result of the inter-system crossing processes. The lifetime of the excited triplet state when put in solid environment such as that of the boric acid glass, becomes rather long approaching the phosphorescence lifetime of the $(T_1 \rightarrow S_0)$ transition. This results in the trapping of molecules in the T_1 state Trapping of molecules in the triplet state reduces the number available for absorption in the ground state S_0. The material absorption coefficient is therefore reduced - the extent of which depends on the actual irradiance level in a non-linear fashion. Some of the largest third order optical nonlinearities have been observed in this class of materials at light intensities as low as few $\mathrm{mW/cm^2}$[7–12]. One can study these non-linearities at power levels available from CW lasers. The dye doped solid films are well suited for non-linear optical investigations and device applications. We begin the discussion on saturable absorbers by introducing the level structure and time scales relevant to these systems.

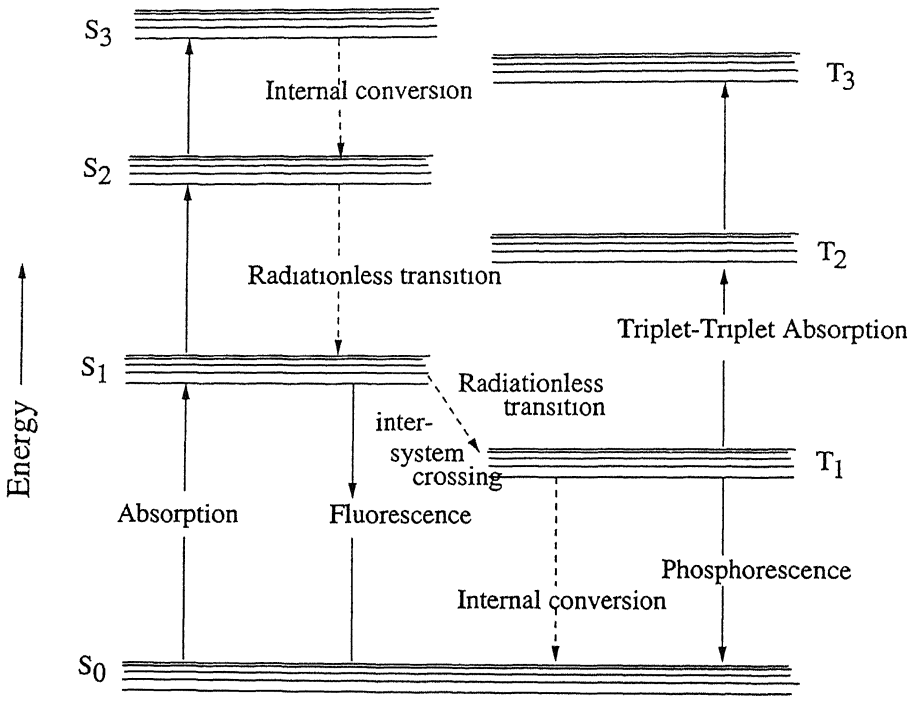

Figure 2.1: Schematic state energy level diagram: S_n are the singlet and T_n are the triplet states. The S_0 state is the ground state.

2.1 Energy Level Structure and Timescales.

Energy level structure of a typical dye molecule consists of a series of singlet (S_n) and triplet (T_n) band states (Fig. 2.1). The band structure arises from the vibrational and rotational substates associated with a given electronic state. The ground state is a singlet, with no associated triplet state. The lowest triplet (T_1) state being associated with the first excited singlet state (S_1). The triplet bands are somewhat lower in energy than the corresponding singlet bands. The spin-forbidden transitions ($S_n \rightarrow T_n$) can take place due to spin-orbit coupling in the molecule. The paramagnetic ions and heavy atoms (either within the molecule or outside) can aid $S_n \rightarrow T_n$ transition. Radiative transition between two states of identical multiplicity is called fluorescence and that between states of different multiplicity is known as phosphorescence[3–5]. The non-radiative between the $S_1 \rightarrow T_1$ intercombination bands is called the intersytsem crossing. A transition between states of the same manifold is called internal conversion. Fig(2.1) shows the possible transitions in a dye molecule. Some of these transitions are quite fast where as some others are rather slow. Fig(2.2) gives orders of magnitudes of the time scales involved in these transitions. Internal conversion from upper states of the same

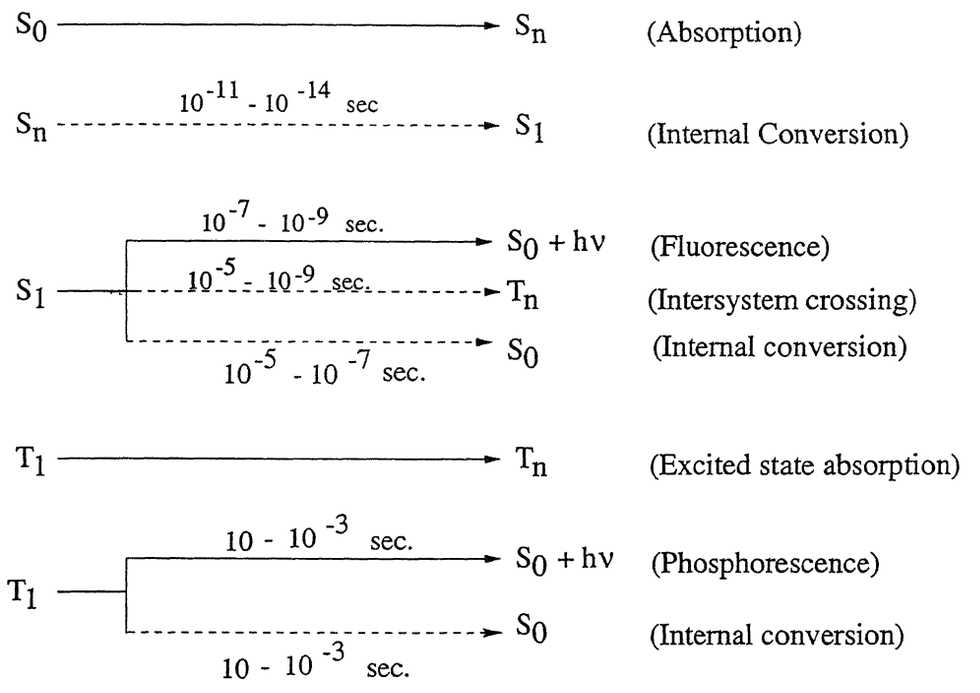

Figure 2.2: Sequence of the optical transitions in a dye doped solid films.

manifold are very rapid (10^{-11} to 10^{-14} sec) whereas the intersystem crossing is comparatively slower (10^{-9} to 10^{-5} sec). Fluorescence and phosphorescence are predominantly observed in $S_1 \rightarrow S_0$ and $T_1 \rightarrow S_0$ transitions respectively indicating high probability for non-radiative conversion among excited levels. Radiative emission from the S_1 to S_0 band can also be caused by a reverse inter-system crossing process from T_1 to S_1 giving rise to the delayed fluorescence, so named to distinguish it from the faster, direct $S_1 \rightarrow S_0$ fluorescence. The T_1 to S_1 excitation can occur via thermally stimulated intersystem crossing, radical and ion recombinations or triplet-triplet annihilative processes. Of the three radiative processes, fluorescence is the fastest (10^{-9} to 10^{-7} sec) and the phosphorescence is the slowest (10^{-3} to 10 sec). Fluorescence is observed in all phases (solid, liquid and gas) while phosphorescence is usually quenched by the non-radiative relaxation in liquids and gases. Impurities particularly those containing oxygen are very effective quenchers of the triplet state. The observation of phosphorescence is facilitated by solid hosts, where many of the non-radiative relaxation routes are not available and the triplet state regains its radiative lifetime. In experiments involving CW lasers most of the processes usually observed in the dye molecules involve the state S_0, S_1, T_1 and in some cases T_2 and higher S_n states. Thus to describe the absorption of light by the dye molecules it is sufficient to have a 3 level model (S_0, S_1, T_0) or a 4 level model if the T_2 state is also involved. It is usually possible to ascertain which of the three models (two- , three-, or four-level) is appropriate under given experimental conditions. Significant signatures of each model help in this classification. In

all these models the levels are assumed sharp - an assumption which may not appear justified at first sight. The absorption profile is generally assumed to be homogeneously broadened though this assumption may also not be quite realistic particularly in the glassy environment. Further for each model, two approaches are possible - the simple approach based on the rate equations and the more rigorous approach involving the density matrix as discussed in the previous chapter in the context of a two level model. In this thesis we shall follow the rate equation approach.

2.2 Three-Level Model

Figure (2.3) shows the level scheme for an atom in which only three levels are involved in the non-linear process.

Let A_{ij} be the radiative transition probability between the i^{th} and the j^{th} levels, W_{ij} be the rate of pumping and τ_{ij}, the radiative lifetime associated with the $i \rightarrow j$ transition. $I(\nu_{13})$ is the irradiance at frequency $\nu_{13}[= (E_3 - E_1)/\hbar]$and σ_{13} is the $1 \rightarrow 3$ absorption cross-section at ν_{13}. The pumping rate W_{ij} can be expressed as,

$$W_{13} = I(\nu_{13})\sigma_{13} \tag{2.1}$$

The rate equations for the fractional populations in the three levels n_i(i=1 to 3) are,

$$\dot{n}_1 = -W_{13}(n_1 - n_3) + n_3A_{31} + n_2A_{21} \tag{2.2}$$

$$\dot{n}_2 = n_3A_{32} - n_2A_{21} \tag{2.3}$$

$$\dot{n}_3 = W_{13}(n_1 - n_3) - n_3(A_{32} + A_{31}) \tag{2.4}$$

with

$$n_1 + n_2 + n_3 = 1 \tag{2.5}$$

The steady state population n_i of the levels can be obtained by requiring

$$\dot{n}_1 = \dot{n}_2 = \dot{n}_3 = 0 \tag{2.6}$$

Under these conditions, the difference population $n = n_1 - n_3$ can be shown to have the value

$$n = \frac{1}{1 + W_{13}\left\{\frac{2+(A_{32}/A_{21})}{A_{31}+A_{32}}\right\}}. \tag{2.7}$$

With $(\tau_{ij} = 1/A_{ij})$, Eq. 2.7 becomes,

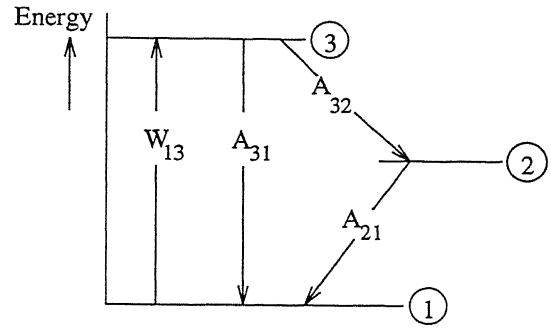

Figure 2.3: Three level energy scheme for the dye molecule

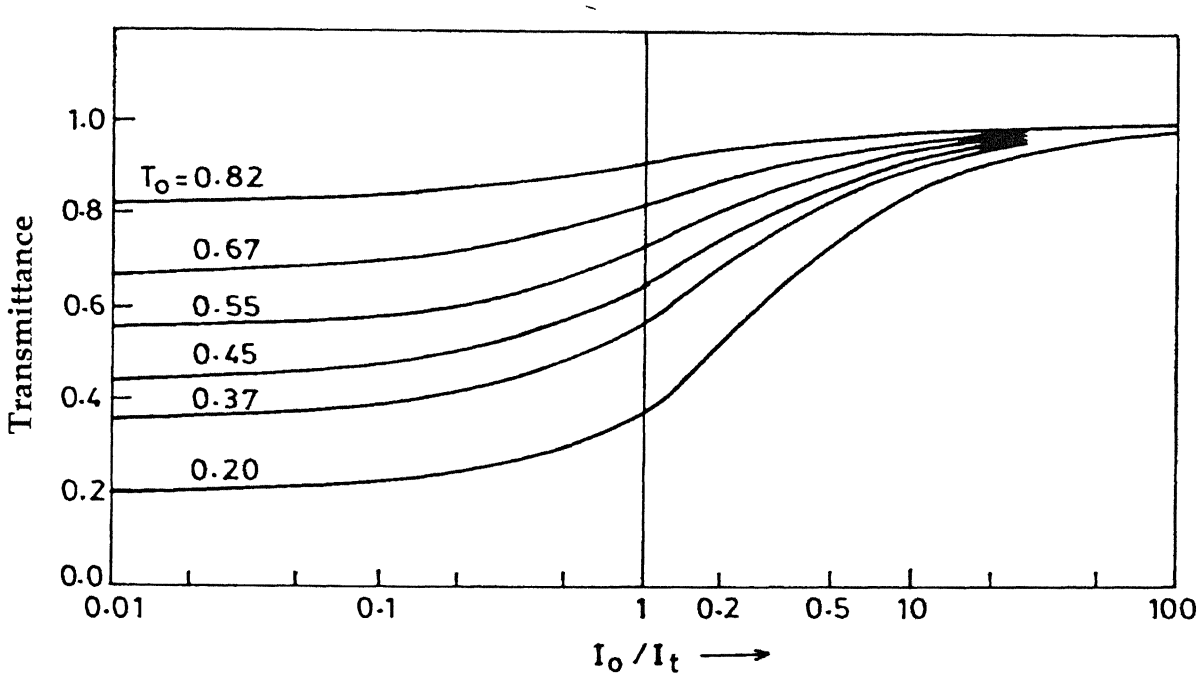

Figure 2.4: Transmission behaviour of a dye medium modelled as a thick 3 level saturable absorber

$$n = \frac{1}{1 + W_{13}\left\{\frac{2\tau_{31}\tau_{32}+\tau_{31}\tau_{21}}{\tau_{31}+\tau_{32}}\right\}} \tag{2.8}$$

$$= \frac{1}{1 + I\sigma_{13}\tau} \tag{2.9}$$

where the effective lifetime is defined as,

$$\tau = \frac{2\tau_{31}\tau_{32} + \tau_{31}\tau_{21}}{\tau_{31} + \tau_{32}} \tag{2.10}$$

For small irradiance, the medium absorption is given by Beer-Lambert's law

$$I_t = I_0 e^{-\alpha_0 L} \tag{2.11}$$

where I_t and I_0 are the transmitted and the incident light irradiances respectively, L is the thickness of the absorbing medium and α_0 is the constant small signal absorption coefficient, $\alpha_0 = \sigma_{13}N$, N being the net concentration of the absorbing species. However, in general

$$\alpha = N(n_1 - n_3)\sigma_{13} \tag{2.12}$$

$$= N\sigma_{13}\frac{1}{1 + I\sigma_{13}\tau} \tag{2.13}$$

$$= \frac{\alpha_0}{1 + (I/I_s)} \tag{2.14}$$

where

$$I_s = \frac{1}{\sigma_{13}\tau} \tag{2.15}$$

Thus we see that the absorption coefficient is intensity dependent. It decreases with increasing irradiance. At sufficiently high level of irradiance, ($I \gg I_s$), the absorption coefficient may approach to zero, making the otherwise strongly absorbing medium transparent. This is what is implied by saturation of absorption For this to happen, the saturation intensity should not be too high. This requires large absorption cross-section for the light absorbing transition ($S_0 \rightarrow S_1$) and long effective lifetime τ of the triplet state. In the three-level model, $I_s = 1/\sigma_{13}\tau$ is the irradiance at which the absorption coefficient is reduced to half its value at small irradiance. I_s is called the saturation irradiance.

2.2.1 Optically Thick Samples

Dye molecules with large absorption coefficient severely attenuate the light beam as it propagates in the sample. It is therefore necessary to take note of the beam attenuation in the sample. The absorption coefficient is intensity dependent for a saturable absorber. Accordingly the absorption coefficient is position dependent in a thick absorbing sample. It is then necessary[1] to go back to the differential form of the Beer-Lamberts' law,

$$\frac{dI(x)}{dx} = -I(x)\alpha(x). \tag{2.16}$$

Since the absorption coefficient is intensity dependent, beam propagation losses lead to spatially dependent absorption coefficient and in the above equation $I(x)$ and $\alpha(x)$ are respectively the intensity and the absorption coefficient at a distance x from the entrance end of the sample, where

$$\alpha(x) = \frac{\alpha_0}{1 + I(x)/I_s} \tag{2.17}$$

Equation(2.16) becomes,

$$\frac{dI(x)}{dx} = -I(x)\frac{\alpha_0}{1 + (I(x)/I(s)} \tag{2.18}$$

Integration of this equation with the boundary condition that at $x = 0$, the incident irradiance is I_i, leads for the sample transmittance,

$$T = \frac{I(L)}{I_i} = ln\frac{I_i}{I(L)} + \frac{I_i - I(L)}{I_s} \tag{2.19}$$

where I_i and $I(L)$ are the incident and transmitted beam intensities for a sample of thickness L. Expression (2.19) is not a convenient expression since the sample transmittance appears on both sides of the equation. Numerical solutions of this equation for different values of T_0 are shown in Fig.2.4, where the low power transmittance is defined as,

$$T_0 = \lim_{I_{in} \to 0} \frac{I(L)}{I_{in}} \tag{2.20}$$

We see from figure 2.4 that irrespective of the low power transmittance which depends on the sample thickness or on the molecular concentration, the transmittance at high powers ($I \gg I_s$) approaches unity and the sample becomes completely transparent at these high powers.

2.3 Four-level Model

In the three level model, if the triplet level T_1 is long lived, substantial population may built up in this level. Further, since the molecular levels are broad the $T_1 \rightarrow T_2$ and $S_0 \rightarrow S_1$ transitions may overlap in energy. Under these circumstances, the light beam which causes $S_0 \rightarrow S_1$ transition may also lead to $T_1 \rightarrow T_2$ absorption. This necessitates, the inclusion of the triplet level T_2 in the cycle leading to the saturation of molecular absorption. We now develop the rate equation for a four level model. Referring to figure 2.5 we can write for the level population

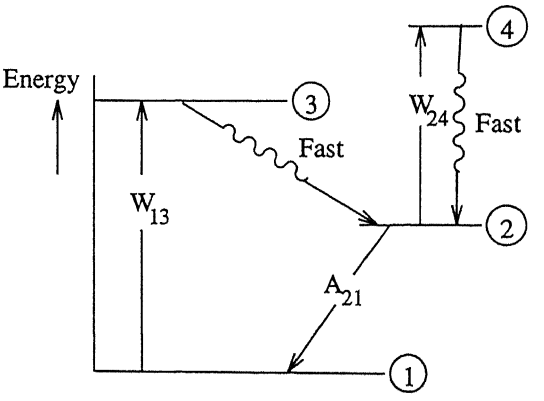

Figure 2.5: Four level energy scheme for the dye molecule.

$$\dot{n_1} = -W_{13}(n_1 - n_3) + n_3 A_{31} + n_2 A_{21} \tag{2.21}$$

$$\dot{n_2} = n_3 A_{32} - W_{24}(n_2 - n_4) + n_2 A_{42} - n_2 A_{21} \tag{2.22}$$

$$\dot{n_3} = W_{13}(n_1 - n_3) - n_3(A_{32} + A_{31}) \tag{2.23}$$

$$\dot{n_4} = W_{24}(n_2 - n_4) - n_4 A_{42} \tag{2.24}$$

with

$$n_1 + n_2 + n_3 + n_4 = 1 \tag{2.25}$$

where,

$$W_{13} = I\sigma_{13}; W_{24} = I\sigma_{24}; A_{ij} = 1/\tau_{ij} \tag{2.26}$$

It should be noted that among the 4 levels (Fig. 2.5), the $T_1 \rightarrow T_2$ and $S_0 \rightarrow S_1$ transitions are the electric dipole allowed transitions and τ_{ij} are the relaxation rates from the i^{th} to j^{th} level. The effective absorption coefficient for the 4 level system can be defined as

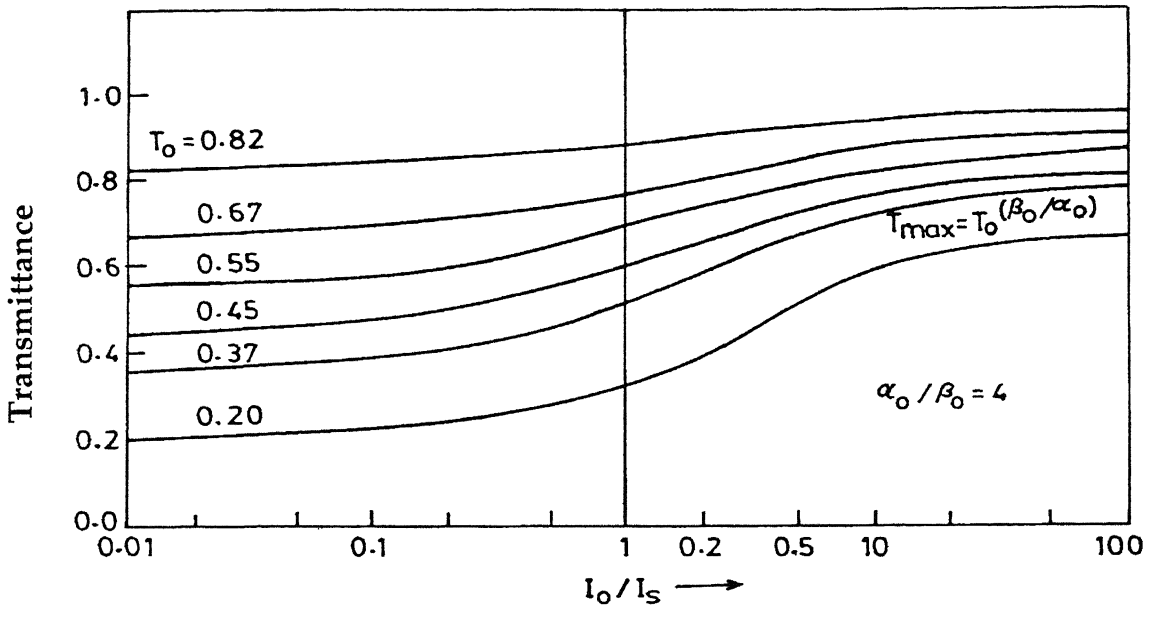

Figure 2.6: Transmission of a dye medium modelled as an optically thick, fast, four-level absorber, for various levels of irradiance.

$$\alpha = \alpha_0(n_1 - n_3) + \beta_0(n_2 - n_4) \tag{2.27}$$

where $\alpha_0 = N\sigma_{13}$ and $\beta_0 = N\sigma_{24}$ are the low power absorption absorption coefficients for $S_0 \rightarrow S_1$ and $T_1 \rightarrow T_2$ transitions respectively, and n_1 to n_4 are the steady state solutions of Eqns. 2.21 to 2.24. Solving the rate equations under the steady state conditions, we can obtain

$$n_1 - n_3 = \frac{(\tau_{31} + \tau_{32})a}{(2\tau_{32} + \tau_{21})ab + \tau_{21}(a-1)b + (\tau_{31} + \tau_{32})a} \tag{2.28}$$

$$n_2 - n_4 = \frac{\tau_{21}}{\tau_{32}} \frac{(\tau_{31} + \tau_{32})a}{(2\tau_{32} + \tau_{21})ab + \tau_{21}(a-1)b + (\tau_{31} + \tau_{32})a} \tag{2.29}$$

(2.30)

where

$$a = 1 + I\sigma_{24}\tau_{42}$$

$$b = I\sigma_{13}\tau_{31}$$

Substituting these expressions in 2.27 we can obtain the steady state absorption coefficient to be

$$\alpha = \alpha_0 \left(\frac{(1/s)(1+r) + p/(s+\gamma_0 p)}{1 + 2q + 1/s(1+r) + s/(s+\gamma_0 p)} \right) \tag{2.31}$$

where,

$$r = \frac{\tau_{32}}{\tau_{31}}; p = \frac{\tau_{21}}{\tau_{42}}; q = \frac{\tau_{32}}{\tau_{21}}; s = \frac{I}{I_s}; \gamma_0 = \frac{\alpha_0}{\beta_0} \tag{2.32}$$

We have obtained this expression for the absorption coefficient with no constraint on the time-scales involved. However in real systems certain approximations may be possible. In case of dye systems in solid hosts with CW laser excitations the $3 \rightarrow 2$ and $4 \rightarrow 2$ transitions are fast i e. τ_{32} and $\tau_{42} \approx 0$ implying that populations in level 3 and 4 are negligible. These may not be justifiable assumptions because τ_{32} is taken zero whereas $\tau_{31} \neq 0$ and as it may turn out, the intersystem crossing time τ_{32} may be larger than τ_{31}. Accepting these assumptions allows us to take $q \rightarrow 0, r \rightarrow 0,$ and $\mathrm{p} \rightarrow \infty$. In these limits, Eq.2.31 reduces to

$$\alpha_{eff} = \alpha_0 \left(\frac{1 + \frac{s}{\gamma_0}}{1+s} \right) \tag{2.33}$$

where $I_s = \sigma_{13}\tau_{21}$. Using this expression for the absorption coefficient in the differential form of the Beer-Lamberts law (Eq 2.16) and integrating over the sample thickness L, we can show that the sample transmittance T satisfies the following equation,

$$ln\frac{T}{T_0} = (\gamma_0 - 1) ln \left\{ \frac{\gamma_0 + I_i/I_s}{\gamma_0 + T I_i/I_s} \right\} \tag{2.34}$$

This is the result originally developed by Hercher[2]. Once again T_0 is the low power sample transmittance as defined earlier. For small values of I_i/I_s i.e. in the limit $I_i \ll I_s$ the above equation reduces to

$$T_0 = \frac{I_{out}}{I_{in}} = exp\{-\alpha_0 L\} \tag{2.35}$$

i.e. there is no effect of excited state absorption at low irradiances and the absorption is essentially due to the $S_0 \rightarrow S_1$ transition. This is understandable since saturation effects will be absent at these power levels. On the other hand for sufficiently large incident beam intensity $I_i \gg I_s$, the beam transmittance again becomes intensity independent with a limiting value of

$$T' = \frac{I_{out}}{I_{in}} = T_0^{1/\gamma_0} = \exp\{-\beta_0 L\} \tag{2.36}$$

implying that at large power levels, the absorption takes place in the $T_1 \rightarrow T_2$ transition and practically no net absorption in $S_0 \rightarrow S_1$ transition This happens because at these power levels, the entire dye population is dynamically transferred to the T_1 level. Since the $T_1 \rightarrow T_2$ transition cannot be saturated at low power levels available from CW lasers, this residual absorption will persist in a four level system. This is in contrast to the three level model which becomes completely transparent in this limit. It is therefore possible to distinguish between a three level saturable absorber and a four level saturable absorber. For power levels between these two limits, numerical solutions must be found to Eq. 2.34. These are shown in Fig.2.6 for some values of T_0. We notice from this figure that the minimum transmittance ($I_i \ll I_s$) and the maximum transmittance ($I_i \gg I_s$) of a four level saturable absorber vary with sample thickness and the absorber concentration. We can have better insight of the population dynamics of a four level saturable absorber if we look into the dependence of the maximum change in the transmittance of a 4 level saturable absorber in the low power absorption constant $\alpha_0 L$. From Eq. 2.35 and Eq. 2.36,

$$\Delta T = T' - T \tag{2.37}$$

$$= \exp(-\beta_0 L) - \exp(-\alpha_0 L). \tag{2.38}$$

The maximum change in the transmittance (ΔT) may be interpreted as the difference with the low power or unsaturated transmittances of the $T_1 \rightarrow T_2$ and the $S_0 \rightarrow S_1$ transitions. In the limit of $\alpha_0 L \rightarrow 0$, the transmittance is 100% for both transitions and consequently $\Delta T \rightarrow 0$ as $\alpha_0 L \rightarrow 0$. On the other hand, the transmittance of both the transitions approaches zero value as $\alpha_0 L \rightarrow \infty$. Once again ΔT approaches zero value in the limit $\alpha_0 L \rightarrow \infty$. In between ΔT must go through a maximum. We may not be able to notice this effect in Fig. 2.6 but Fig.2.7 which shows $\alpha_0 L$ dependence of ΔT clearly demonstrates this fact. In this figure, we have plotted the two exponentials $\exp(-\alpha_0 L)$ and $\exp(-\beta_0 L)$ also for a value of $\gamma_0 = 2.18$. It can be shown that the maximum change in the transmittance (ΔT) takes place when

$$\alpha_0 L = \left(\frac{\gamma_0}{\gamma_0 - 1} \ln \gamma_0\right) \tag{2.39}$$

This may be a useful result in determining γ_0 from experimental observations. The two exponential curves in Fig.2.7 clearly show that the maximum change in transmittance cannot be a monotonic function of $\alpha_0 L$ but must go through a maximum. We conclude by saying that a

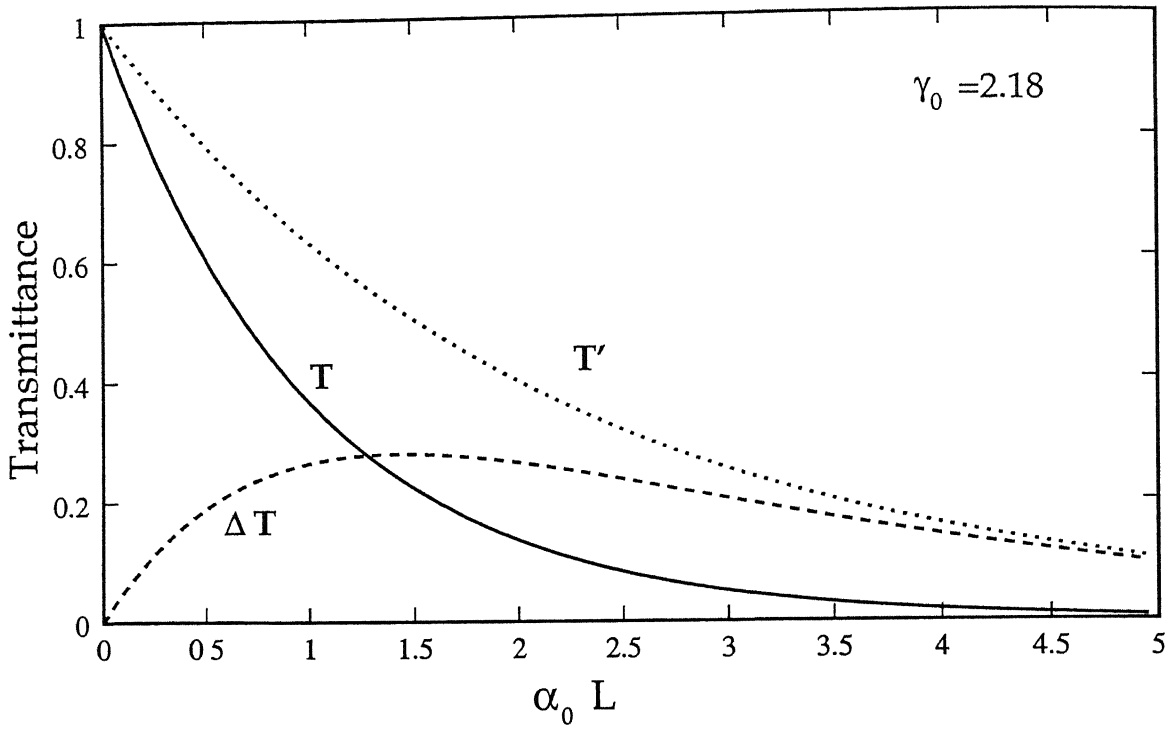

Figure 2.7: Dependence of low power and high power transmittance on $\alpha_0 L$ for $\gamma_0 = 2.18$

four level saturable absorber acts like two level system at very low and also at very high levels of irradiance.

2.3.1 Low Power Absorption

Let us return to Eq.2.31. We have already mentioned that the relaxation time τ_{32} may actually be longer than the radiative lifetime τ_{31}. This will make $r \gg 1$. This actually is the case for most of the systems exhibiting saturation absorption (e.g. R6G and Fluorescein doped in boric acid glass have $\tau_{32} \approx$msecs and $\tau_{31} \approx$ nanoseconds). We now explore the low power limit ($s \ll 1$) of equation 2.31 and numerically calculate the sample transmittance for a range of values around this limit i.e for $r \gg 1$ and $s \gg 1$. We find that instead of the flat linear response at low powers we get marked deviations from it. The deviations are more pronounced with systems having higher saturation intensities (Fig.2.8). However the amplitudes of these oscillations at low incident beam powers are quiet small to be observed. Nevertheless it points to interesting features at the low irradiance levels.

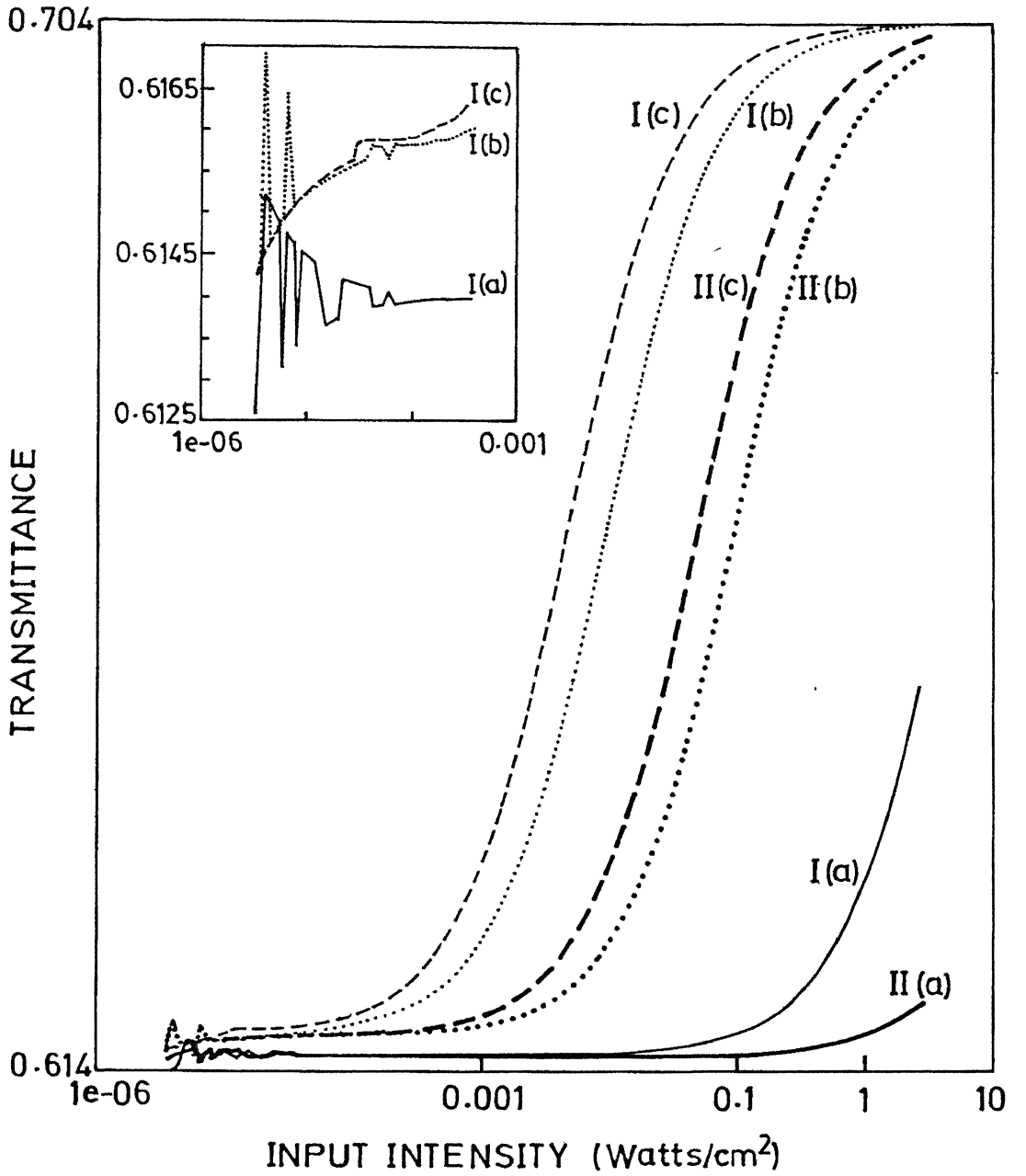

Figure 2.8: Transmission curves for four level model with $r \gg 1, s \gg 1$. Inset shows the deviations in transmittance more clearly at low powers[14].I,II corresponds to s=3.5mW, 35mW whereas a,b,c corresponds to r=1000, 1, 0.001

2.4 Origin of Nonlinear mechanisms

Having seen as to how the changes in the populations bring about changes in the absorption coefficient we would now like to see how population changes affect the macroscopic polarization of the medium. In order to see the connection between the microscopic and the macroscopic properties, let us have an ensemble of dye molecules having a ground state '0' and only one excited state '1' with population N_0 and N_1 respectively. A resonant monochromatic field

$$\frac{1}{2}\left[\vec{E}(\vec{r})\exp(-i\omega t) + C.C\right] \tag{2.40}$$

produces in this ensemble, a polarization[15]

$$\vec{P} = \epsilon_0(n_0\chi_0 + n_1\chi_0)\vec{E} \tag{2.41}$$

where χ_0 is the contribution of the ground level, and χ_1 is that of th excited level to the total susceptibility and n_0 and n_1 are the probabilities for the occupancy of the ground and excited levels, respectively, where

$$n_0 = \frac{N_0}{N_1 + N_0}; \tag{2.42}$$

$$n_1 = \frac{N_1}{N_1 + N_0} \tag{2.43}$$

Since the probabilities for occupancy are functions of the intensity and also $\chi_1 \neq \chi_0$ we can write,

$$\vec{P} = \vec{P_L} + \vec{P_{NL}} \tag{2.44}$$

where,

$$\vec{P_L} = \epsilon_0 n_0 \chi_0 \vec{E} \tag{2.45}$$

$$\vec{P_{NL}} = \epsilon_0 n_1(\chi_1 - \chi_0)\vec{E} \tag{2.46}$$

ϵ_0 is the free-space permittivity and $I = \frac{1}{2}\epsilon_0\eta c|E|^2$ (η is the linear refractive index of the medium). This nonlinear polarization $\vec{P}_{NL}$ is the source of generation of new waves when substituted in wave equation1.2. This is how the saturation of absorption leads to the nonlinear effect.

We shall explore the nonlinear polarization in more detail in the next chapters.

References

[1] R. W. Keyes, *I.B.M Journal*, **7**, (1963), 334

[2] M.Hercher, *Applied Optics*, **6**, (1967), 947

[3] C.A. Parker, *Photoluminescence of Solutions, Elsevier, Amsterdam*, 1968.

[4] J.B.Birks,*Photophysics Of Aromatic Molecules, John Wiley, London*,(1970).

[5] R.S.Becker,*Theory and Interpretation of Fluorescence and Phosphorescence, Wiley Interscience, New York* ,(1969).

[6] R.C. Hoffman, K.A. Ktetyick, R.S. Potember and D.G. McLean, *J. Opt. Soc. Am.*, **B 6**, (1989), 772.

[7] W.R.Tompkin, M. S. Malicut and R.W. Boyd*App. Opt.*, **29**,(1990),3921.

[8] M.A. Kramer, W.R. Tompkin, J. Krasinski, and R.W. Boyd, *J. Lumin*, **31-32**, (1984), 789.

[9] M.A. Kramer, W.R. Tompkin and R.W. Boyd, *Phys. Rev. A*, **34**, (1986), 2026.

[10] W.R Tompkin, R.W. Boyd, D.W. Hall and P.A. Tick, *J. Opt. Soc. Am*, **B 4**, (1987), 1030.

[11] T. Todorov, L. Nikolova, N. Tomova and V. Prayostinova, *Opt. Quant. Elec.*, **13**, (1981), 209.

[12] Y. Silberberg and J. Bar-Joseph, *Opt. Commun.*, **30**, (1981), 265.

[13] S.N.Sandhya, R.C.Sharma, Alok Sharan and K.K.Sharma, *Proceedings of National Laser Symposium,I.I.T.Kanpur*, (1998), 174.

[14] S.N.Sandhya, Alok Sharan and K.K Sharma, *Proceedings of National Laser Symposium,I.I.T.Kanpur*, (1998), 180.

[15] H.L. Fragnito, S F. Periera and A. Kiel, *J. Opt. Soc. Am.*, **B** 4, (1987), 1309.

Chapter 3

Sample Preparation and characterisation

This thesis deals with the study of nonlinear optical interactions in saturable absorbers. We have chosen some of the xanthene dyes doped in boric acid glass film for these studies. As explained in chapter 2, these dyes when hosted in solid matrix approach the lifetime of the phosphorescence ($T_1 \rightarrow S_0$) transition making it possible to observe the nonlinearity even with CW lasers. We chose boric acid glass as the host medium because of the ease of preparation, high durability and good thermal stability. Further, it is known that this host does not go any chemical and structural changes. This rules out the possibility of creating host based permanent gratings. This allows us to investigate the dynamics of the dye molecules over a wide range of input powers. In this chapter we describe the preparation and characterization of the dye-doped glass samples in terms of the refractive index, spectral details and saturation characteristics.

3.1 Sample Preparation

Films of dye doped boric acid glass were prepared by the method first suggested by Lewis *et.al.*[1] and later used by Shankoff[2], Todorov *et.al.*[3] and Boyd[4] and coworkers. Required amounts of the dye and the boric acid powders were mixed in a test tube and heated to about 270^0C. The resulting melt was stirred by a glass rod to affect homogenization. Drops of the melt were then placed between microscope glass slides preheated to 140^0C to 170^0C, and a weight of about 3-4 kg was placed on them to press the melt to obtain thin films. The slides were then allowed to cool to room temperature. The films have the tendency to develop cracks. However, film of good optical quality with high degree of transparency can be grown. There were however, significant variations in the thickness of these films, because of the different

amounts of melts used and at times due to uneven pressure. Besides there were variation in the thickness of the glass slides. The homogenization of the boric acid melt too posed problems. Similar films have been used by earlier workers in the laboratory. We now briefly discuss the characterization of these films.

3.2 Spectral Characterization

The absorption spectra of these sandwiched films were recorded using a 1000 W water cooled tungsten lamp, a GDM-1000 double monochromator, an M12FC51 photomultiplier and an EG&G-PARC 4402-4420 Boxcar-Processor. A dye-free boric acid film is transparent in the visible region The emission spectra were recorded using light of appropriate wavelengths from a 15-W Coherent Innova-100 laser to excite the dye-glass films. The collection, detection and recording setup was similar to the one used for absorption studies.

3.3 Rhodamine 6G doped in Boric acid

The absorption spectrum of a typical 10^{-4} M Rhodamine 6G(R6G)-boric acid film is shown in Fig.3.1. The absorption spectrum is rather broad with peak at around 470 nm and two shoulders at 510 nm and 445 nm. The absorption profile is similar in shape to the one reported by Todorov *et.al.*[3] for a concentration of 4.2×10^{-4} M though the main peak in their case is at 450 nm. The Rhodamine 6G films absorb all Argon ion laser wavelengths to lesser or greater extent. The emission spectrum shown in the Fig.3.1 was obtained by exciting the film at 476.5 nm. The emission peak is at 526 nm giving a Stokes shift of 56 nm. The emission at this wavelength is quite strong because this laser line is close to the absorption peak.

3.3.1 Saturation Characteristics

The experimental setup used for measuring the saturation characteristics of these films is shown in Fig.3.2. A glass plate was introduced before the sample and the beam reflected from this plate was monitored for power fluctuations using the IL1700 Radiometer. Neutral density (Balzers) filters were used to vary the light power entering the sample. The light transmitted through the sample was collected by a lens and measured by the NRC Digital Power Meter815 The same powermeter was also used to measure the incident light beam power.

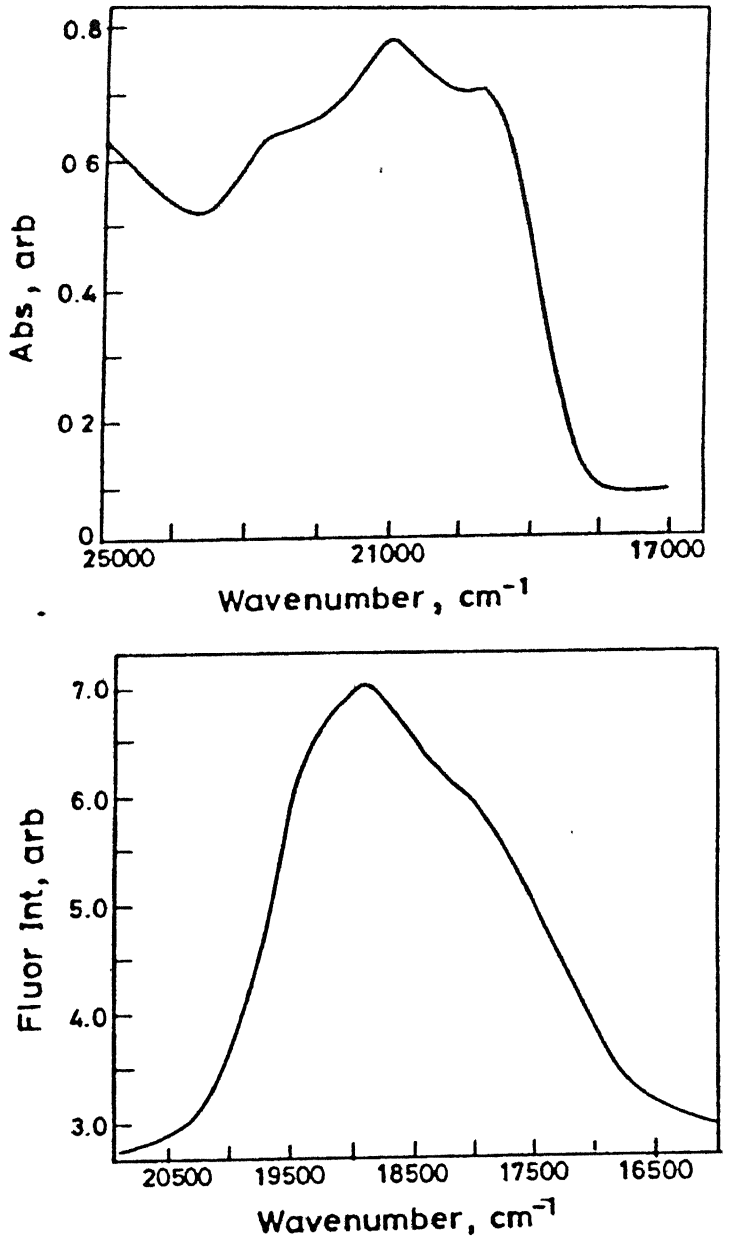

Figure 3.1: Absorption and emission spectra of R6G - boric acid (10^{-4}) glass

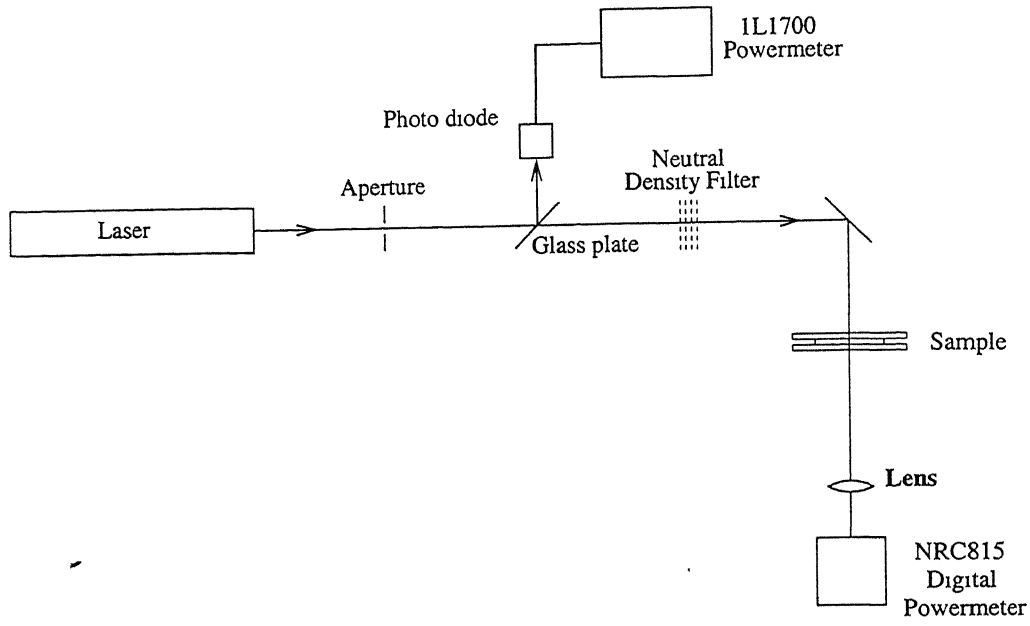

Figure 3.2: Experimental setup for saturation

3.3.2 Results

The transmittance of the films was measured at 476.5 nm (laser line closest to the absorption peak), 457.9 nm and 514.5 nm. For excitation at 476.5 nm, the absorbance for the films used was near 75% at low power (upto an intensity of $31mW/cm^2$): At high powers, the sample is almost completely bleached with a residual absorbance of only 12% around $310mW/cm^2$. The saturation characteristics shown in Fig.3.3 clearly display an initial flat portion followed by a linear rise which tapers off into a plateau at high powers. The saturation intensity at 476.5 nm is estimated to be $130mW/cm^2$. The transmission change as a result of saturation at 457.9nm is much less as compared to the one observed when the film was excited at 476.5nm. This is due to the reduction of the absorption coefficient at this wavelength. The saturation takes place at much higher input intensities at this wavelength. The saturation intensity in this case is about $1.3W/cm^2$. The absorption constant ($\alpha_0 L$) as calculated from the low power flat regions, has values of 1.3 at 476.5 nm and 0.59 at 457.9 nm[5]. A similar measurement at 514.5 nm gives a value of about 0.3. The saturation characteristics at 514.5 nm is shown in Fig.[?] is for a different sample. Low power absorption constant($\alpha_0 L$) at 514.5nm for this film is 0.86 and the saturation intensity is about $1.58W/cm^2$. In all the three samples, the saturation of absorption is clearly established. The samples are, however, not fully bleached. For all these cases, there is a residual absorption since the saturation yields less than unit transmittance. Thus the four

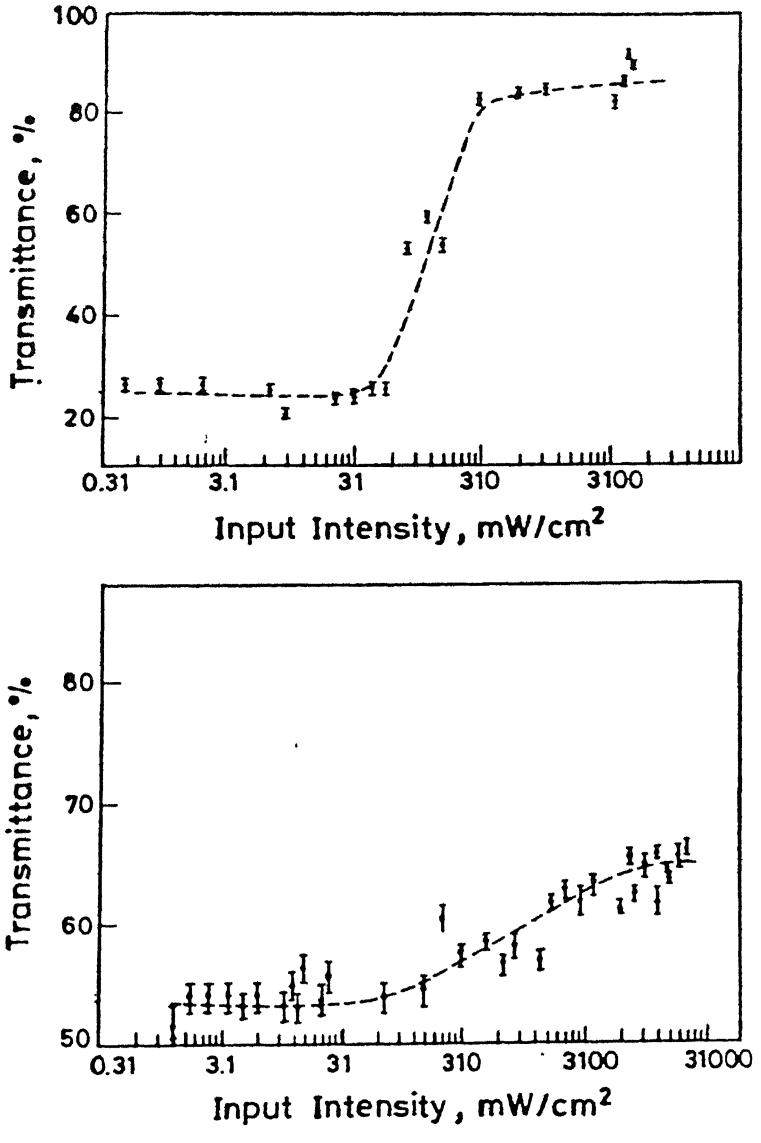

Figure 3.3: Saturation characteristics of R6G-boric acid glass (10^{-4}) Top at 476.5 nm bottom at 457.9 nm

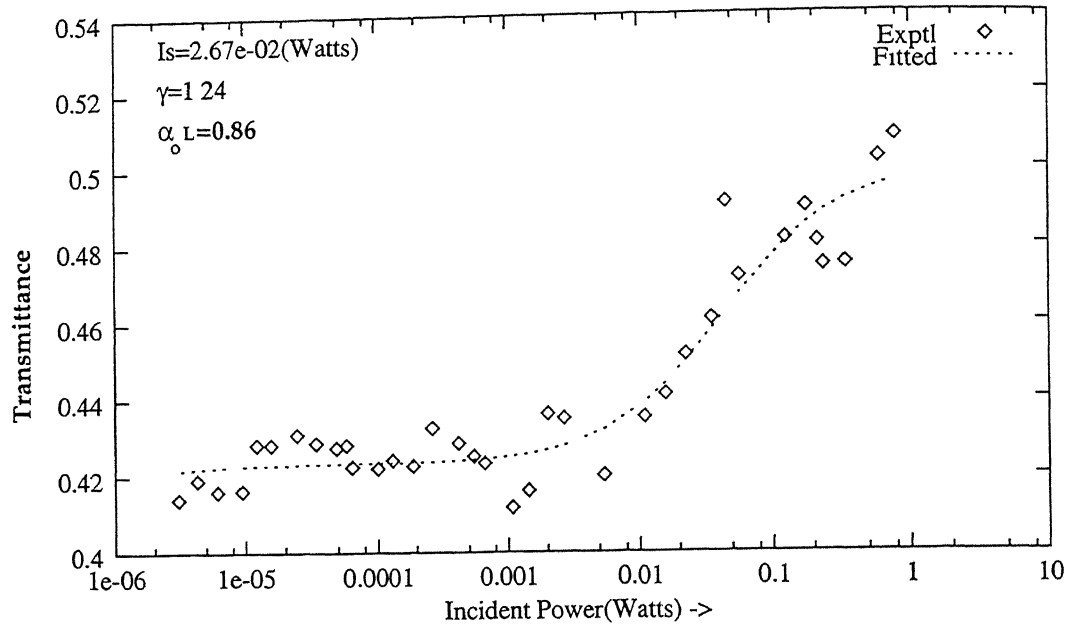

Figure 3.4: Saturation characteristics of R6G -boric acid glass (10^{-4}) At 514.5 nm

level model should be more appropriate to describe these samples. The saturation behaviour of these samples was fitted with the four level model as described in chapter 2. Table 3.1 gives optimum values of the parameters.

Table 3.1: Table showing the saturation intensities at different Argon ion wavelengths. γ_0= Ratio of low power absorption coefficient to high power absorption coefficient; α_0= Low power absorption coefficient; $\beta 0$= high power absorption coefficient

λ	$\alpha_0 L$	$\beta_0 l$	$\gamma_0 = \frac{\alpha_0}{\beta_0}$	I_s
457.9 nm	0.62	0.412	1.51	$1.3 W/cm^2$
476.5	1.3	0.13	10.	$130 mW/cm^2$
514.5*	0.86	0.69	1.24	$1.58 W/cm^2$

*This measurement is for a different sample. The first two wavelengths measurement are in the same sample.

We see from this table that the ratio (γ_0) of the low power ground state absorption coefficient to the excited state absorption coefficient is about 10 for 476.5 nm and 1.51 for 457.9 nm and 1.25 for 514.5nm. This would suggest that the laser exciting line 514.5 nm and 457.9 nm are close to the excited state absorption band. This is in agreement with the experiments of K. Divakar et.al.[6] who predicted an excited $T_1 \rightarrow T_2$ transition around 540 nm. The variation in the low power transmission in different portions of the film was about 15%.

3.4 Fluorescein-Boric acid glass films

The absorption and emission spectra of a 10^{-3} M fluorescein sample are shown in Fig 3.3. The peak of absorption occurs around 453 nm. This is somewhat red-shifted from the value of 440 nm reported by Kramer*et. al.*[4] for the same concentration. The absorption falls off rapidly at higher wavelengths, reaching nearly zero at about 498 nm Unlike R6G, Fluorescein can be excited only on the red side of the absorption peak. Moreover, not all Argon wavelengths can be used for excitation. The spectrum of fluorescein doped film does not show any structure unlike that of R6G. The shape of the spectrum is similar to that reported by Kramer*et. al.*[4] and that by Todorov for a much higher concentration (0.12M). The emission spectrum shows a peak at 482 nm giving a stokes shift of 29 nm. The saturation characteristics of Fluorescein films are not discussed because they are available in the literature[1, 3, 4, 7]

3.5 Thickness and refractive index.

Standard methods of thickness measurement of films are not applicable to sandwiched films. The thickness of our films was measured by a non-linear technique to be described in Chapter 4. The normal thickness of these films is around 30-50 μm. Approximate value of the linear refractive index was calculated from the measurements of the light power reflected from the glass slide-film interface. The linear refractive index of the dye-glass film at 514.5 nm. was obtained to be 1.1 with respect to the glass, giving a value of 1.36 for the refractive index with respect to air. This value is in agreement with the values reported in the literature. This value of the film refractive index was used to correct the reflective losses at the glass-film interface. The absorption spectrum of other samples like Tetraphenylporphyrin (TPPH), $TPP(NO_2)_4$, S_2TPP, BrTPP doped in boric acid glass will be presented as a part of the complete study in chapter 6.

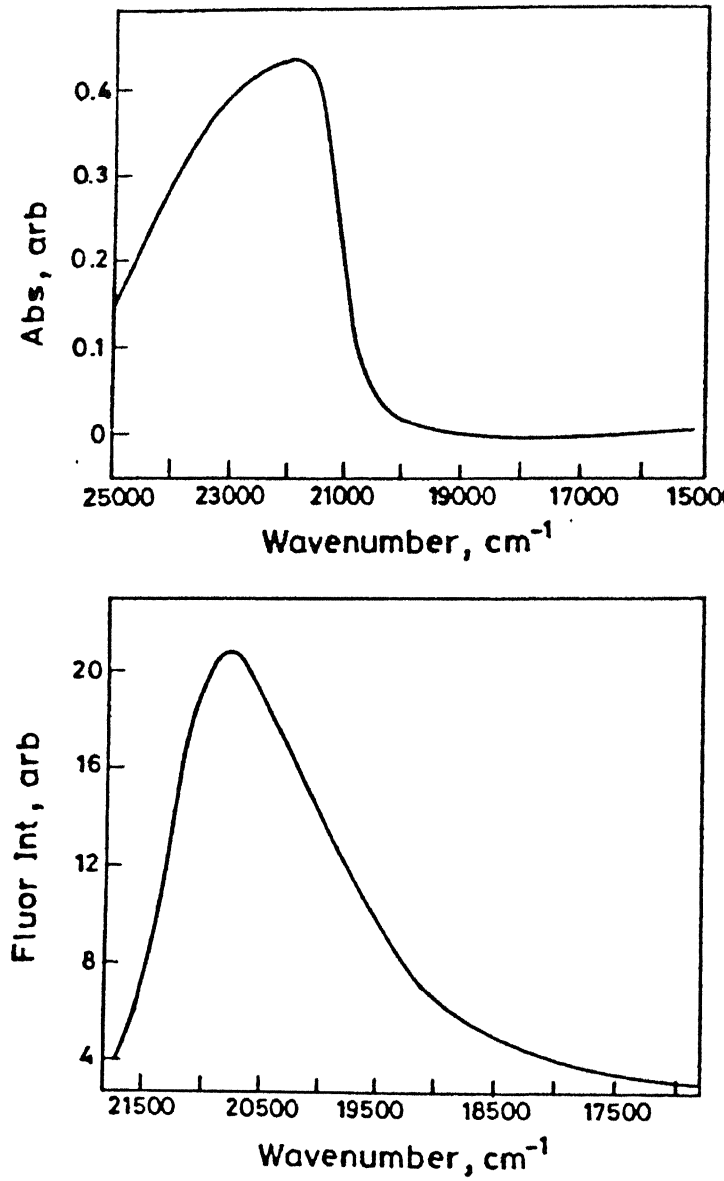

Figure 3.5: Absorption and emission spectra of Fluorescein-boric acid (10^{-3}) glass

References

[1] G.N. Lewis, D. Lipkin and T T mayer, *J. Am. Chem. Soc.*, **63**, (1941), 3005.

[2] T A. Shankoff, *Appl. Opt.*, 8, (1969), 2282

[3] T. Todorov, L Nikolova, N. Tomova and V. Prayostinova, *Opt. Quant. Elec.*, **13**, (1981), 209.

[4] M A. Kramer, W.R Tompkin and R.W. Boyd, *Phys. Rev. A*, **34**, (1986), 2026.

[5] G. Ravindra Kumar, Ph.D. Thesis, Indian Institute of Technology, Kanpur, 1990.

[6] K. Divakara Rao, Ph.D. Thesis, Indian Institute of Technology, Kanpur, 1994.

[7] M.A. Kramer, W.R. Tompkin, J. Krasinski, and R.W. Boyd, *J. Lumin*, **31-32**, (1984), 789.

Chapter 4

Two Beam Coupling in Rhodamine 6G Doped Boric Acid Glass Films

4.1 Introduction

In two beam coupling, two light beams degenerate or non-degenerate in frequency interact in a nonlinear material such that the energy is transferred from one beam to the other. This coupling between the two beams is brought about by the fact that each beam sees the medium refractive index which has been modified by the presence of the other beam. Two beam coupling is exhibited in a variety of non-linear optical phenomena. Notable among them are the stimulated Brillouin scattering and stimulated Raman scattering[1, 2, 17]. The two beam coupling can not only be used to transfer information from one beam to another but it may also be used to amplify the probe beam in the presence of the pump beam. Two beam coupling has been studied in a host of materials like photo-refractive crystals, Kerr-like media and saturable absorbers. In saturable absorbers it has been used to determine the response time of the non-linearity, the saturation intensity, the real and imaginary parts of the complex nonlinear index of refraction of the medium[3–5, 7, 8, 20]. Two beam coupling is used in real-time holography, self-pumped phase conjugators, ring resonators, laser gyros, nonreciprocal transmission, image amplification, vibrational analysis, image processing, etc[17].

In this chapter we first review the two beam coupling process in general terms and then discuss in some detail the two-wave mixing process specifically in the context of the saturable absorbers. This will be followed by the presentation of our results on two beam coupling in Rhodamine 6G doped Boric Acid Glass films.

4.2 Description of Two Beam Coupling

We shall first consider two beam coupling in a Kerr medium where the optical non-linearity arises from the dependence of the refractive index of a non-linear medium on the intensity distribution of the light field in the medium[1, 11]. The non-linearity in a Kerr medium can be characterised by the steady state non-linear refractive index

$$n_{NL} = n_2 I \tag{4.1}$$

and the response time τ of the medium. Two beam coupling in a Kerr medium was first studied in detail by Silberberg, and Bar Joseph and Boyd. Fig 4.1(a) shows two waves of complex amplitude A_1 and A_2 with propagation vectors $\vec{k_1}$ and $\vec{k_2}$ and frequencies ω_1 and ω_2 entering a nonlinear medium. The resultant real optical field in the region of interference is given by,

$$\vec{E}(\vec{r},t) = \frac{1}{2}\left[A_1 e^{\imath(\vec{k_1}.\vec{r}-\omega_1 t)} + A_2 e^{i(\vec{k_2}.\vec{r}-\omega_2 t)} + C.C\right] \tag{4.2}$$

where $C.C$ stands for the complex conjugate and,

$$k_\imath = \frac{n_0 \omega_\imath}{c} \tag{4.3}$$

n_0 being the linear refractive index of the medium. The intensity distribution in the medium can be expressed as

$$\begin{aligned} I &= \frac{n_0 c}{2\pi}\left\{A_1.A_1^* + A_2.A_2^* + \left[A_1.A_2^* e^{+\imath(\vec{k_1}-\vec{k_2}).\vec{r}-(\omega_1-\omega_2)t} + C.C\right]\right\} \\ &= \frac{n_0 c}{2\pi}\left\{A_1.A_1^* + A_2.A_2^* + \left[A_1.A_2^* e^{-\imath(\vec{q}.\vec{r}-\delta t)} + C.C\right]\right\} \end{aligned} \tag{4.4}$$

where the vector $\vec{q} = \vec{k_1} - \vec{k_2}$ is shown in the figure and $\delta = \omega_1 - \omega_2$. For the nonlinear material the changing light intensity interference pattern modulates the optical properties such as the refractive index and turns the exposed portion of the medium into a grating. For $\delta \neq 0$, the grating is not stationary but is moving. The direction of movement of the grating depends on the sign of δ(Fig.4.1(b)). This grating diffracts the waves which produced the grating in the first place or any other wave which may be incident on it. We now describe why it is necessary to create a moving interference pattern to create conditions for the energy transfer to take place between the beams. The modulated index of the medium can be written as,

$$n(t) = n_0 + n_{NL}(t) \tag{4.5}$$

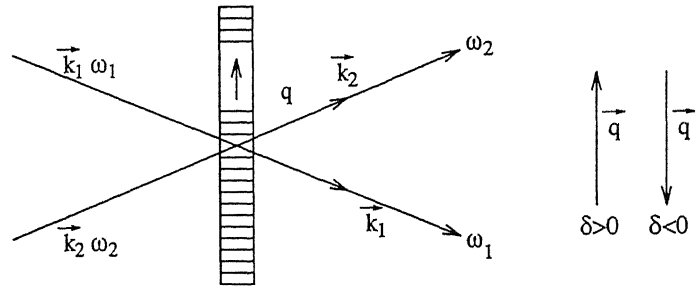

(a) Formation of interference fringes

(b) Direction of movement of interference pattern

Figure 4.1: Movement of interference pattern created by two interacting waves

Since the resultant intensity varies spatially in the medium, the refractive index will also vary spatially The medium in general will not be able to respond to changing intensity pattern instantaneously because the medium polarization results from the displacement of the bound charges. We assume a Debye type relaxation for the non-linear refractive index,

$$\tau \frac{dn_{NL}}{dt} + n_{NL} = n_2 I \tag{4.6}$$

where $n_2 I$ is the steady state value of the non-linear refractive index n_{NL} suggests that under transient conditions, the nonlinearity develops in a characteristics time interval of the order of τ. Silberberg*et.al.*[11] obtained the following solution of Eq.4.6,

$$n_{NL} = \frac{n_2}{\tau} \int_{-\infty}^{t} I(t') e^{(t'-t)/\tau} dt' \tag{4.7}$$

Substituting Eq 4.4 in Eq.4.7, one obtains for the non-linear refractive index as,

$$n_{NL} = \frac{n_0 n_2 c}{2\pi} \left[(A_1 A_1^* + A_2 A_2^*) + \frac{A_1 A_2^* e^{i(\vec{q}.\vec{r} - \delta t)}}{1 - i\delta\tau} + \frac{A_1^* A_2 e^{-i(\vec{q}.\vec{r} - \delta t)}}{1 + i\delta\tau} \right] \tag{4.8}$$

We note that the non-linear refractive index n_{NL} has a dc bias term and a time dependent term. Because of the appearance of the complex denominator in Eq.4.8, the time dependent refractive index is not in phase with the instantaneous intensity distribution as long as the medium response is not instantaneous i.e as long as $\tau \neq 0$. This term is responsible for the energy coupling between the two waves. The first terms in Eq.4.8 correspond to the stationary grating and the last two terms represents the moving grating because the refractive index changes are time dependent

We can now substitute Eq.4.2 for the electric field in the wave equation.

$$\nabla^2\vec{E} - \frac{n^2}{c^2}\frac{\partial^2\vec{E}}{\partial t^2} = 0 \tag{4.9}$$

where

$$\begin{aligned} n &= n_0 + n_{NL} \\ \text{and} & \\ n^2 &= n_0^2 + 2n_0 n_{NL} \end{aligned}$$

Here we have assume $|n_{NL}| \ll n_0$, so that the term $|n_{NL}|^2$ can be neglected. If the spatial variation of the amplitude is neglected in the x and y directions, we can write for the propagation of the wave with amplitude A_2.

$$\begin{aligned} \frac{d^2A_2}{dz^2} &+ 2ik_2\frac{dA_2}{dz} - k_2A_2^2 + \frac{n_0^2\omega_2^2}{c^2}A_2 \\ &= -\frac{n_0^2 n_2\omega_2^2}{\pi c}(|A_1|^2 + |A_2|^2)A_2 - \frac{n_0^2 n_2\omega_1^2}{\pi c}\frac{(|A_1|^2)A_2}{1+i\delta\tau} \end{aligned} \tag{4.10}$$

A similar equation for the propagation of the other wave can also be written.

We can immediately identify the last term with the moving grating and the first two terms with the stationary grating. With the slowly varying amplitude approximation, the equation (4.10)reduces to

$$\frac{dA_2}{dz} = \frac{in_0 n_2\omega}{2\pi}(|A_1|^2 + |A_2|^2)A_2 + \frac{in_0 n_2\omega}{2\pi}\frac{(|A_1|^2)A_2}{1+i\delta\tau} \tag{4.11}$$

where $\omega_1 \approx \omega_2 \approx \omega$. We can write for the spatial dependence of the intensity distribution,

$$\frac{dI_2}{dz} = (\frac{n_o c}{2\pi})\left(A_2^*\frac{dA_2}{dz} + A_2\frac{dA_2^*}{dz}\right) \tag{4.12}$$

We notice that when $\frac{dA_2}{dz}$ and $\frac{dA_2^*}{dz}$ are substituted from Eq.4.11 into Eq.4.12 the stationary grating terms disappear and the spatial dependence of I_2 takes the form,

$$\frac{dI_2}{dz} = \frac{2n_2\omega}{c}\frac{\delta\tau}{1+\delta^2\tau^2}I_1I_2 \tag{4.13}$$

For positive value of n_2 and δ, Eq.4.13 predicts gain for the beam with intensity I_2. Further in the limit of a fast nonlinearity $\tau \to 0$, the coupling between the two waves vanishes. It also vanishes when $\delta \to 0$ i.e. when the input waves have the same frequency. It should be noted that for large detuning, the energy transfer goes down. Thus there is an optimum detuning for energy transfer to take place. When the product $\delta\tau$ is nonzero the field generated by the

changing polarization can lag behind the driving field leading to an exchange of energy between the two beams. It is instructive to note that the stationary grating does not contribute to the growth or decay of the beam with the intensity I_2. It is the moving grating which modifies the intensity of the beam as it propagates . This explains why it is necessary to have unequal frequencies of the beam to obtain any coupling between them.

In photorefractive crystals[21], even with waves of the same frequency, energy transfer occurs because the charge carriers produced by the incident light can move with respect to the interference pattern The movement of the carriers introduces the necessary phase shift between the refractive index grating and the optical intensity distribution. The direction of energy flow depends upon the orientation of the wave vectors of the optical beams w.r.t. the symmetry axis of the photorefractive crystal.

4.3 Nondegenerate two wave mixing in saturable absorbers

We have seen in the previous section that it is possible to couple two beams inside a Kerr medium and affect an energy transfer between them provided the interfering beams have slightly different frequencies. Saturable absorbers do not involve any charge carriers and hence there is need to produce frequency mismatch between the interfering beams to exchange energy between them. The frequency shift between the beams needed for energy transfer in saturable absorbers can be achieved quite easily. The most common method employed involve the reflecting of one of the interfering beams off a moving mirror thereby introducing a Doppler frequency shift. Energy transfer in saturable absorbers such as ruby, fluorescein doped boric acid glass films, acridine orange doped in lead tin fluorophospate glass, erythrosin B-doped PVA film etc., has been achieved using this technique.

In one of the earliest studies on fluorescein doped in boric acid glass films, Boyd *et. al.*[1, 3, 4] described analytically the two beam coupling process in saturable absorbers on lines outlined in the previous section in the context of a Kerr medium. In order to include the effects of absorption in saturable absorbers they allowed the refractive index to become complex, i.e.,

$$n = n' + in'' + (n_2' + in_2'')I \tag{4.14}$$

where the linear refractive index has the usual form $n_0 = n' + in''$ and the nonlinear contribution to the refractive index has been written as $n_2 = (n_2' + in_2'')I$. Following a procedure similar to the one used in the previous section, they obtained for the spatial dependence of intensity of

beam one,

$$\frac{dI_1}{dz} = -\alpha I_1 + 2n_2''k(I_0 + I_1)I_1 + \frac{2n_2''k(I_0I_1)}{1+\Delta^2} + 2n_2'k(I_0I_1)\frac{\Delta}{1+\Delta^2} \tag{4.15}$$

where k is the wave number of light($= 2\pi/\lambda$) and $\Delta = (\omega_1 - \omega_2)\tau$. The first term in Eq.4.15 describes the linear absorption of the host with absorption coefficient α, the second and the third terms predict increase in transmission at high intensities due to saturation effects. And the last term is due to dispersion and is responsible for the two beam coupling signal The last two term may be compared to (Eq.4.13) except that now n_2 has both real and imaginary parts.

A similar expression for the other beam can also be written down. Expression (4.15) was used by authors to account for the observed energy transfer between the two beams in fluorescein doped boric acid glass films. They obtained an empirical value for the non-linear refractive index n_2. $n_2 = 0.23(1+0.2i)$e.s.u. However it does not explain the saturation effects and the intensity dependence of the lifetimes of these films. Major drawback in their approach was to treat a saturable absorber like fluorescein doped BAG as a medium displaying Kerr like non-linearity which neglects the strong absorption of the dye molecules.

In a later work Zhou*et. al.*[20] theoretically analyzed the saturation effects in non-degenerate two-wave mixing and tested their theoretical predictions with experimental results in acridine yellow doped boric acid glass. They used a two-level model to represent saturable absorbers and predicted that the frequency difference of the two incident waves, at which the gain reaches its maximum increases with the pump intensity. They were also able to determine quantities such as relaxation time T_1, the saturation intensityI_s and the third order susceptibility $\chi^{(3)}$ in the process.

For a weak probe beam (I_2) in the presence of a relatively strong pump beam (I_1), they obtained the following expression for the probe transmittance.

$$\frac{I_2(z)}{I_2(0)} = \exp\left\{-\frac{2\alpha_0/(\delta T_2)^2}{1+I_1/I_s} - \frac{2\alpha_0/(\delta T_2)^2}{I_s}\frac{(\delta T_2)\Omega'}{1+(\Omega')^2}\frac{I_1}{(1+I_1/I_s)^2}\right\} \tag{4.16}$$

This expression suggests amplification (attenuation) of the beam with intensity I_2 depending on the product $\delta\Omega' < 0 (\delta\Omega' > 0)$. Here, T_2 is the transverse relaxation time or the dipole dephasing time and $\delta = \omega_0 - \omega_j$ is the detuning from the line center, I_s is the saturation intensity and

$$\Omega' = (\omega_1 - \omega_2)\frac{T_1}{1+I_1/I_s}. \tag{4.17}$$

Defining the gain parameter

$$\Gamma(\Omega') = ln\frac{I_2(L,+\Omega')}{I_2(L,-\Omega'} \tag{4.18}$$

equation(4 16)yields

$$\Gamma(\Omega') = \frac{-4\alpha_0}{I_s(\delta T_2)^2}\frac{T_2\delta\Omega'}{1+\Omega'^2}\frac{I_1 L}{(1+I_1/I_s)^2} \tag{4.19}$$

For $I_1 \ll I_s, \Gamma$ is proportional to I_1 but for $I_1 \gg I_s, \Gamma$ decreases with the pump intensity I_1. Thus the gain first increases with the pump intensity, reaches a maximum value and then on further increase in pump intensity, the gain falls. Further, we see that the gain Γ is maximum at $|\Omega'| = 1/T_1'$ (with $T_1' = T_1/(1 + I_1/I_s)$) and the maximum value is dependent on the pump intensity. They applied their analysis to acridine yellow doped boric acid glass and found $I_s = 109\text{mW/cm}^2$ with $\chi^{(3)} = \pm 0.04 + 0.7i$ e.s.u. as compared to $I_s = 100\text{mW/cm}^2$ with $\chi^{(3)} = \pm 0.06 + 0.8i$e.s.u. at $\lambda = 488\text{nm}$ using degenerate four wave mixing results. Despite this agreement, this approach based on a two level model is inadequate to describe the non-linear effects in dye molecules with energy level structure far from a two-level model. Fragnito *et.al.*[22] developed a treatment for self-diffraction for three level saturable absorber model based on population gratings. Later Zilio*et.al.*[8] proposed an alternative theory to describe nearly degenerate two wave mixing in saturable absorbers where the energy exchange is regarded as the zero-order diffraction process in the theory of self-diffraction. They applied this model to the two-beam coupling in ruby. We have extended this model to conditions existing in our experiment. We outline this approach in the next section.

4.4 Theoretical Framework

Consider two mutually coherent and co-polarized beams propagating in $\vec{k_0^+}$ and $\vec{k_0^-}$ directions crossing each other at an angle of 2θ inside a non-linear medium (Fig(4.2)). Let the beam in the $\vec{k_0^+}$ direction be the strong saturating beam (hereafter called the pump beam) and the one propagating in the k_0^- direction be the weak probe beam. We assume the two beams to be plane waves. There is a small frequency difference $\Omega = \omega_+ - \omega_-$ between these two beams such that the interference pattern is somewhat non-stationary. The electric field for the pump and the probe beams can be written as

$$E^{pump} = E_0^+ exp\{i(\vec{k_0^+}.\vec{r} - \omega_+ t + \phi_0^+)\} \tag{4.20}$$

$$E^{probe} = E_0^- exp\{i(\vec{k_0^-}.\vec{r} - \omega_- t + \phi_0^-)\} \tag{4.21}$$

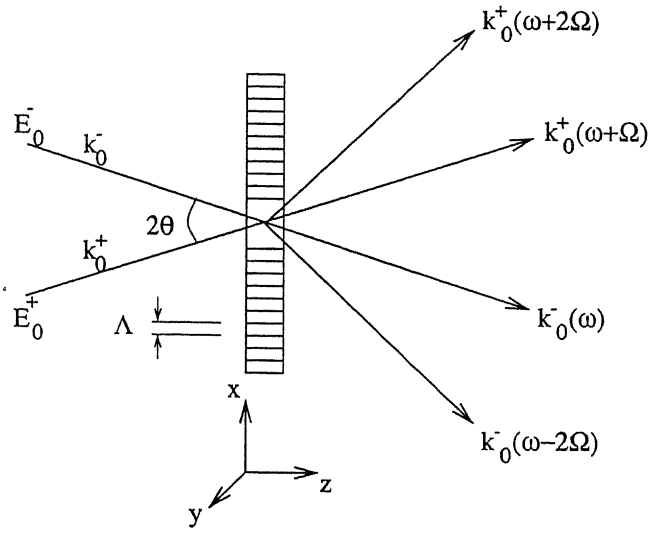

Figure 4.2: Schematic of non-degenerate two wave mixing

with the resultant intensity as

$$I^0(x,t) = \frac{1}{2} \in_0 \eta c|E|^2 \tag{4.22}$$

$$= I_0 + I_1 cos(kx - \Omega t + \Delta\phi). \tag{4.23}$$

where $\in_0$ is the dielectric permittivity of vacuum, η is the refractive index of the host medium. $\vec{k} = \vec{k_0^+} - \vec{k_0^-}$ is the direction of the grating vector as shown in the Fig. 4.2 with magnitude

$$K = \frac{2\pi}{\Lambda}; \Lambda = \frac{\lambda}{2sin\theta} \tag{4.24}$$

$$K = \frac{4\pi sin\theta}{\lambda} \tag{4.25}$$

where Λ is the spatial period of the interference pattern. $\vec{E_0^+}$ and $\vec{E_0^-}$ may be taken to have constant magnitude before entering the non-linear medium. However, they will decrease in magnitude as the beams propagate in the saturable absorber. The intensities I_0 and I_1 are defined as,

$$I_0 = I_0^+ + I_0^- \tag{4.26}$$

$$I_1 = 2\sqrt{I_0^+ I_0^-} \tag{4.27}$$

where I_0^+ and I_0^- are the intensities of the pump and the probe beams and $\Delta\phi = \phi_0^+ - \phi_0^-$. In order to solve the wave equation it will be necessary to find a suitable expression for the medium

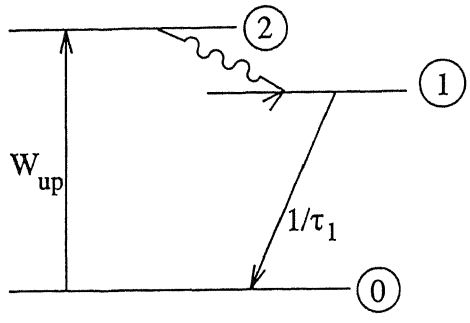

Figure 4.3: Three level energy diagram

polarization which is responsible for the generation of the new waves. We begin by assuming that the saturable absorber can be characterised by three levels (Fig. 4.3). We further assume that 0 to 2 transition is dipole allowed and 2 to 1 is a very fast non-radiative transition with unit quantum efficiency and level 1 is metastable. Medium polarization can then be expressed as,

$$\vec{P} = \epsilon_0 (\eta^2 - 1)\vec{E} + \epsilon_0 (n_0\chi_0 + n_1\chi_1\vec{E} \quad (4.28)$$

$$= \epsilon_0 (\eta^2 - 1 + \chi_0)\vec{E} + \vec{P_{NL}} \quad (4.29)$$

where

$$\vec{E} = \vec{E_0^+} + \vec{E_0^-} \quad (4.30)$$

$$\vec{P_{NL}} = \epsilon_0 n_1(\chi_1 - \chi_0)\vec{E} \quad (4.31)$$

Here, n_0 and n_1 are the fractional populations densities of the ground and the first excited levels respectively, so that $n_0 + n_1 = 1$. It has been assumed that the population of level 2 is very nearly zero.

We can find n_0 and n_1 from the rate equations.

$$\frac{dn_1}{dt} = (1 - n_1)W_{up} - \frac{n_1}{T_1} \quad (4.32)$$

where T_1 is the longitudinal relaxation time or population decay time of level 1; W_{up} is the rate of photon absorption in the $0 \rightarrow 2$ transition and is given by

$$W_{up} = \frac{\sigma_0 I}{\hbar\omega} \quad (4.33)$$

where

$$\sigma_0 = \frac{\mu^2\omega T_2}{\hbar c\eta \epsilon} \quad (4.34)$$

is the absorption cross-section $\omega_+ \approx \omega_- \approx \omega$ and T_2 is the transverse relaxation time or the dipole dephasing time Since the beam intensity is depleted as the beam propagates in the saturable absorber, the transfer rate W_{up} changes with propagation. As a result, Eq 4.32 is a non-linear differential equation. Instead of trying to solve the non-linear differential equation(4.32) to obtain an expression for the fractional population n_1 of level 1, we exploit the grating interpretation of the non-linear process. The spatial distribution of the dye molecules in the excited state (level 1) should follow the light interference pattern created in the region of overlap of the two-input beams. Eq.4.23 describes the intensity distribution which suggests a sinusoidal variation in the x-direction superposed on the uniform distribution described by the dc term I_0. The distribution of excited dye molecules may however, not be sinusoidal due to a number of reasons, saturation of level populations being one It is reasonable to expect this distribution to be anharmonic in which case we can Fourier expand the population function $n_1(x)$. The anharmonic modulation so generated leads to the appearance of many orders of diffraction. Fourier expansion of population distributions can be expressed as,

$$n_1(x,t) = \frac{1}{1+S_0} \sum_{n=-\infty}^{\infty} A_n \exp\{in(Kx - \Omega t + \Delta\phi\} \tag{4.35}$$

where $S_0 = I_0/I_s$ with $I_s = \hbar\omega/\sigma_0 T_1$. The higher diffraction orders represent the manifestation of the self-diffraction of the incident beams from the anharmonic population grating created by the beams themselves. For $I_s \ll I_0$ Fragnito *et. al.*[22]have evaluated the Fourier coefficients A_n under steady state conditions($t \gg T_1$) and found,

$$A_0 = S_0 \tag{4.36}$$

$$A_n = (\dot{-}1)^{n+1} \left(\frac{S_1/2}{1+S_0}\right)^{|n|} \left[\prod_{m=1}^{|n|} (1 - i\mathrm{sign(n)m}\Omega\mathrm{T}_1'\right] \tag{4.37}$$

$$\text{for} \quad n \neq 0$$

where $S_1 = I_1/I_s$ and $T_1' = T_1/(1 + I_0/I_s)$. Defining $\chi_{NL} = \chi_1 - \chi_0$ and using $P_{NL} = \sum_n P_{NL}(nK, n\Omega)$ as a source term in the wave equation we get

$$\left(\frac{c}{\omega}\right)^2 \nabla^2 E + \left(\eta^2 + \chi_0 + \frac{1}{1+S_0} \sum_{n=-\infty}^{\infty} \chi_{NL} A_n \exp in(Kx - \Omega t + \Delta\phi)\right) E = 0 \tag{4.38}$$

Following Fragnito*et.al.* we expand the electric field $\vec{E}$ in the nonlinear medium in terms of its Fourier coefficients

$$\vec{E} = \vec{E_0} + \vec{\delta}$$

$$= \sum_{n=0}^{\infty} \Big\{ \varepsilon_n^+ \exp[\imath((n+1/2)Kx - (n+1)\Omega t)] + \varepsilon_n^- \imath \exp[-\imath((n+1/2)Kx - n\Omega t)] \Big\} \times \exp\{i\beta_n z\} \quad (4.39)$$

here

$$\beta_n = \frac{\omega_n}{c} \left\{ (1 - (2n+1)^2 \sin^2\theta) \right\}^{1/2} \quad (4.40)$$

and E_0 is the net field entering the nonlinear medium and ε_n may be interpreted as the field associated with the beams representing different orders of diffraction. The $\pm$ sign refer to positive and negative orders of diffraction. With this definition of β_n, the dispersion relation

$$K_{nx}^2 + K_{nz}^2 = (\frac{\omega\eta}{c}) \quad (4.41)$$

holds. Further, assume

$$\frac{\partial \varepsilon_n^{\pm}}{\partial x} = \frac{\partial \varepsilon_n^{\pm}}{\partial y} \equiv 0 \quad (4.42)$$

and

$$\frac{\partial \varepsilon_n^{\pm}}{\partial z} \ll \beta_n \varepsilon_n^{\pm}, \quad (4.43)$$

we obtain the following equation for the spatial evolution of the slowly varying field amplitude.

$$\begin{aligned} 2i\left(\tfrac{c}{\omega}\right)^2 & \sum_{n=0}^{\infty} \beta_n \left(\frac{d\varepsilon_n^+}{dz} \exp[i((n+1/2)Kx - (n+1)\Omega t)] \right. \\ & \left. + \frac{d\varepsilon_n^-}{dz} \exp[-i((n+1/2)Kx - n\Omega t)] \right) \exp(i\beta_n z) \\ = & -\left(\chi_0 + \frac{1}{1+S_0} \sum_{n=0}^{\infty} \chi_{NL} A_l \exp[il(Kx - \Omega t + \Delta\phi)] \right) \\ \times & \sum_{n'=0}^{\infty} \Big(\varepsilon_n^+ \exp[i((n'+1/2)Kx - (n'+1)\Omega t)] \\ & + \varepsilon_n^- \exp[-\imath((n'+1/2)Kx - n'\Omega t)] \Big) \exp(i\beta_{n'} z) \end{aligned} \quad (4.44)$$

In the above equation terms proportional to A_l represent diffraction of the input beam from the anharmonic grating. Subsequent diffraction of these diffracted beams from the induced anharmonic grating are not important under our experimental conditions. For $I \approx I_s$, such effects can be neglected. We compare terms with the same x and t dependences in order to obtain a set of coupled equations. By comparing term by term in the sum on both sides of

equation(4.44), we can deduce the z-dependence of each diffracted wave as it propagates in the non-linear medium.

$$\frac{d\varepsilon_n^+}{dz} = \frac{\imath}{2\beta_n}\left(\frac{\omega}{c}\right)^2\left[\chi_0\varepsilon_n^+ + \frac{1}{1+S_0}\sum_{l=0}^{\infty}\left\{\chi_{NL}^* A_{l-n}^*\varepsilon_l^+ \exp[-\imath(l-n)\Delta\phi]\right.\right. \\ \left.\left. + \chi_{NL}^* A_{l+n+1}^*\varepsilon_l^- \exp[-\imath(l+n+1)\Delta\phi]\right\} \times \exp[-\imath(\beta_l-\beta_n)z]\right] \quad (4.45)$$

and

$$\frac{d\varepsilon_n^-}{dz} = \frac{\imath}{2\beta_n}\left(\frac{\omega}{c}\right)^2\left[\chi_0\varepsilon_n^- + \frac{1}{1+S_0}\sum_{l=0}^{\infty}\left\{\chi_{NL}^* A_{l+n+1}^*\varepsilon_l^+ \exp[-i(l+n+1)\Delta\phi]\right.\right. \\ \left.\left. + \chi_{NL}^* A_{l-n}^*\varepsilon_l^- \exp[-\imath(l-n)\Delta\phi]\right\} \times \exp[-\imath(\beta_l-\beta_n)z]\right] \quad (4.46)$$

where $A_l^* = A_{-l}$ Here the field terms ε_n^+ represent the input pump beams ε_0^+ and its various diffractions orders which are generated by the diffraction of the pump beam from the induced grating. Similarly the ε_n^- terms can also be interpreted as the diffraction of the probe beams. From these set of equations one can calculate the electric field associated with any order of diffraction. However we shall consider the propagation of the zero order diffraction beams which are in fact the pump and probe beams themselves. Our experimental conditions to be described later ensure that higher order diffractions are insignificant. As such we need to solve the following equations only.

$$\frac{d\varepsilon_0^+}{dz} = i\gamma\left[\left(\chi_0 + \frac{\chi_{NL}A_0^*}{1+S_0}\right)\varepsilon_0^+ + \frac{\chi_{NL}A_1}{1+S_0}\varepsilon_0^- \exp(i\Delta\phi)\right] \quad (4.47)$$

$$\frac{d\varepsilon_0^-}{dz} = i\gamma\left[\frac{\chi_{NL}^*A_1^*}{1+S_0}\varepsilon_0^+ \exp(-i\Delta\phi) + \left(\chi_0 + \frac{\chi_{NL}A_0^*}{1+S_0}\right)\varepsilon_0^-\right] \quad (4.48)$$

The phase dependent exponentials cancel out because $\varepsilon_0^+ \sim \exp(+i\phi_0^+)$ and $\varepsilon_0^- \sim \exp(+i\phi_0^-)$ and $\gamma = \frac{1}{2\beta_0}\left(\frac{\omega}{c}\right)^2$. Two beam coupling is not expected to be a strong effect, consequently the probe beam continues to be much weaker than the pump beam inside the non-linear medium as well. Further it is expected that higher order diffractions would be weaker than lower order diffractions -in particular we expect the coefficient A_1 to be less than A_0. It is therefore reasonable to assume that

$$\frac{\chi_{NL}A_1}{1+S_0}\varepsilon_0^- \ll \left(\chi_0 + \frac{\chi_{NL}A_0^*}{1+S_0}\right)\varepsilon_0^+ \quad (4.49)$$

with this equation(4.47) reduces to

$$\frac{d\varepsilon_0^+}{dz} = i\gamma\left[\left(\chi_0 + \frac{\chi_{NL}A_0^*}{1+S_0}\right)\varepsilon_0^+\right] \quad (4.50)$$

which has the solution

$$\varepsilon_0^+(z) = \varepsilon_0^+(0) \exp\left[i\gamma\left(\chi_0 + \frac{\chi_{NL}A_0}{1+S_0}z\right)\right] \tag{4.51}$$

Using this solution of ε_0^+ we can solve equation4.48 to obtain the field strength of the probe beam. We get

$$\varepsilon_0^-(z) = \varepsilon_0^-(0)\left\{1 + i\gamma\left(\chi_0 + \frac{\chi_{NL}^* A_1^*}{1+S_0}\frac{\varepsilon_0^+(0)}{\varepsilon_0^-(0)}z\right)\right\} \times \exp\left[i\gamma\left(\chi_0 + \frac{\chi_{NL}A_0}{1+S_0}z\right)\right] \tag{4.52}$$

Zilio replaced

$$\left\{1 + i\gamma\left(\chi_0 + \frac{\chi_{NL}^* A_1^*}{1+S_0}\frac{\varepsilon_0^+(0)}{\varepsilon_0^-(0)}z\right)\right\} \tag{4.53}$$

by

$$\exp\left\{i\gamma\left(\chi_0 + \frac{\chi_{NL}^* A_1^*}{1+S_0}\frac{\varepsilon_0^+(0)}{\varepsilon_0^-(0)}z\right)\right\} \tag{4.54}$$

This requires

$$\left\{\gamma\left(\chi_0 + \frac{\chi_{NL}^* A_1^*}{1+S_0}\frac{\varepsilon_0^+(0)}{\varepsilon_0^-(0)}z\right)\right\} \ll 1 \tag{4.55}$$

This condition is generally not satisfied under our experimental conditions. We retain Eq.4.52 as such and obtain the following expression for the intensity of the probe beam exiting the sample,

$$\begin{aligned} I_0^-(L) &= \frac{1}{2}\in_0 \eta c|\varepsilon_0^-(L)|^2 \\ &= I_0^-(0)\exp\left\{-2\gamma L(\chi_0'' + \frac{\chi_{Nl}'' S_0}{1+S_0})\right\} \\ &\times \left\{1 + \frac{2X}{1+\Omega^2 T_1'^2(\chi_{NL}'' + \Omega T_1'\chi_{NL})}\right. \\ &+ \left.\frac{X^2((\chi_{NL}')^2 + (\chi_{NL}'')^2)}{(1+\Omega^2 T_1'^2)}\right\} \end{aligned} \tag{4.56}$$

where $X = \gamma L(I_0^+/I_s)/(1+S_0)^2$ and $\chi_{NL} = 2\eta n_2$ have been used. We use $\Delta = \Omega T_1'$; $n_2 = n_2' + in_2'' = n_2'(1+i\gamma)$ with $r = n_2''/n_2'$. Defining $\alpha_0 = (\omega/\eta c)\chi_0''$, $\beta_0 = (\omega/\eta c)\chi_1''$, as absorption coefficients of the ground and the excited states respectively and also using the fact that $\chi_{NL}'' = \chi_1'' - \chi_0''$ equation(4.56) becomes

$$
\begin{aligned}
I_0^-(L) &= I_0^-(0)\exp\left\{\frac{\alpha_0 L}{\cos\theta(1+S_0)}\left(1+\frac{I_0^+}{I_s}\frac{\beta_0}{\alpha_0}\right)\right\} \\
&\times \left[\left\{1+\frac{2\pi n_2' L}{\lambda\cos\theta}\frac{I_0^+/I_s}{(1+S_0)^2}\frac{(r+\Delta)}{(1+\Delta^2)}\right\}^2\right. \\
&+ \left.\left\{\frac{2\pi n_2' L}{\lambda\cos\theta}\frac{I_0^+/I_s}{(1+S_0)^2}\frac{(1-r\Delta)}{(1+\Delta^2)}\right\}^2\right]
\end{aligned} \tag{4.57}
$$

We can rewrite this equation in a compact notation,

$$
\begin{aligned}
I_0^-(\Delta,L) &= I_0^-(0)\exp\{-\alpha_{eff}L\} \\
&\times \left[\left\{1+gL\frac{(r+\Delta)}{(1+\Delta^2)}\right\}^2+\left\{gL\frac{(1-r\Delta)}{(1+\Delta^2)}\right\}^2\right]
\end{aligned} \tag{4.58}
$$

where

$$
\alpha_{eff} = \frac{\alpha_0/\cos\theta}{(1+I_0^+/I_s)}\left(1+\frac{I_0^+}{I_s}\frac{\beta_0}{\alpha_0}\right) \tag{4.59}
$$

$$
\text{and} \quad g = \frac{2\pi n_2' L}{\lambda\cos\theta}\frac{I_0^+/I_s}{(1+S_0)^2} \tag{4.60}
$$

This should be compared with the corresponding expression obtained by Zilio,

$$
I_0^-(\Delta,L) = I_0^-(0)\exp\left[\left(g\frac{(r+\Delta)^2}{(1+\Delta^2)}-\alpha_{eff}\right)L\right] \tag{4.61}
$$

For $\Delta = 0$, the expression (4.58) reduces to the degenerate case which shows how the probe beam gets modified during propagation in the non-linear medium in the presence of a relatively strong pump.

$$
\begin{aligned}
I_0^-(0,L) &= I_0^-(0)\exp\{-\alpha_{eff}L\} \\
&\times \left[\{1+gLr\}^2+\{gL\}\right]
\end{aligned} \tag{4.62}
$$

More explicitly, we can write,

$$
\frac{I_0^-(0,L)}{I_0^-(0,0)} = \exp\left\{\frac{\alpha_0 L}{\cos\theta}\frac{(1+\beta_0/\alpha_0 I_0^+/I_s)}{(1+S_0)}\right\}\left[\left\{1+\frac{2\pi n_2'' L}{\lambda\cos\theta}\frac{I_0^+/I_s}{(1+S_0)^2}\right\}^2+\left\{\frac{2\pi n_2' L}{\lambda\cos\theta}\frac{I_0^+/I_s}{(1+S_0)^2}\right\}^2\right] \tag{4.63}
$$

In our two beam coupling experiment, we use a triangular ramp voltage to the peizo-mirror. This results in upshift in the probe frequency during half the period of the ramp waveform and downshift in the second half. Thus in one half of the mirror motion the probe will gain energy

from the pump and in the other half it will lose energy. We define gain parameters as

$$\frac{\Delta I_0^-(\Delta, L)}{I_0^-(0, L)} = \frac{|I_0^-(\Delta, L) - I_0^-(-\Delta, L)|}{I_0^-(0, L)} \tag{4.64}$$

where $I_0^-(\Delta, L)$ and $I_0^-(-\Delta, L)$ are the transmitted probe intensities during the two half cycles of the motion of the peizo-mirror. The gain parameter has been normalized to the transmitted probe intensity in the absence of the mirror motion. With (4.58), the gain parameter takes the form (with$I_0^+/I_s = I_0/I_s = S_0$)

$$\frac{\Delta I_0^-(\Delta, L)}{I_0^-(0, L)} = \frac{\frac{4\pi L}{\lambda \cos\theta} \frac{n_2' S_0}{(1+S_0)^2} (2\Delta)}{\left[\left\{1 + \frac{2\pi n_2'' L}{\lambda \cos\theta} \frac{S_0}{(1+S_0)^2}\right\}^2 + \left\{\frac{2\pi n_2' L}{\lambda \cos\theta} \frac{S_0}{(1+S_0)^2}\right\}^2\right]} \tag{4.65}$$

Writing $X = \frac{2\pi L}{\lambda \cos\theta}$, Eq.4.65 becomes

$$\frac{\Delta I_0^-(\Delta, L)}{I_0^-(0, L)} = \frac{2X \frac{n_2' I_0^+/I_s}{(1+S_0)^2} (2\Delta)}{\left[\left\{1 + \frac{X n_2'' S_0}{(1+S_0)^2}\right\}^2 + \left\{\frac{X n_2' S_0}{(1+S_0)^2}\right\}^2\right]} \tag{4.66}$$

This expression for the gain parameter will be used to interpret the result of our two beam coupling experiment to be described in the next section.

4.5 Experimental Setup

Fig(4.4) gives the schematic of the experimental configuration. The pump and the probe beams are derived from the same laser (in our case Argon ion Laser Model Coherent Innova-70). The beam splitter BS_1 splits the laser beam in the ratio 90:10 The pump beam is directly steered to the sample with the help of mirrors M_2 and M_5. The probe beam is sent to another beam splitter (BS_2). The reflected beam from BS_2 is made to fall normally on a mirror mounted on a peizo-electric transducer. The beam reflected from the peizo mirror traverses the same beam splitter on return and is then steered to the sample with the help of mirrors M_3 and M_4. Appropriate neutral density filters are introduced in its path to bring down the probe power to the desired level. This peizo transducer is driven by a triangular voltage waveform obtained from a function generator (Systronics function generator 1012) and further amplified by a home-made voltage amplifier. Voltage amplifier is of cascode type so that it does not distort the impressed triangular waveform and had the same gain over the ramp repetition rate of our interest. The uniformity of the mirror displacement is important so that the frequency shift is the same for the light falling on different portions of the mirror throughout the range of the frequency shifts

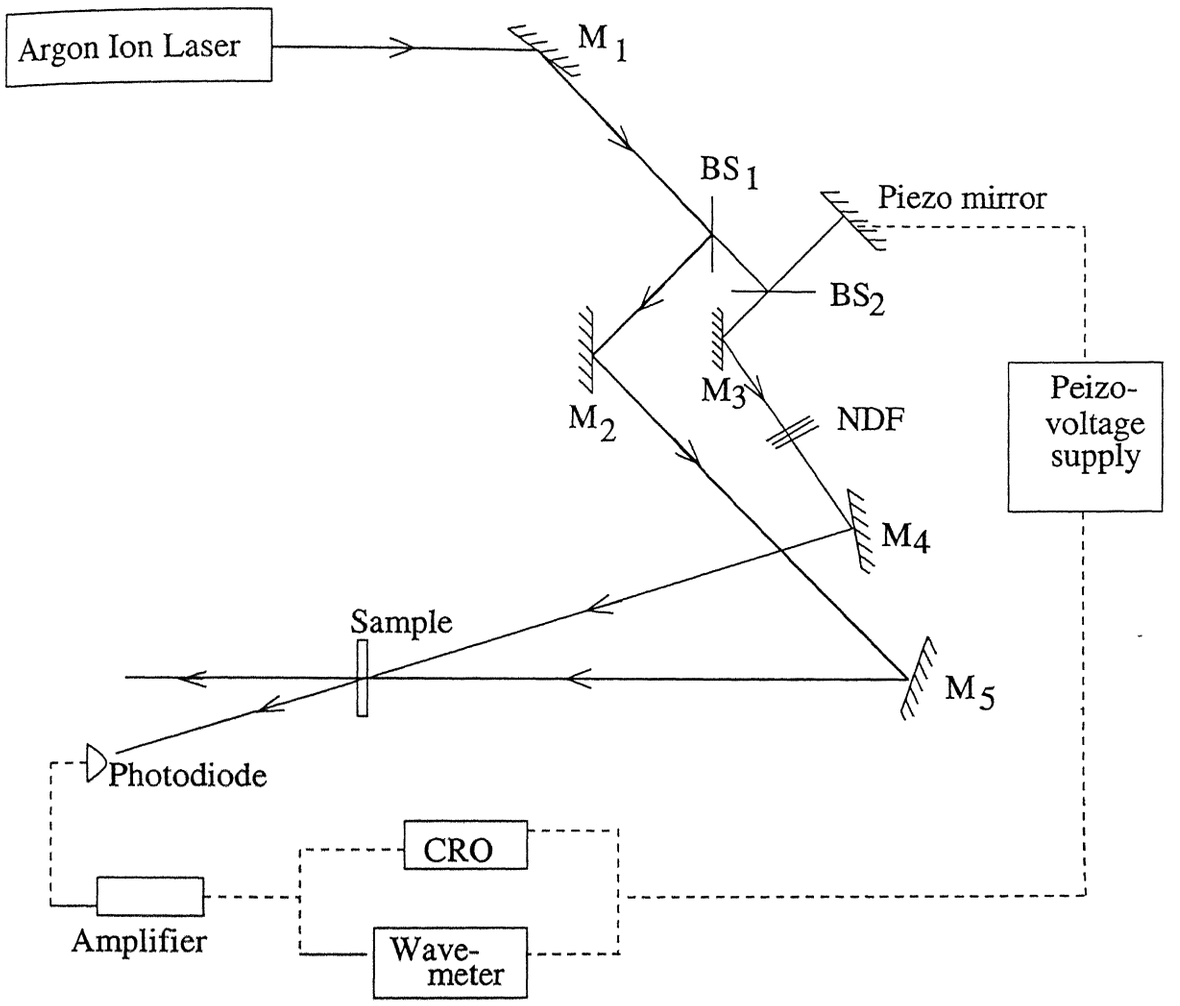

Figure 4.4: Experimental Setup for two-beam coupling setup ; M_1 to M_5 mirrors, BS-Beam-splitters, NDF- Neutral Density Filters

carried out in our experiments. This was achieved by examining the mechanical-resonances of the peizo-mirror in a Michelson interferometric setup. The ramp voltage was amplified to the level so that the maximum displacement of the mirror is $\lambda/2$ where λ is the wavelength of the Ar^+ ion laser line used viz. 514.5nm.

Under these conditions the frequency shift of the reflected beam is twice the ramp repetition rate i.e. $\Omega = \pm 2\pi f$. Here Ω is the shift in angular frequency of the reflected light beam and $f/2$ is the inverse of the ramp repetition rate. The $\pm$ sign correspond to the up and down frequency shifts of the probe beam.

In order to determine the voltage to the peizo for a $\lambda/2$ excursion, we substituted the peizomirror for one of the end mirror of the Michelson interferometer. Michelson fringes were displayed on the screen for a fixed position of the peizo-mirror. For an arbitrary displacement

of the mirror, the fringe pattern gets disturbed and the visibility of fringes is affected. However for displacement of $\lambda/2$ of the peizo- mirror, the fringe visibility remains unchanged. There was no change in the visibility of Michelson fringes over the desired frequency range for the $\lambda/2$ movement of the mirror. Voltage ramp of 72 volts was applied to the peizo-mirror for $\lambda/2$ excursion at 514.5nm.

The pump.probe intensity ratio was changed by using neutral density filters close to the sample, so as to avoid any beam narrowing or clipping resulting in change of the spot size. Efforts were made to maintain the spot size of the two beams throughout the experiment Spot size was measured by the standard knife-edge method. The beams were ensured to have parallel polarization. Good overlap of probe and pump beams were also ensured. The path difference between the pump and the probe beams was kept within 1cm, much less than the coherence length of the Coherent laser model I-70. The probe transmission through the sample was monitored by a Si-photodetector which was fed to an amplifier and then displayed on Kikusui digital storage scope DSS 6521 (C R.O) and recorded on a wave meter(Hioki 8801). The depth of the modulated signal is quite small in comparison to the d.c. signal on which the modulation rides. This presented some difficulty in measuring the depth of modulation and its variation as seen on the C.R.O. Therefore we had to use an additional amplifier to amplify the weak a.c. signal which represents the modulation caused by frequency shifting the probe beam with the peizo-mirror. The actual strength of the weak a.c. signal was calculated from the known amplification factor of the amplifier. However in the process we lost the d.c signal which represents the probe transmission in the absence of the modulation. But this information can be obtained using a calibrated photo-diode system. It is therefore possible eventually to get the actual values of the d.c. and the modulated signals for comparison. The two beam coupling signal is the difference between the a.c. signals recorded during the upshift and downshift of the probe frequency. The upshift takes place when the peizo-mirror is moving into the beam with a constant velocity and the downshift is when beam is moving away from it.

4.6 Results and Discussion

Rhodamine 6G doped films of boric acid glass with 10^{-4} molar concentration in the melt were prepared by the method discussed in chapter 3. Films of varying thickness were prepared from the same melt so that the molar concentration in different samples were nearly the same. These films are sandwiched between two microscope slides. It is difficult to measure the thickness of the sandwiched films. We have used the measured values of $\alpha_0 L = \ln I_o/I_t$ at low intensities ($I_0 \ll I_s$) to characterize a film. Here I_0 is the incident and I_t is the transmitted intensity. Most of the work on the beam coupling was carried out on one spot of a film with $\alpha_0 L$ value of 0.63

at 514.5 nm line of the Argon^+ ion laser. This wavelength lies in the wings of the absorption profile of the dye doped BAG film The line was selected for two beam coupling studies because the signal strength observed at this wavelength is maximum The probe power during the experiment was kept fixed at 1.1 mW with the beam spot-size of 3 8mm at the location of the sample which corresponds to $I = 9.7\mathrm{mW/cm^2}$. The beam coupling was studied at pump beam power of 73mW,195mW,380mW and 600mW which correspond to beam intensities of $.643\mathrm{W/cm^2}, 1.72\mathrm{W/cm^2}, 3.35\mathrm{W/cm^2}, 5.29\mathrm{W/cm^2}$ respectively. Some of the recorded profiles of the two beam coupling signals are shown in Figs.4.5 The frequency modulation of the probe beam was confined to some discreet values in the interval $0 - 30$Hz. The two beam coupling signal is recorded along with the ramp voltage waveform for comparison The two beam signal is reasonably clean at low frequencies but the signal to noise ratio degrades as the probe frequency increases. Eq.4.64 was used to extract the two beam coupling signal from the recorded profiles and measured values of the transmitted probe intensity in the absence of any modulation. The two beam coupling data appear in table(4.1to 4.4)

Before we attempt to fit these data to the expression (4.65) we need to take a close look at this expression. There are several unknown quantities in this expression. The film thickness L, the saturation intensity I_s, the real and imaginary part (n_2', n_2'') of the non-linear refractive index n_2, and the relaxation time T_1 are the five unknowns in this expression It would not be proper to fit all these parameters by fitting the two beam coupling data to Eq.4.65. In fact such an attempt was made but it was not possible to get a reliable set of values for these quantities. This happens because in this process we effectively transfer the inadequacies of the basic saturation process in these films to the two beam coupling process. It was decided to determine the best values for the film thickness and the saturation intensity from other considerations. It is the non-linear susceptibility parameter χ_{NL} or equivalently the real and the imaginary components of the non-linear refractive index n_2 which are basic to the beam coupling process. These will be determined from the two beam coupling results.

Table 4.1: TBC data of R6G doped BAG film (α_0L=0 63 at 514.5 nm, pump power=73 mW, probe power = 1.1 mW)

Sr. No.	Frequency (Hz)	$\Delta I_{probe}(\Delta)$ (mV)	$I_{probe}(0)$ (mV)	$\frac{\Delta I_{probe}(\Delta)}{I_{probe}(0)}$ %
1	1.3	0.70	32.7	2.15
2	2.0	0.96	32.5	2.95
3	4.0	1.13	32.5	3.48
4	5.0	1.22	32.5	3.75
5	6.0	1.39	32.5	4.28
6	8.0	1.30	32.5	4.00
7	8.8	1.39	32.0	4.34
8	10.0	1.39	32.0	4.34
9	12.0	1.30	31.0	4.19
10	15.0	1.22	31.0	3.94
11	20.0	0.78	31.0	2.50
12	25.0	0.70	31.0	2.25
13	30.0	0.52	31.0	1.68

Table 4.2: TBC data of R6G doped BAG film(α_0L=0.63 at 514.5 nm , pump power=195 mW, probe power = 1.1 mW)

Sr. No.	Frequency (Hz)	$\Delta I_{probe}(\Delta)$ (mV)	$I_{probe}(0)$ (mV)	$\frac{\Delta I_{probe}(\Delta)}{I_{probe}(0)}$ %
1	1.3	0.70	33.0	2.12
2	2.0	0.96	32.75	2.93
3	4.0	1.13	32.75	3.45
4	5.0	1.22	32.25	3.78
5	6.0	1.39	32.75	4.24
6	8.0	1.39	32.75	4.24
7	8.8	1.39	32.75	4.34
8	10.0	1.48	32.0	4.77
9	12.0	1.48	31.0	4.77
10	15.0	1.48	31.0	4.77
11	20.0	1.22	31.0	3.93
12	25.0	1.04	31.0	3.35
13	30.0	0.70	31.0	2.25

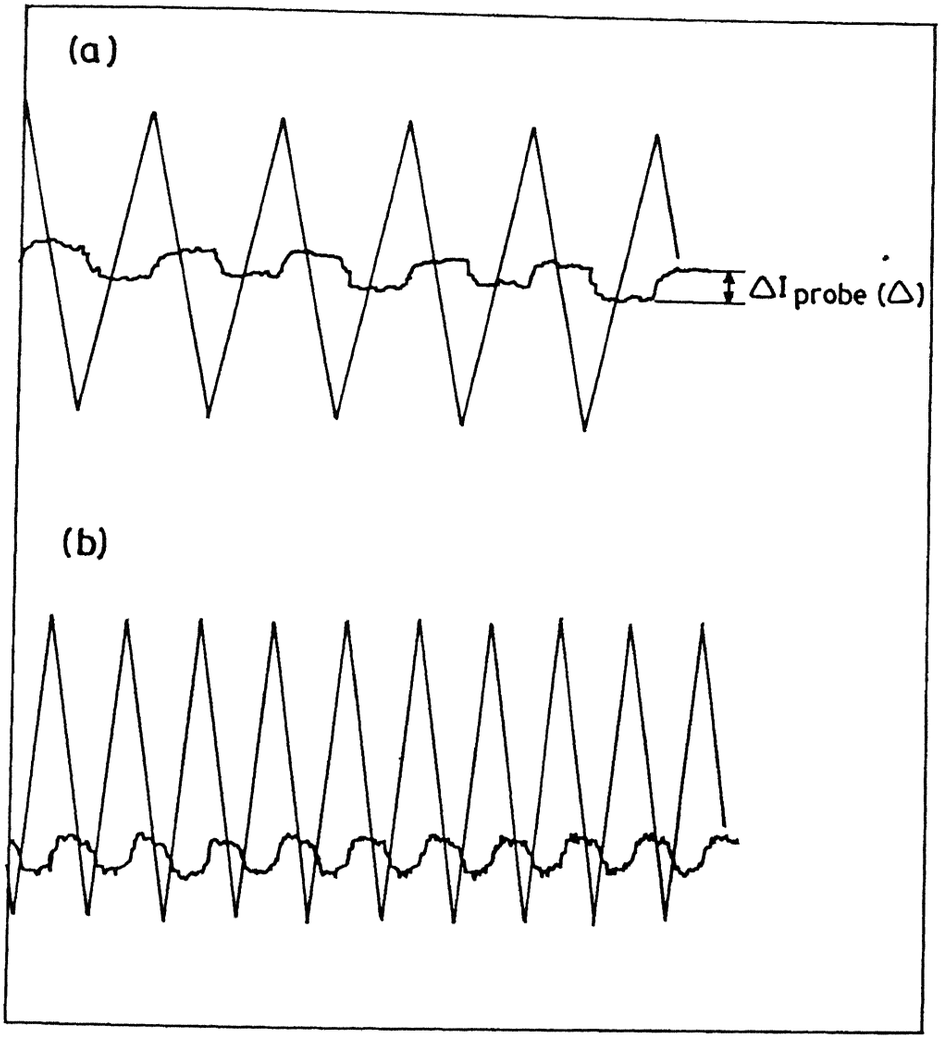

Figure 4.5: Two beam coupling signal recorded in Rhodamine6G doped BAG at 514.5nm $\Delta I_{probe}(\Delta)$ =modulation depth of the two beam coupling signal at the detuning Δ for (a)Δ=2.0Hz, (b)Δ= 8.8Hz,(c)Δ= 10.0Hz, (d)Δ=25Hz

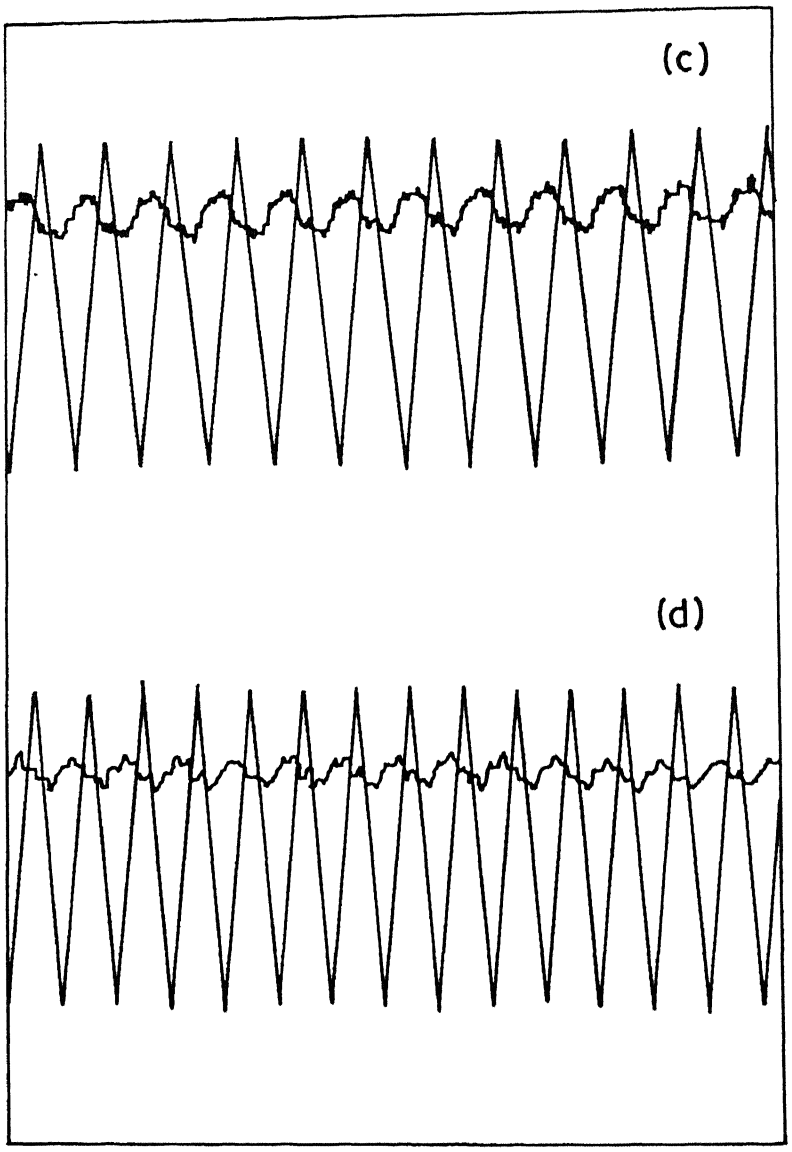
(c)
(d)

Table 4.3: TBC data of R6G doped BAG film(α_0L=0.63 at 514.5 nm ,pump power=380 mW, probe power = 1.1 mW)

Sr. No.	Frequency (Hz)	$\Delta I_{probe}(\Delta)$ (mV)	$I_{probe}(0)$ (mV)	$\frac{\Delta I_{probe}(\Delta)}{I_{probe}(0)}$ %
1	1.3	0.61	33.25	1.83
2	2.0	0.78	33.0	2.34
3	4.0	1.13	33.0	3.42
4	5.0	1.22	33.0	3.70
5	6.0	1.48	33.0	4.48
6	8.0	1.48	33.0	4.48
7	8.8	1.48	33.0	4.48
8	10.0	1.48	31.0	4.77
9	12.0	1.48	31.0	4.77
10	15.0	1.57	31.0	5.06
11	20.0	1.39	31.0	4.48
12	25.0	1.30	31.0	4 19
13	30.0	0.96	31.0	3.10

Table 4.4: TBC data of R6G doped BAG film(α_0L=0.63 at 514.5 nm, pump power=600 mW, probe power = 1.1 mW

Sr. No.	Frequency (Hz)	$\Delta I_{probe}(\Delta)$ (mV)	$I_{probe}(0)$ (mV)	$\frac{\Delta I_{probe}(\Delta)}{I_{probe}(0)}$ %
1	1.3	0.52	33.25	1.54
2	2.0	0.70	33.25	2.10
3	4.0	1.13	33.25	3.40
4	5.0	1.13	33.25	3.40
5	6.0	1.30	33.25	3.91
6	8.0	1.48	33.25	4.45
7	8.8	1.48	33.25	4.45
8	10.0	1.48	31.0	4.77
9	12.0	1.48	31.0	4.77
10	15.0	1.57	31.0	5.06
11	20.0	1.39	31.0	4.48
12	25.0	1.39	31.0	4.48
13	30.0	1.04	31.0	3.35

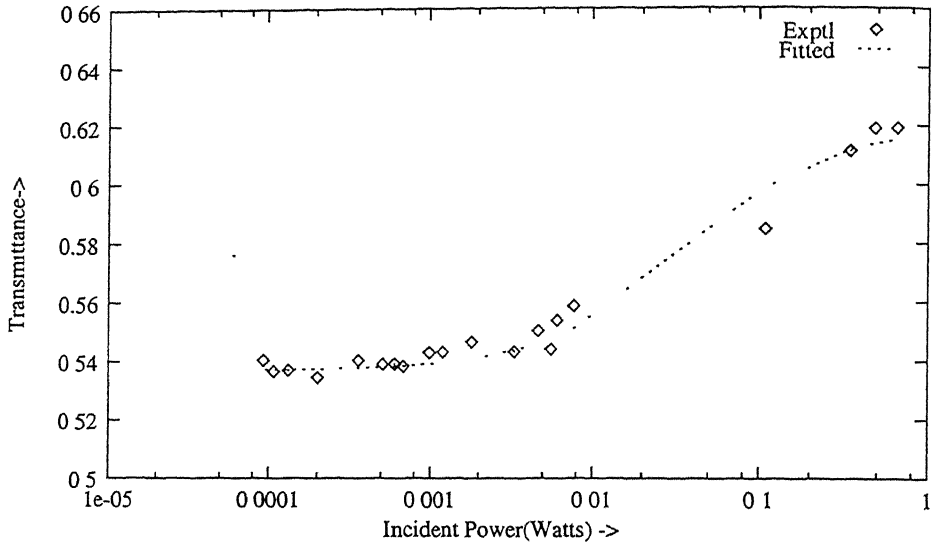

Figure 4.6: Single beam transmission experiment

4.6.1 Transmission Experiments

Single beam transmission measurements were carried out as the beam power was varied from 10 μW to nearly one Watt. For these measurements, the beam was made to fall at the same spot on the sample at which the two beam coupling measurements were carried out. The transmission behaviour of the sample is shown in Fig.4.6. Data was fitted to expression 2.34 obtained for the 4 level model. Equation2.34 is a transcendental equation for which straight forward solutions were not possible. So a numerical approach to obtain the roots of this equation was adopted. This equation basically involves three unknown quantities, namely, the low power absorption constant α_0L, the high power absorption constant β_0L or equivalently $\gamma = \frac{\alpha_0 L}{\beta_0 L}$ and the saturation intensity I_s. These quantities were treated as parameters in an effort to fit the observed transmittance changes with input beam power with those calculated numerically from Eq.2.34 A non-linear least squares fitting algorithm due to Marquardt and Levenberg was used for this purpose. We faced serious convergence difficulties in this fitting when all these quantities were simultaneously parameterized. To get out of this problem, optimum values for α_0 L and γ were directly read from the saturation plots Fig.4.6 and only saturation intensity I_s was initially treated as a parameter in the Marquardt-Levenberg algorithm. With the best value for I_s so obtained, the remaining parameter α_0 L and γ were also optimized in a similar manner. The best values for these parameters are listed in table 4.5. We would like to emphasize the fact that a three level model has been used for beam coupling studies but results of our saturation studies confirm the participation of the fourth level in the basic non-linear process.

Table 4.5: Best fit values for R6G doped BAG from single beam transmission experiments

$\alpha_0 L$	γ	I_s
0.63	1.28	1.58 W/cm^2

4.6.2 Measurement of Film Thickness

It was mentioned earlier that measurement of thickness for the sandwiched film by the standard methods is difficult. We have used the third beam diffraction technique first used by K Divakar Rao[24] to measure the film thickness. In this technique the population grating is induced in the film by two coherent pump beams of equal power which cross each other at a small angle in the non-linear medium. The third beam is the weak probe which is derived from the same laser, from which the pump beams are derived but is made incoherent with the pump beams by introducing a large path difference between the pump and the probe beams. The probe beam is incident normally on the film. Fig.4.7 shows schematically the experimental

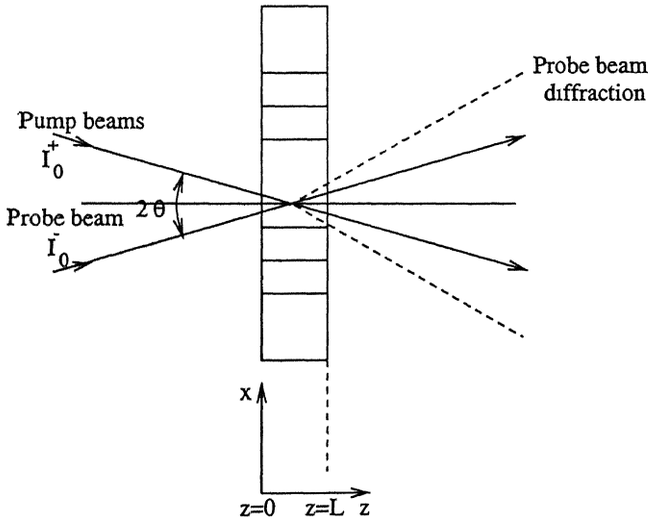

Figure 4.7: Schematic of three beam experiment.

configuration. In this figure, we have not shown the self diffracted beams but the diffraction associated with the third beam are shown. The diffraction efficiency of the third beam was obtained by Divakar

$$\eta_n' = \frac{I_n'(L)}{I_0'}$$

$$= \left|\frac{\omega^2 \chi_{NL} L}{2\beta_n' c^2}\right|^2 \mathrm{sinc}^2\left(\frac{\pi \mathrm{L}}{\mathrm{L_n}}\right) |\mathrm{c_n}|^2 \tag{4.67}$$

where the argument of the Sinc function involved the sample thickness L and the coherent length L_n given by

$$L_n = \frac{2\pi}{\beta_0' - \beta_n'} \tag{4.68}$$

where

$$\beta_n' = \left(\frac{\omega n_0}{c}\right)\left\{1 - (\sin\theta_1 \pm (2n\sin\theta)^2)\right\}^{1/2} \tag{4.69}$$

Here θ_1 is the incidence angle of the probe beam (zero in the present case) and θ is the angle between the pump beams. Equations 4.67 and 4.69 suggest that the diffraction efficiency of the third beam changes with the angle between the pump beam. The efficiency starts from a maximum value for $\theta = 0$ and goes to successive minimum (zero) and maximum values. The first zero in the first order diffraction of the third beam appears for an angle $\theta = \theta_0$ between the pump beams such that L_1=L in equation(4.68) This gives for the sample thickness as

$$L = \frac{2\pi}{\omega n_0/c - (\omega n_0/c)\left\{1 - 4\sin^2\theta_0\right\}^{1/2}} \tag{4.70}$$

Hence for a fixed intensity of the incident beams, varying the angle between the pump beams (keeping probe normal to the film) we can estimate the thickness of the sample. Thus by experimentally determining the angle at which the first order diffraction of the third beam goes to zero (or reaches a minimum value), we have at our disposal a nonlinear technique for measuring the thickness of sandwiched dye-doped films. The first minimum of the third beam diffraction for our sample with $\alpha_0 L = 0.63$ was found at 4.2^0 (Fig 4.8). This gives an estimated thickness of our sample as $35\mu m$. We are still left with three unknown quantities namely, the real and imaginary parts of the refractive index (n_2', n_2'') and the relaxation time T_1. In order to estimate values of some of these quantities, we carried out pump-probe experiments. Transmission coefficient of the probe beam of a fixed power $(470\mu m)$ was measured in the presence of the pump beam of varying power. The experimental result are shown in Fig.4.9. The observed transmission behavior of the probe beam was fitted with Eq.4.71 obtained earlier and reproduced here,

$$\frac{I_0^-(0,L)}{I_0^-(0,0)} = \exp\{\frac{\alpha_0 L}{\cos\theta}\frac{(1+\alpha'/\alpha I_0^+/I_s)}{(1+S_0)}\}\left[\left\{1 + \frac{2\pi n_2' L}{\lambda\cos\theta}\frac{I_0^+/I_s}{(1+S_0)^2}r\right\}^2 + \left\{\frac{2\pi n_2' L}{\lambda\cos\theta}\frac{I_0^+/I_s}{(1+S_0)^2}\right\}^2\right] \tag{4.71}$$

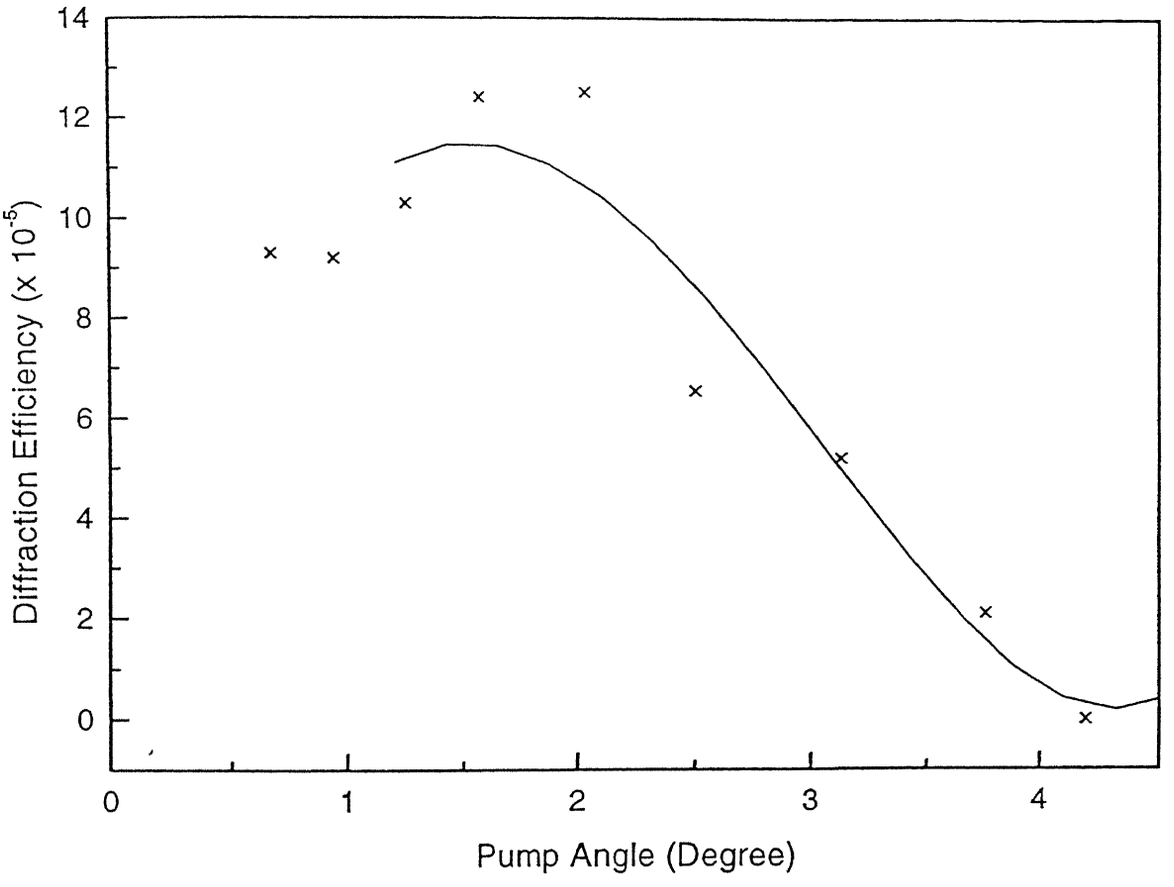

Figure 4.8: Third beam ($\eta = +1$)probe diffraction as a function of angle

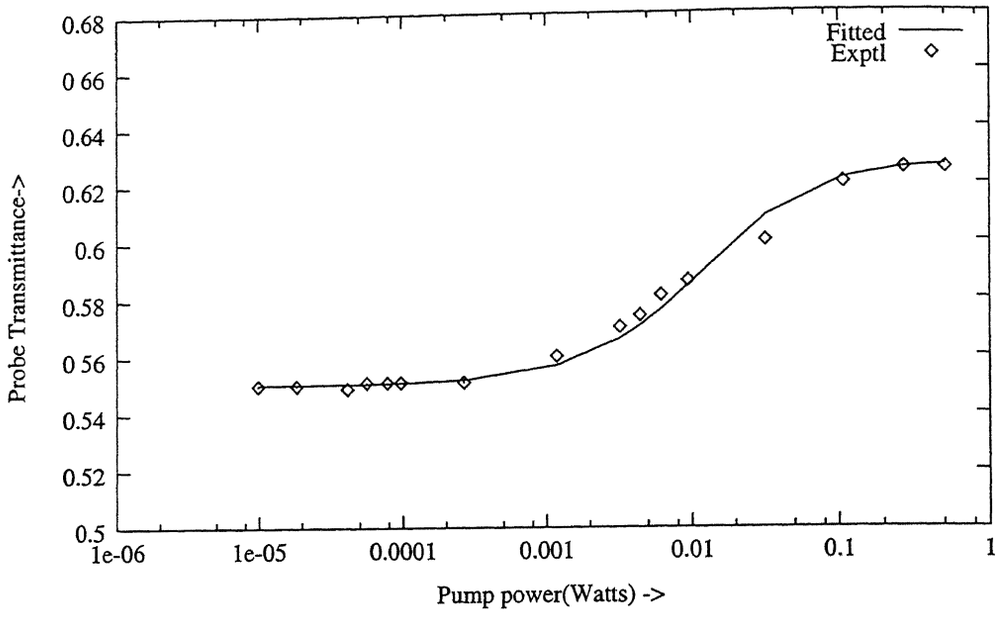

Figure 4.9: Two beam saturation

Here θ is the angle between the pump and the probe beams and $\beta_0/\alpha_0 = 1/\gamma_0$. For this fit, values of $I_s = 1.58\mathrm{W/cm}^2$ and sample thickness L= $35\mu m$ determined earlier were used. however, $\alpha_0 L = 0.60$ in place of 0.63 was used. It is possible that the spot might have shifted slightly in the experiment. It was found that the fitting routine was insensitive to the values of n_2'. Actually the term involving $n_2' L$ makes very little contribution to expression (4.71). As such n_2' remained undetermined in the pump-probe experiment but we found a fitted value of $n_2'' = 5.4 \times 10^{-4}$. Having determined the saturation intensity I_S, the sample thickness L and the imaginary part of the non-linear refractive index (n_2'') from these auxiliary experiment, we now return to two beam coupling measurements. Two beam coupling data of (Table(4.1)to(4.4)) are plotted as a function of the frequency shift of the probe beam at four different powers in Fig.4.10 to 4.13 There is a certain amount of scatter in these measurements. However, the general trends are well established. The two beam signal start from zero value when the pump and probe are degenerate in frequency. The signal then increases as the probe shift frequency increases, it goes through a maximum and then decreases with further increase in the frequency shift. The appearance of peak in the two coupling signal is understandable. It occurs when the inverse of the frequency shift of the probe matches with the relaxation time of the non-linearity in the medium. Fig.(4.15) shows the shift in the peak position with pump power. Such a shift is expected since the degree of saturation changes with the pump power. For a detailed comparison between the experimental and theoretical results of two beam coupling we have fitted the experimental results with expression (1.64), treating the real part (n_2') of

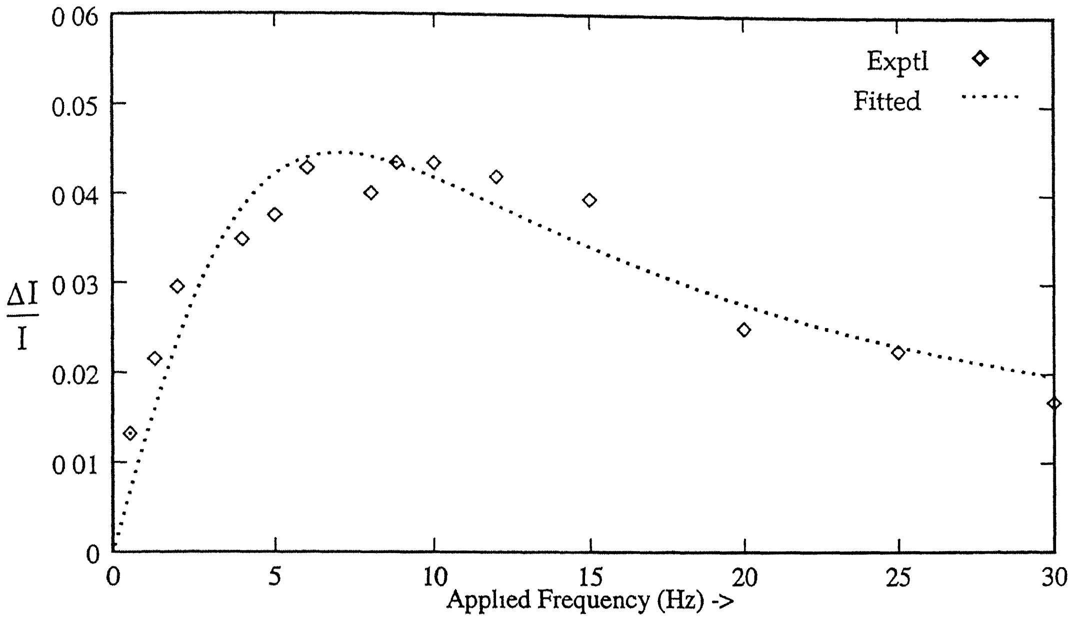

Figure 4.10: Two beam coupling in R6G doped BAG at 514.5 nm as a function of shift in the probe frequency:pump power =73mW,probe power=1.1mW

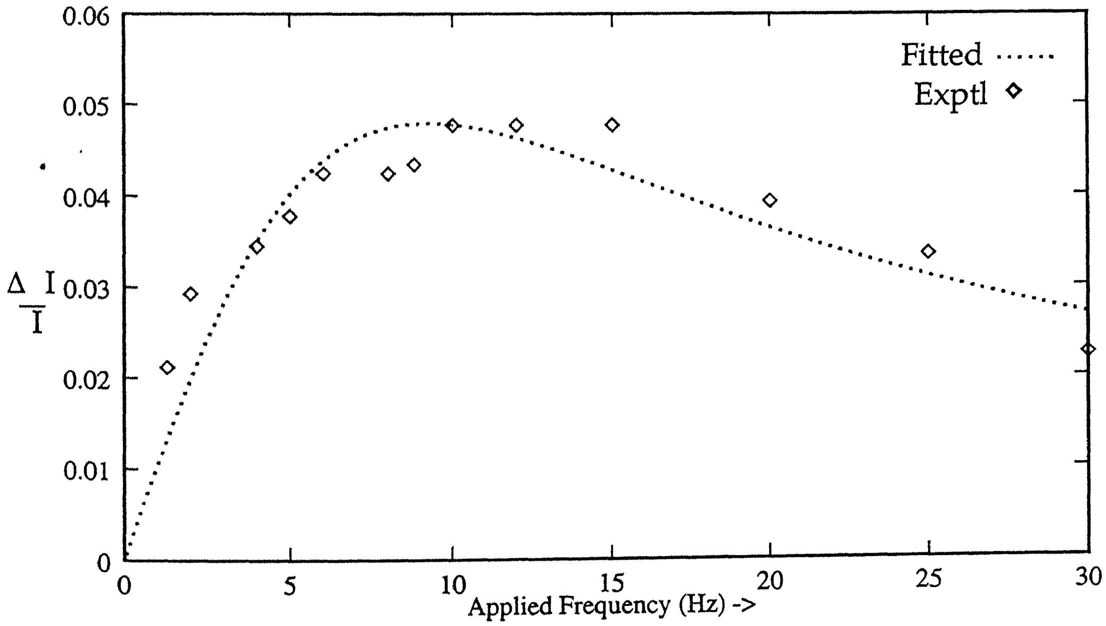

Figure 4.11: Two beam coupling in R6G doped BAG at 514.5 nm as a function of shift in the probe frequency :pump power=195mW, probe power=1.1mW

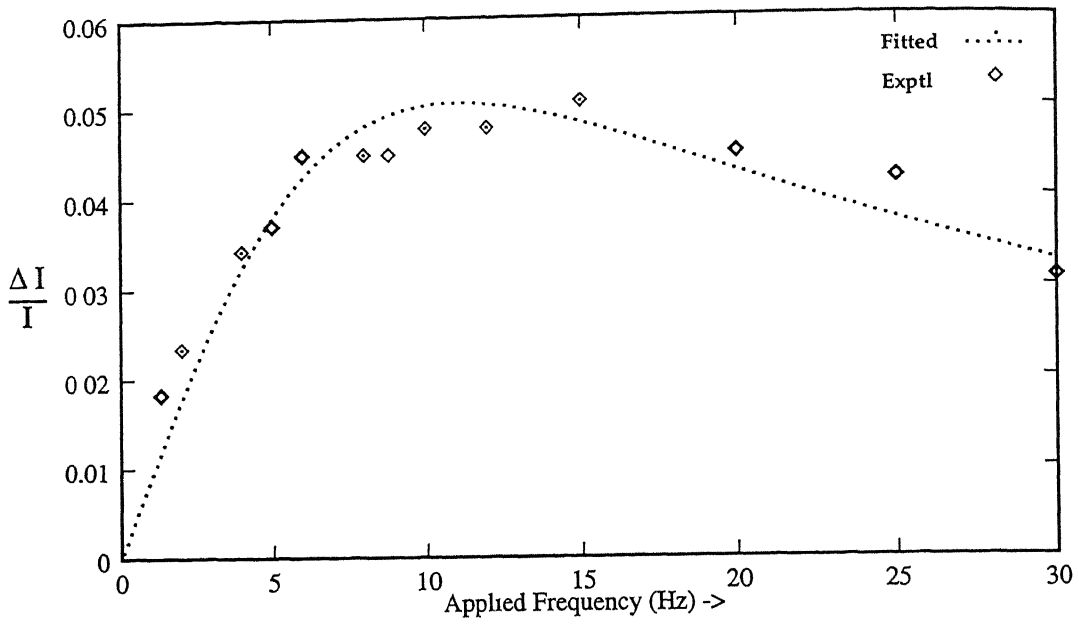

Figure 4.12: Two beam coupling in R6G doped BAG at 514.5 nm as a function of shift in the probe frequency:pump power=380mW,probe power=1.1mW

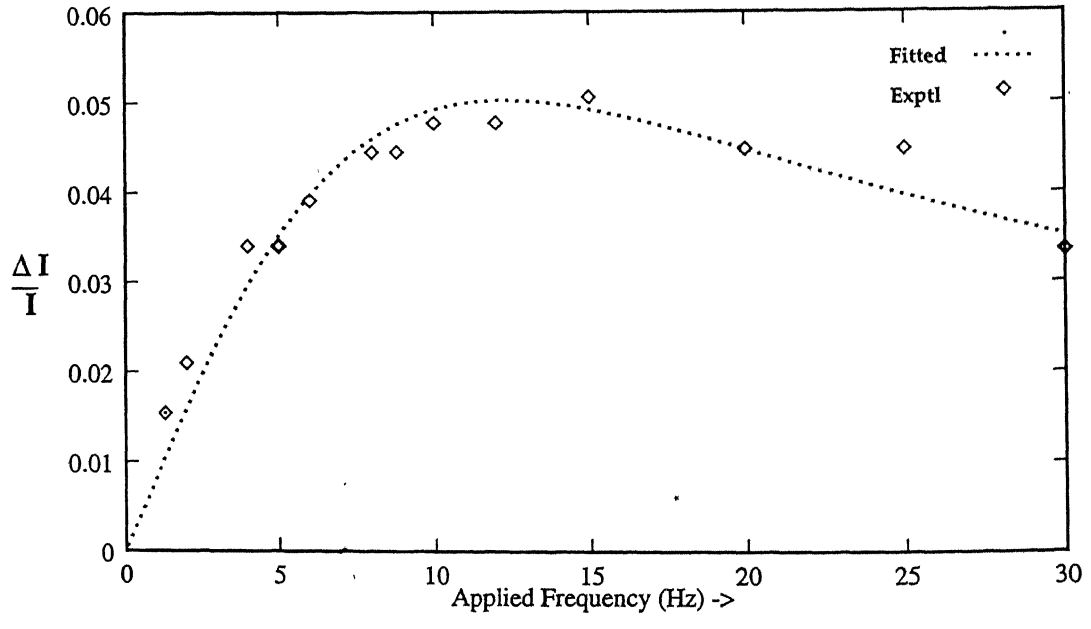

Figure 4.13: Two beam coupling in R6G doped BAG at 514.5 nm as a function of shift in the probe frequency:pump power=600mW,probe power=1.1mW

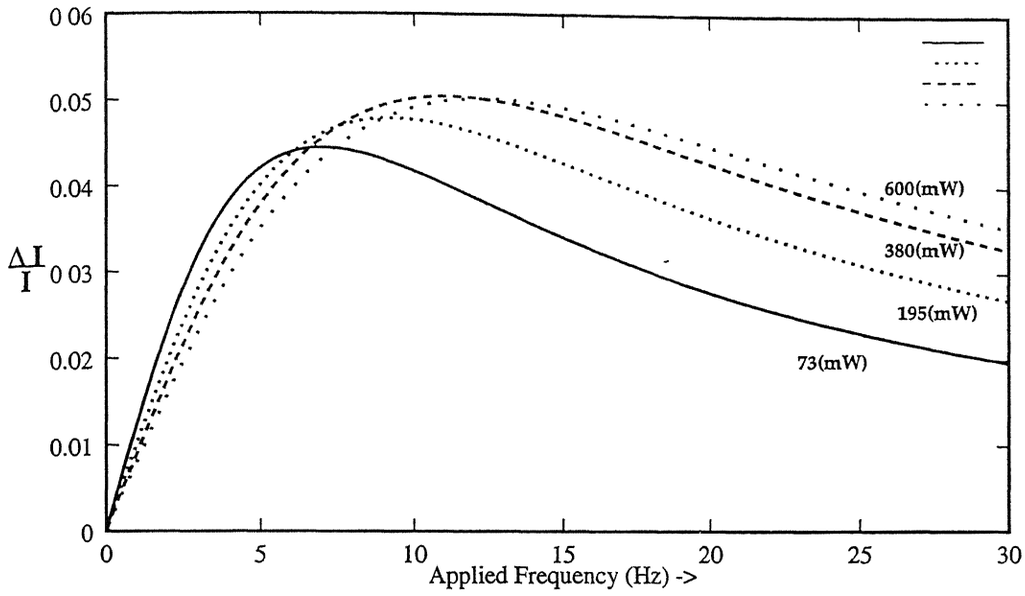

Figure 4.14: Two beam coupling signal in R6G doped BAG at 514.5 nm as a function of shift in probe frequency at different pump powers, probe power=1.1mW (only fitted plots from the previous figures are shown)

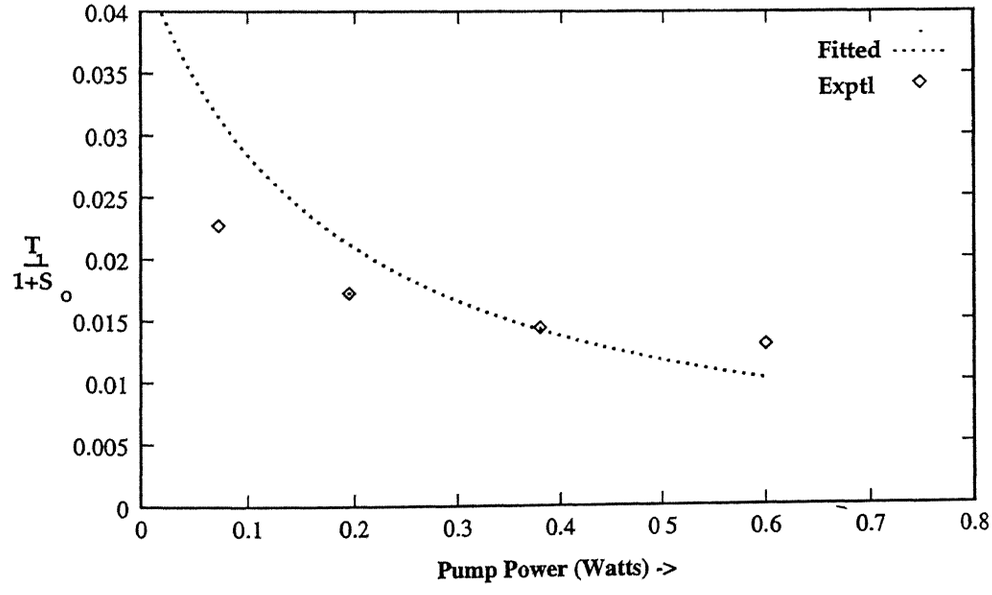

Figure 4.15: Best fit of T_1=36msecs obtained by fitting $T_1/(1+S_0)$ vs I_0.

the non-linear refractive index and the effective relaxation time $T_1' = T_1/(1 + I/I_S)$ as two parameters using Marquardt-Levenberg algorithm. It was possible to get excellent convergence in these fits We could start with widely different values of n_2' and T_2', but they always converged to the same set for measurements at a given power The best values obtained from the real part of the refractive index n_2' by fitting data of different pump powers were very nearly the same. However, there was large dispersion in the values of the effective relaxation time T_1' The best values for the calculated relaxation time T_1 with the known values of I_S are plotted in Fig.4.15 We see a systematic variation in the relaxation time from 32 to 56 msec. At this stage we are not certain whether this variation in the relaxation time T_1 with pump power is genuine or is due to the presence of substantial scatter in the experimental results or due to some other experimental uncertainties. In view of these uncertainties, we preferred to optimize n_2' and T_1' using data for all powers. This gives the optimum values of $n_2' = 1.1 \times 10^{-4}$ and $T_1 = 36msec.$

4.7 Conclusion

We have studied two beam coupling in sandwiched films of R6G doped boric acid glass by Doppler shifting the probe beam frequency with a peizo mirror. No beam coupling occurs in the absence of the Doppler shift. There is some scatter in the experimental results but the general trends of the two beam coupling process are well established. We have used the three level model, first described by Zilio in the context of two beam coupling to interpret the experimental results. Some of the assumptions made by Zilio*et.al.* have been relaxed. In the absence of ab-initio estimates of some of the physical quantities such as the non-linear susceptibility and the saturation intensity, the theoretical model could be tested by parameterizing these unknown quantities. Efforts have been made to determine best estimates of these parameters using a number of experimental considerations. Within these limitations, we find the theoretical model was reasonably adequate in describing two beam coupling process in saturable absorbers. In the process, we have been able to obtain optimum values for the magnitudes of the real and imaginary parts of the non-linear refractive index and the relaxation time T_1. This was not quite possible in earlier work because of bimolar quenching and to a relatively poor signal to noise ratio in the earlier works.

We however like to state in conclusion that there is a clear indication in our experimental results that the 4^{th} level (T_2) is actively involved in the non-linear process in these samples. It will be worthwhile to develop a theoretical model for two beam coupling in saturable absorbers based on four participating levels.

References

[1] R W.Boyd *Nonlinear Optics ,Academic Press, San Diego,*(1992).

[2] Y. R. Shen, *The Principles of Nonlinear Optics, John Wiley, New York,*(1984). Mark A. Kramer, W.R.Tompkin, R.W.Boyd *Phys Rev A*,**34**,(1986), 2026.

[3] Mark. A. Kramer, W.R.Tompkin, R.W.Boyd *Phys Rev A*,**34**,(1986), 2026.

[4] W.R.Tompkin,R.W.Boyd, D.M.Hall, P.A.Tick *et.al.*, *J.O.S.A B*, **4(6)**,(1987),1030

[5] H.Fujiwara, K.Shio, S Miyanaga, *J.O.S.A.B*, **8**,(1991), 1740.

[6] H.Fujiwara, K.Shio, S.Miyanaga, K.Nakaguchi *Jap. J. App.Phy.*, **29(7)**,(1990), L1235.

[7] S.A.Boothroyd, J.Chrostowskii, M.S.O'Sullivan,*Optics Letters*, **14(17)**,(1984), 946

[8] S.C.Zilio, J.C.Penforte, F.A.Gouveia, M.J.V.Bell,*Optics Communication*,**86**,(1991), 81.

[9] S.A.Boothroyd, J.Chrostowskii, M.S.O'Sullivan,*J.O.S.A.B*, **6(4)**,(1989),760.

[10] R.Saxena, I.McMicheal, P.Yeh *Appl. Phys B.*,**51**,(1996),243.

[11] Y.Silberberg, Isarel Bar-Joseph, *J.O.S.A.B*,**1(4)**,(1984),662.

[12] I.McMicheal, P.Yeh, P.Beckwith, *Optics Letters*,**13(6)**,(1988),

[13] Andrei.G.Skirtach, D.J.Simkin,S.A.Boothroyd, *J.O.S.A.B*,**13(3)**,(1996),546.

[14] I.McMichel, R.Saxena, T.Y.Cheng,Q.Shu, S.Rand,J Chen,H.Tuller, *Optics Letters*,**19(19)**,(1994), 1511.

[15] Andrei.G.Skirtach, D.J.Simkin,S.A.Boothroyd, *J.O.S.A.B*,**13(10)**,(1996),2164.

[16] V.L.Vinetskiii, N.Kukhtarev, S,G,Odulev, M.S.Soshkin, *Sov. Phy. Usp*,**22(9)**,(1979), 742

[17] Pochi Yeh *I.E.E.E J of Quantum Electronics*,**25(3)**,(1989),484.

[18] Aviad Peda'el, Ron Daisy, M.Horowitz, B,Fischer, *Optics Letters*,**23(15)**,(1998), 1173

[19] Pochi Yeh, *J.O.S.A.B*,**3(5)**,(1986),747

[20] H.Zhou,Xin Mi, Qian Jiang, Ruihua Zhang, Peixian Ye, *Opt. Communication*,**78** ,(1990),382.

[21] J.Freinberg, D.Heiman,A.R.Tanguay,Jr., R.W.Hellwarth*J. Appl. Phys.* ,**51** ,(1980),1297.

[22] H.L.Fragnito, S.F.Pereira, A.Kiel*J.O.S.A.B*,**4** ,(1987), 1309.

[23] D.Grandelement, G.Grynberg and M.Pinard *Phys. Rev. Lett*,**59**,(1987),40.

[24] K.Divakara Rao *Ph.D Thesis, I.I.T.Kanpur*,(1992)

Chapter 5

Nearly Degenerate Four Wave Mixing in Dye Doped Solids

We begin this chapter with a brief introduction to the nearly degenerate four wave mixing (NDFWM) process and its applications to high resolution spectroscopy of gases and solids. This will be followed by a discussion on the density matrix formulations of the NDFWM processes developed by S.C.Rand *et. al.*[1] in the context of a three level model. We shall then describe the experiments used in the present study to record the optical phase conjugation signal under conditions of nearly degenerate four wave mixing. We shall then present our results on Rhodamine 6G and Fluorescein doped boric acid glass films.

5.1 Introduction

The subject of optical phase conjugation using degenerate four wave mixing (DFWM) approach has been investigated in great depth both for its application potential to real-time holography, information processing and storage as well as for the basic understanding of the non-linear process[2–4]. In the DFWM configuration, a weak probe beam traverses a non-linear medium in the presence of two relatively strong counter-propagating pump beams. The probe and the pump beams are derived from the same laser and have the same frequency. The medium generates the fourth beam at the same optical frequency which counter-propagates the probe beam with spatial phase, which is exact conjugate of the spatial phase of the probe beam. There is exact energy and and momentum phase-matching in this process. However, there are situations where the probe beam frequency may differ somewhat from the pump beam frequency. The probe beam may have been derived from a laser different from the one used to obtain the pump beams, or the three beams may be derived from the same laser but the probe beam is

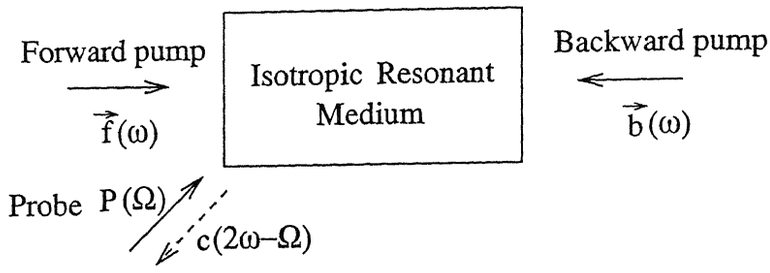

Figure 5.1: Geometry for Nearly Degenerate Four-Wave Mixing

somewhat frequency shifted with respect to the pump beams. In the later case, the shift could be the Doppler shift experienced by a moving receiver or the transmitter system or when the gain-bandwidth of an external resonator differs from that of this phase conjugate mirror or if the laser system drifts in frequency during operation. These practical situations require us to obtain the frequency response of the phase conjugation when the frequency of the probe beam differs from the frequency of the pump beams. This is the non-degenerate four wave mixing (NDFWM) process We shall examine optical phase conjugation when the frequency shift of the probe beam is rather small. This is sometimes called as nearly degenerate four wave mixing (NDFWM) process. It provides a convenient method to investigate non-linear optical processes including spectroscopic ones also. In the frequency domain the phase conjugated signal under NDFWM condition has the frequency response of a narrow-band optical filter.

The interaction process in the nearly degenerate four wave mixing is shown in Fig.5.1 The counter-propagating pump beams at $\omega = \omega_0 + \Delta$ are detuned from the atomic resonance at ω_0 , Δ is the extent of detuning The probe beam with frequency $\Omega = \omega + \delta$ is detuned by δ from the pump beam frequency ω. The interference between the forward pump $\vec{\varepsilon_f}$ and the detuned probe $\vec{\varepsilon_p}$ produces a moving interference pattern. As a result, the medium experiences a traveling wave excitation which propagates in the $\vec{k_p} - \vec{k_f}$ direction with the phase velocity $(\omega - \delta)/|\vec{k_b} - \vec{k_f}|$. Interaction of this traveling wave with the medium generates an induced grating which is also moving but lags behind the exciting traveling wave because of the finite response time of the medium. The induced grating represents the spatial modulation of excited species. The scattering of the backward pump wave $\vec{\varepsilon_b}$ from the moving population grating gives rise to the phase conjugate wave of frequency $\omega - \delta$ and propagates in a direction opposite to the direction of the probe beam. In this process the energy conservation is exact and the momentum mismatch given by $2\delta/c$ is vanishingly small for the range of δ covered in these experiments.

In a similar manner, the backward pump wave $\vec{\varepsilon_b}$ and the input probe wave $\vec{\varepsilon_p}$ generate a traveling wave excitation with frequency $\omega - \delta$ and phase velocity $(\omega - \delta)/|\vec{k_b} - \vec{k_p}|$. The direction of this traveling wave excitation is given by $\vec{k_p} - \vec{k_b}$. The scattering of the forward

$\vec{\varepsilon_f}$ pump from the traveling wave excitation also generates the phase conjugate wave which propagates in the same direction as the one generated by the scattering of the backward pump. The efficiency of the generation of the phase conjugate wave is determined in part by the amount of phase mismatch that arises in the four wave mixing process. If counterpropagating geometry is maintained for the pump waves, the $\vec{k}$ vector mismatch is given by

$$\begin{aligned} \Delta\vec{k} &= \vec{k_f} + \vec{k_b} + \vec{k_p} + \vec{k_c} && (5.1) \\ &= \vec{k_p} + \vec{k_c} && (5.2) \\ &\neq 0 && (5.3) \end{aligned}$$

The mismatch occurs because the frequency of the probe wave differs from that of the generated conjugate wave. As a result the magnitude of $\vec{k_p}$ and $\vec{k_c}$ are somewhat unequal although their direction are exactly opposite. One defines the coherence length L_c as,

$$L_c = \frac{\pi}{|\Delta k|}. \tag{5.4}$$

If the interaction length L in the medium exceeds the coherence length L_c, the generation of the phase conjugate signal becomes rather inefficient.

The frequency dependence of the phase conjugate reflectivity defined as $R = |\varepsilon_c|^2/|\varepsilon_p|^2$ is a function of the difference between the pump and the probe frequencies for the two level homogeneously broadened system. This can be understood from the following argument. The build-up of the phase conjugate signal in a stationary two-level system as a function of $\omega - \Omega$ is determined by the energy relaxation rate $1/T_1$. For $\omega = \Omega$ a standing wave excitation is generated. This will lead to a distribution of excited atomic species which is spatially stationary. As Ω is tuned away from ω, the standing wave changes to a traveling wave. The time for the traveling wave to move through a spatial period is given by $(\omega - \Omega)^{-1}$. This time needs to be compared with the finite lifetime T_1 of the upper level. For $(\omega - \Omega)$ much greater than $1/T_1$, the atomic excitation cannot be sustained and the spatial modulation is washed out, driving the reflectivity to zero. Thus only for the pump-probe detuning of less than $1/T_1$, will the reflectivity remain appreciable. We shall now discuss the application of NDFWM to spectroscopy.

The NDFWM has been used by Raj *et.al.*[5] to study the lineshapes of atomic and molecular system. They took advantage of the fact that in the collinear geometry two conjugate waves at frequencies $\omega+\delta$ and $\omega-\delta$ are generated inside the nonlinear medium if the counterpropagating pump waves oscillate at frequency ω and the collinear probe at frequency $\omega + \delta$. Then the interference of these phase conjugate waves with co-propagating pump beams yields beat signal at δ. The increased sensitivity of high frequency optically heterodyned signal permitted them

to record Doppler-free signal at I_2. Subsequently, using phase-sensitive detection Raj *et.al.* were able to achieve shot-noise limited detection for the hydrogen Balmer line under similar experimental conditions, surpassing (in sensitivity) all other nonlinear spectroscopic techniques available at that time(Bloch *et.al.*[6]).

MacDonald *et.al.*[7] using optical waves of slightly different frequencies showed that the efficiency of four wave mixing in photorefractive materials can be enhanced. Andrei *et.al.*[10] took the cue from the study of the influence of the ratio of beam intensities on the energy transfer in the photorefractive media They investigated the influence of energy transfer by two-wave mixing in a nonlinear absorptive Kerr medium on the four wave mixing phase conjugate signal. For a fixed ratio of intensities of pump beams and a detuned probe beam they obtained a narrow band optical filter like frequency response of the conjugate signal which can be tuned by changing the ratio of the incident beam intensities.

In an earlier study, Duncan G Steel *et.al.*[8] and S.C.Rand[1] using the NDFWM technique obtained for the first time a direct measurement of the ground state relaxation rate of the optically excited Cr^{3+} ions in $Cr : YAlO_3$. In their experiment the two counterpropagating pump beams and the frequency shifted probe beam were obtained from the same laser and this completely removed the influence of the laser jitter in the measured line-width. We consider their scheme in some detail in the the next section because it resembles closely our approach to the study of NDFWM in dye doped films of boric acid glass.

5.2 NDFWM in a Three level system

Steel and Rand[8] and Rand[1] developed a theoretical model for the optical phase conjugation reflectivity, applicable to a three level system when the probe beam is somewhat detuned from the pump beam (NDFWM). Fig.5.2 describes the three level systems.

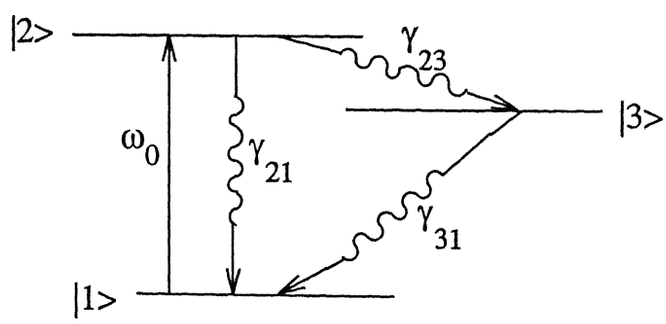

Figure 5.2: Three level system, γ_{ij} are relaxation rates where i,j=1,2,3

Levels $|1\rangle$ and $|2\rangle$ have the same multiplicity so that the $|1\rangle$ to $|2\rangle$ transition is spin-

allowed Levels $|3\rangle$, on the other hand possesses different multiplicity and is therefore long-lived Consequently the condition $\gamma_{31} \ll \gamma_{21}$ is satisfied. Further it is assumed that the inter-system crossing ($|2\rangle - |3\rangle$) is efficient so that $\gamma_{31} \ll \gamma_{23}$ also holds. The evolution of this system when the pump and the probe beams are in near resonances with the $|1\rangle$ to $|2\rangle$ transition can be described by the equation of motion of the density matrix,

$$\imath\hbar\frac{d}{dt}\rho = [H_0, \rho] + [V, \rho] + i\hbar\frac{d}{dt}\rho|_{decay} \tag{5.5}$$

Here, H_0 is the atomic Hamiltonian with eigen state $|1\rangle$, $|2\rangle$, and $|3\rangle$; V is the light matter interaction Hamiltonian. The decay term includes all possible decay processes including the dephasing of the off-diagonal terms. In the perturbation approach adopted by Rand[1], the light matter interaction Hamiltonian in the zeroth order includes contributions from the pump waves only. The probe and the conjugate waves are assumed weak and contribute in higher orders.

Thus the zero-order optical interaction Hamiltonian with equal amplitude for the counter-propagating pump beams can be expressed as

$$V^{(0)} = -\frac{1}{2}\mu_{12}E_0(e^{\imath kz} + e^{-\imath kz})e^{-\imath\omega t} + c.c. \tag{5.6}$$

while the first order term contains only the probe and the signal waves

$$V^{(1)} = -\left[\frac{1}{2}\mu_{12}E_1 e^{i(k_1 z - \omega_1 t)} + \frac{1}{2}\mu_{12}E_2 e^{-\imath(k_2 z + \omega_2 t)}\right] + c.c. \tag{5.7}$$

The probe wave is asssumed to have frequency $\omega_1 = \omega + \delta$ and the signal wave will then have frequency $\omega - \delta$. We further write

$$\begin{aligned} \rho &= \rho^{(0)} + \lambda\rho^{(1)} \\ V &= V^{(0)} + \lambda V^{(1)} \end{aligned} \tag{5.8}$$

where λ is a perturbation series parameter. This leads to

$$i\hbar\frac{d}{dt}\rho^{(0)} = [H, \rho^{(0)}] + [V^{(0)}, \rho^{(0)}] + i\hbar\frac{d}{dt}\rho^{(0)}|_{decay} \tag{5.9}$$

$$i\hbar\frac{d}{dt}\rho^{(1)} = [H, \rho^{(1)}] + [V^{(1)}, \rho^{(0)}] + [V^{(0)}, \rho^{(1)}] + i\hbar\frac{d}{dt}\rho^{(1)}|_{decay} \tag{5.10}$$

with

$$\begin{aligned} V_{21}^{(0)} &= -\hbar\Omega_{21}(e^{\imath kz} + e^{-\imath kz})e^{\imath\omega t} + c.c. \\ V_{21}^{(1)} &= -\hbar\Omega_{21}(\epsilon_1 e^{-\imath(k_1 z+\omega_1 t)} + \epsilon_2 e^{\imath(k_2 z-\omega_2 t)}) + c.c \end{aligned} \tag{5.11}$$

where $\epsilon_1 = E_1/E_0$; $\epsilon_2 = E_2/E_0$; and $\omega_{21} = \mu_{21}E_0/2\hbar$.

Following by Rand[1] the first order solution for the off diagonal matrix elements can be written as

$$\rho_{21}^1 = -\frac{\imath N\Omega_{21}|\Omega_{21}|^2}{1+I'}(e^{\imath kz} + e^{-\imath kz})^2 L_2 L_3 \times \left(2 + \frac{\gamma_{23}}{\gamma_{31} - i\delta}\right)\varepsilon^* e^{-\imath(k_1 z+\omega_2 t)}(L + L_1^*) \tag{5.12}$$

where

$$\begin{aligned} \Delta &= \omega_j - \omega_0; j = 1,2,3 \\ L &= (\Gamma_{21} - i\Delta)^{-1} \\ L_1 &= (\Gamma_{21} - i\Delta - \imath\delta)^{-1} \\ L_2 &= (\Gamma_{21} - \imath\Delta + i\delta)^{-1} \\ L_3 &= \left(\gamma_2 + \frac{\gamma_2\gamma_{31}}{2\gamma_{31}+\gamma_{23}}\left(2 + \frac{\gamma_{23}}{\gamma_{31} - i\delta}\right) I' + i\delta\right)^{-1} \end{aligned} \tag{5.13}$$

and

$$\begin{aligned} I' &= \frac{2|\Omega_{21}|^2(2\gamma_{31}+\gamma_{23})}{\gamma_2\gamma_{31}}(1 - cos(2kz))(L + L_1^*) \\ &= 2(1 + cos(2kz))\frac{I}{I_{sat}} \\ \Gamma_{21} &= (\gamma_{21} + \gamma_{23})/2 \\ &= \gamma_2/2 \end{aligned} \tag{5.14}$$

Medium polarization can be expressed in terms of the matrix elements ρ_{21}

$$P = Tr(\mu\rho) \tag{5.15}$$

The saturation behaviour of the microscopic polarization is contained in L_3. Its magnitude squared varies as

$$|L_3|^2 = \left(\frac{1}{\gamma_{31}^2 + \delta^2}\right)\gamma_2^2\left(\gamma_{31}^2[1 + I']^2 + \delta^2\right) \tag{5.16}$$

where $\gamma_2 \gg \gamma_{31}, \delta$ is assumed.

The non-linear polarization(5.15) can be used as the source with wave equation. Rand *et.al* concluded for optically thin samples under conditions specified above ($\gamma_{21}, \gamma_{23} \gg \gamma_{31}, \delta$) the NDFWM signal has the proportionality,

$$I_{sig} \propto \left(\gamma_{31}^2[1 + \frac{4I}{I_{sat}}]^2 + \delta^2\right)^{-1} \tag{5.17}$$

for homogeneous broadened line For inhomogeneous 3-level systems, an additional integration of $\rho_{21}^{(1)}$ over the frequency distribution of the absorption line is necessary It gives

$$I_{sig} \propto \left(\gamma_{31}^2[1 + \frac{4I}{I_{sat}}] + \delta^2\right)^{-1} \tag{5.18}$$

at low intensities.

Eqns(5.17 and 5.18) represent power broadened Lorentzian profiles. When the pump intensity approaches the saturation value, we obtain intensity dependent line-widths. In the homogeneous case it's determined by (Eq.5.17) and for the inhomogeneous case by(Eq.5.18).

Before we end this section, we would like to give a very important detail of the derivations of the results given in Eqn(5.17, 5.18). These results involve the resonant Lorentzian which actually appears for the first time in the ground state population term - actually in the second order contribution to $\rho_{11}^{(2)}$. This implies that the NDFWM signal is caused by changes in the population of the ground state. Several terms contribute to this population change. One such term corresponds to the re-population of the ground through transition (radiative and non-radiative) from level 3 to level 1 (Fig.5.2). There can be many other contributions. But if the dominant contributions comes via repopulation from the decay of level 3, then the frequency response of the NDFWM signal(a measurement in the frequency domain) can complement the time domain measurement of the decay of level 3. However it must be emphasised that the NDFWM has the potential to investigate population kinetics of the ground state.

We now use this technique to study NDFWM in R6G and Fluorescein doped BAG thin films.

5.3 Experimental Setup

Fig.5.3 shows the experimental setup used to carry out the NDFWM experiments. The configuration is similar to the one used for the optical phase conjugation studies in the backward degenerate four wave mixing geometry. The laser beam obtained from the Coherent I-70 Argon ion laser is split by a 90:10 beam splitter BS_1. The 90% transmitted beam from BS_1 is further

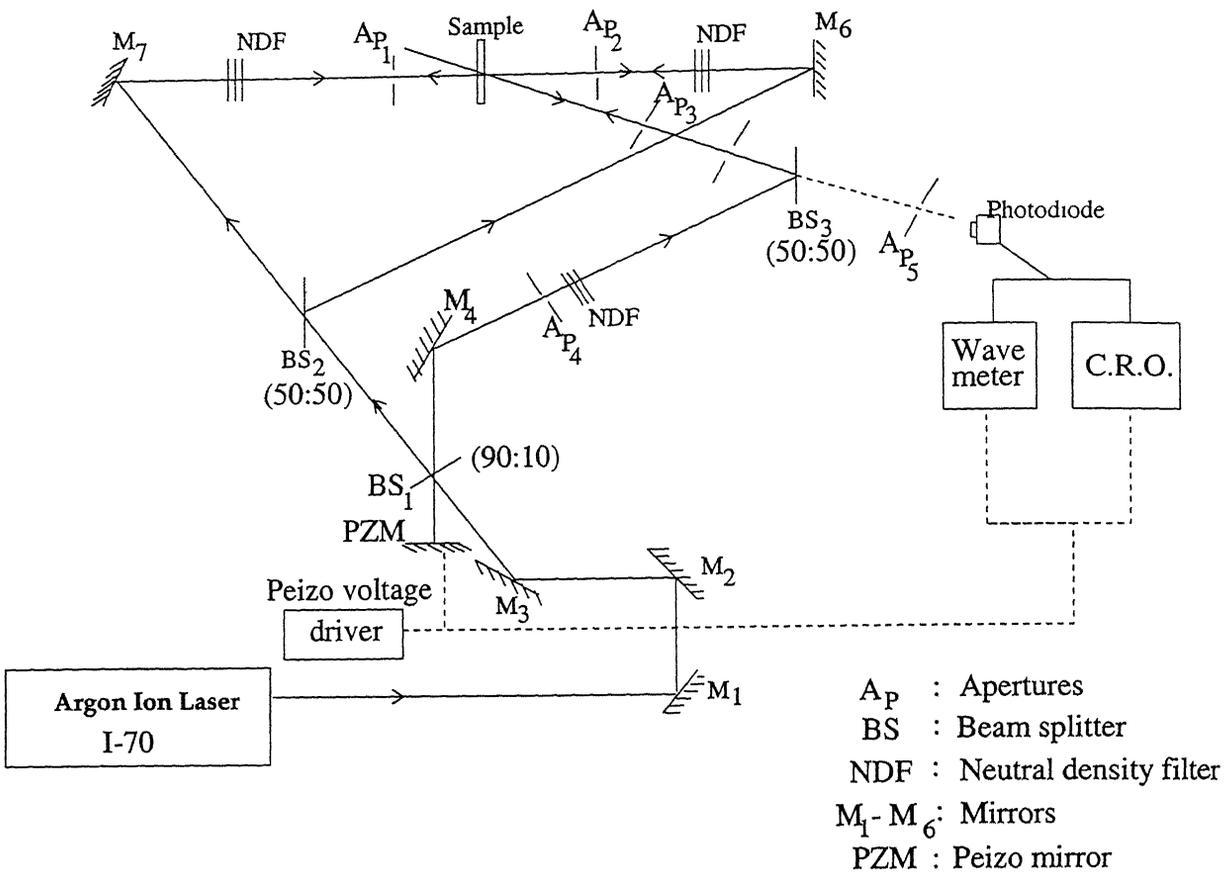

Figure 5.3: Experimental setup for OPC measurements under NDFWM conditions

split by the 50:50 beam-splitter BS_2. These split beams constitute the counterpropagating pump beams of nearly equal intensities. The 10% reflected beam is frequency shifted by reflecting it normally (to avoid any angular dependence on the frequency shift induced by the moving peizo -mirror) off the peizo-mirror (PZM). This beam steered by the guiding mirrors is made to fall on the sample after reflection from the beam-splitter BS_3. This is the probe beam. The beam-splitter BS_3 is primarily used to allow the separation of the phase conjugate wave which counter-propagates the probe beam.

The phase conjugated wave collected far from the table is focussed on to the Si-2386K photodiode and the signal recorded on the wave-meter. The peizo-mirror is driven by the same voltage driver as used for the two-beam coupling experiment. The triangular ramp voltage used to drive the peizo-mirror is adjusted to give a $\lambda/2$ one way excursion to the peizo mirror. The entire experiment is performed on the NRC vibration-isolation table. Two samples (with Rhodamine 6G and Fluorescein doping) were used for these experiments. The Rhodamine 6G doped boric acid glass film had 10^{-4} M concentration with $\alpha_0 L$ of 0.27 at 514.5 nm. The backward and the forward pump powers used for this sample were 202 mW and 210 mW

respectively and the probe was kept at 8.95 mW with beam spot size of 3.8mm at the sample. The beam powers were measured with NRC 815 Digital powermeter. Fluorescein doped sample had 10^{-3} M concentration with $\alpha_0 l$ of 0.6 at 488.0nm. The backward pump power used in this case was 31.7 mW and the forward pump power was 31.3 mW with probe power of 1.97 mW.

5.4 Results and Discussions

Figures5.4 and 5.5 depict typical recordings of the optical phase conjugated signal under conditions of NDFWM for Rhodamine 6G and Fluorescein doped boric acid glass samples respectively. The triangular voltage waveforms used for driving the peizo-mirror are also shown in these figures. As expected the phase conjugated signal has the maximum value under DFWM conditions (zero frequency shift of the probe beam). The OPC signal decreases with increasing frequency shift of the probe beam. We notice some ringing effects in the recordings. Because of the triangular nature of the voltage waveform, the probe beam experiences an up-shift in frequency when the peizo-mirror moves into the probe-beam and a down-shift during the reverse motion of the peizo-mirror. Before we discuss our results it may help to make some qualitative observations as to what do we expect from these measurements. The peizo mirror has certain amount of inertia as a result the peizo mirror will not go through zero velocity in a smooth manner at the turning points of its motion. If it did acquire zero velocity at the turning points, the situation would be more or less the same as for DFWM and the OPC signal should recover its maximum value. But this does not quite happen as for all traces given here and those not given here, the maximum of signal under NDFWM is always less than that for the degenerate case. It may be further argued that even if the mirror did come to rest at at the turning point, the OPC signal may not get restored to the degenerate case because the medium non-linearity does not build up instantaneously but has a certain response time. It is a bit intriguing to note that not in all cases, the maximum signal is at or close to the cross-over points. For the intermediate range of frequencies (Fig.5.4b &c and Fig.5.5b&c), it is very nearly true but not quite so for the recording at the lowest frequencies (Fig.5.4a and Fig.5.5) reported here. We are not exactly sure of the reasons for this departure from the expected results. Further, we expect the peizo-mirror would acquire the steady (and maximum) velocity somewhere in the middle of its swing in either direction. We therefore expect the least values for the OPC signal somewhere near the middle of the linear portions of the triangular waveforms. Once again this nearly holds for the intermediate range of frequencies (Fig.5.4b&c and Fig.5.5b&c), but not for (Fig.5.4a and Fig.5.5a). Once again we fail to see the reasons for this observation. Perhaps this is some experimental artifact which shows up at very low frequencies. Further, one would expect equal degradation of the OPC signal in the two halves of the triangular waveform. Consequently the

maximum and the minimum OPC signals in the two halves of the waveforms should be equal i.e. the maximum signal in the one way swing should equal the maximum signal in the reverse swing and a similar result is expected for minimum signals in the two halves of the swing. Although this holds in some cases but does not hold in all cases.. There is a certain amount of asymmetry in the signal in the two halves. A similar asymmetry has been observed when these experiments are performed in Kerr media. Andrei *et.al.*[10] have correlated the asymmetry to the unequal ratio of the pump intensities. We are not exactly sure if this explanation holds in the present case where the origin of non-linearity is saturation of absorption. Another notable feature in the present work and also found in earlier works[8, 1], is an almost complete absence of noise in the OPC signal for the full range of frequency shifts of the probe beam. Even when the reflectivity goes to zero, at large values of the frequency shift there is hardly any accompanying noise. This is in marked contrast to the two beam coupling experiments where the signal is overwhelmed with noise and it is difficult to extract signal out of the noise. The OPC signal is free from laser jitter because all interfering beams are derived from a single laser. A small amount of noise can be noticed in the OPC signal recorded with 0.04 Hz shift in the probe frequency. But no noise is seen at larger values of the probe frequency shift.

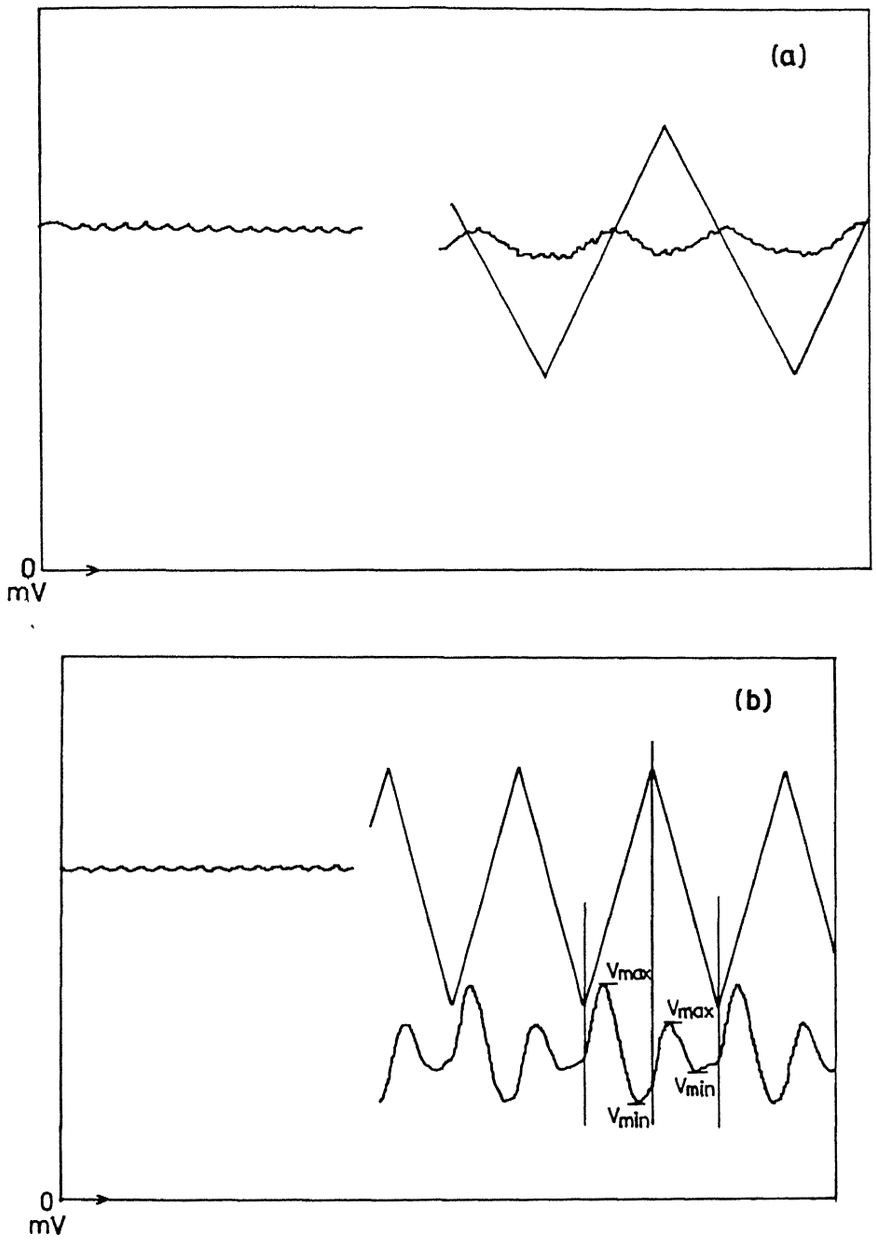

Figure 5.4: (a,b,c,d) OPC signal from Rh6G doped boric acid glass film recorded under nearly degenerate four wave mixing conditions a:δ=0.08Hz, b:δ=14Hz, c:δ=45Hz, d:δ=190Hz The triangular voltage waveforms used to drive the peizo-mirror are also shown. All voltages are measured from zero baseline

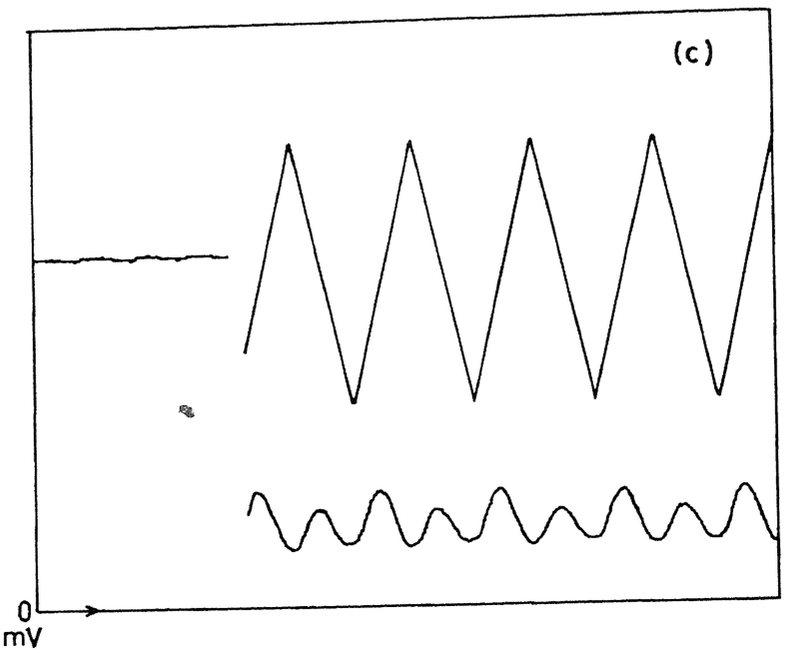
(c)
0
mV

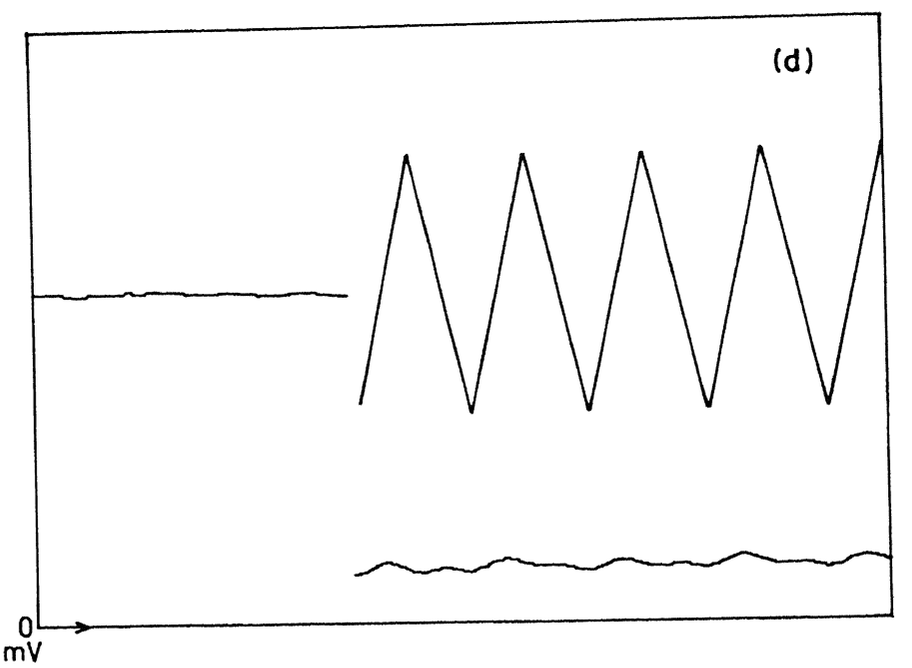
(d)
0
mV

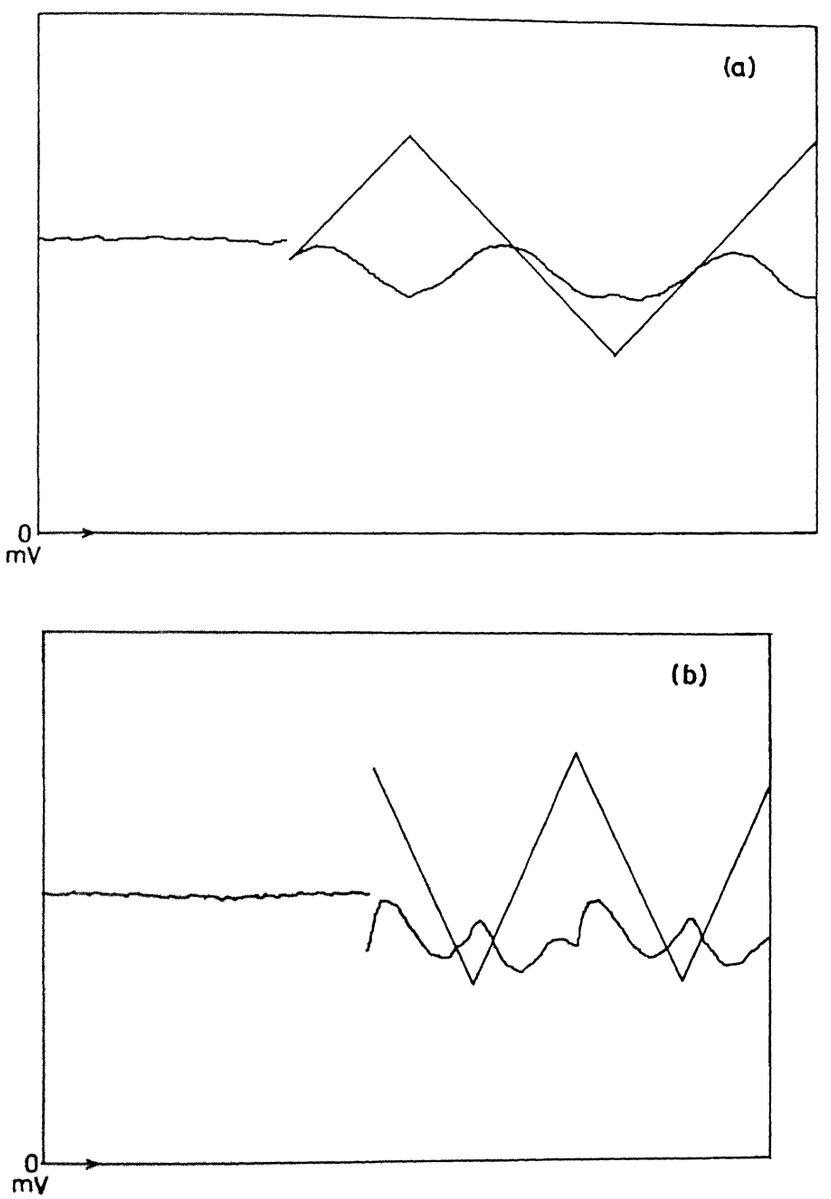

Figure 5.5: (a,b,c,d) OPC signal from Fluorescein doped boric acid glass film recorded under nearly degenerate four wave mixing conditions a:δ=0.04Hz, b:δ=.2Hz, c:δ=.66Hz, d:δ=5.6Hz The triangular voltage waveforms used to drive the peizo-mirror also shown (All voltage levels are measured with respect to the zero baseline)

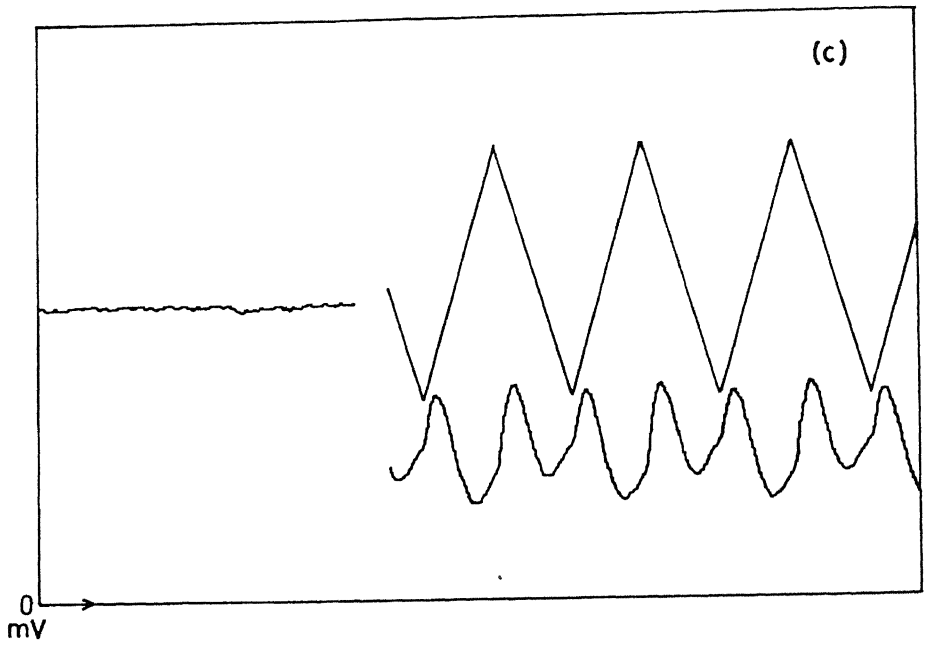
(c)
0
mV

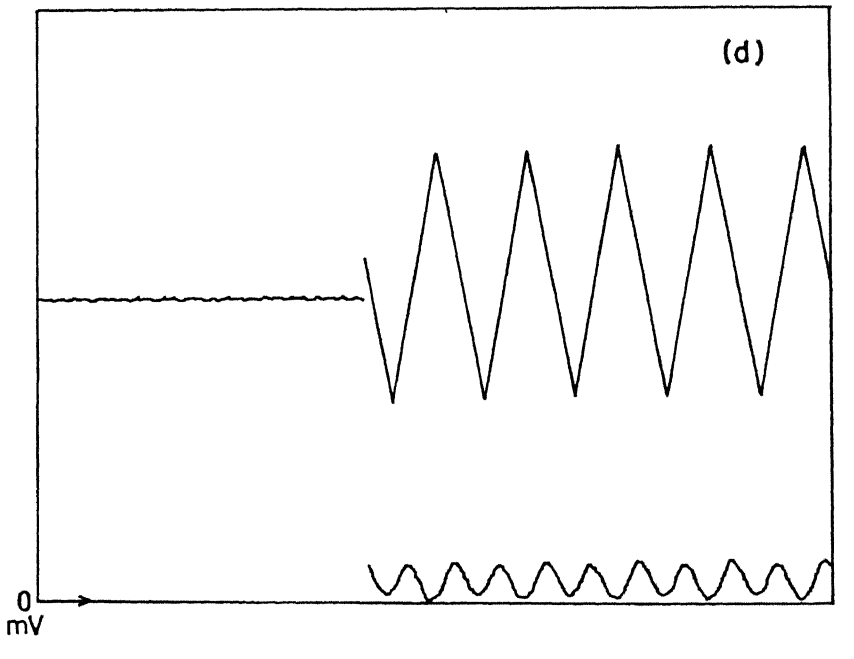
(d)
0
mV

Table 5.1: NDFWM OPC data for R6G doped in boric acid glass

Sr. No.	Time period of the triangular voltage waveform T=1/f	Probe frequency shift 2f(Hz) (a)	Minimum OPC signal during		Maximum OPC signal during		Modulation depth during	
			upshift (b) V_{max}	downshift (c) V_{min}	upshift (d) V_{max}	downshift (e) V_{min}	upshift (d)-(b) V_{mod}	downshift (e)-(c) V_{mod}
1	D.C	0.0	60					
2	46sec	0.04	55.2	54.6	58	58.5	2.8	3.9
3	26sec	0.8	53.0	53.5	58.5	59.4	5.5	5.9
4	11.6sec	0.18	52	53	59.6	60.7	7.6	7.7
5	3.1sec	0.64	51	53	58.5	60.7	7.5	7.7
6	1.7sec	1.2	41.8	47.4	59.6	63.5	17.8	16.1
7	1.1sec	1.8	44	46.3	58.5	58.5	14.5	12.2
8	540msec	3.7	32.3	32.9	48.5	45.1	15.2	12.2
9	280msec	7.14	21.7	28	45.1	41.8	23.4	13.8
10	210msec	9.6	16.7	23	41.8	37.3	25.1	14.3
11	142msec	14	10.	16.1	34.	26.5	24.0	10.4
12	100msec	20	5.6	9.48	26.5	21.7	16.1	17.0
13	60msec	35.4	3.32	2.78	17.5	13.9	14.2	11.1
14	44msec	45.4	1.67	2.23	12.8	11.5	11.1	9.3
15	32msec	62.6	0.55	0.55	17.2	13.9	16.7	13.4
16	25msec	80	0.5	0.5	15.0	12.8	14.5	12.3
17	16msec	125	1.1	0.6	12.8	11.7	11.7	11.1

Table 5.2: NDFWM OPC data for Fluorescein doped boric acid glass

Sr. No.	Time period of the triangular voltage waveform T=1/f	Probe frequency shift 2f(Hz) (a)	Minimum OPC signal during		Maximum OPC signal during		Modulation depth during	
			upshift (b) V_{max}	downshift (c) V_{min}	upshift (d) V_{max}	downshift (e) V_{min}	upshift (d)-(b) V_{mod}	downshift (e)-(c) V_{mod}
1	D.C	0.0	130.5					
2	47sec	0.04	105	106	129	131	24	25
3	22.5sec	0.09	101	105	117	122	16	17
4	12.8sec	0.16	103.5	94.5	114	117	10.5	22.5
5	9.2sec	0.22	80	87.8	112	116	32	28.5
6	7.6sec	0.26	75.4	85.5	105	109.5	29.6	24
7	4.6sec	0.434	56.3	65.3	94	96	37.7	30.7
8	3.0sec	0.66	35.13	46.1	81.3	83.5	46.2	37.4
9	2.0sec	1.0	24.8	30.4	66.6	7.5	41.2	44.1
10	1.4sec	1.43	11.3	14.6	54.2	57.6	43.0	43.0
11	0.95sec	2.10	7.9	13.5	27.1	29.3	24.9	24.8
12	610ms	3.28	2.3	4.5	27.1	29.3	24.9	24.8
13	360ms	5.56	11.3	3.4	15.8	18.0	4.55	14.6
14	180ms	11.2	0	1.1	6.8	7.9	6.8	6.8
15	125ms	16.0	0	1.1	2.3	4.5	2.3	3.4
16	68ms	29.4	0	0	1.1	2.3	1.1	2.3
17	42ms	47.6	0	0	1.1	1.1	1.1	1.1

The OPC signal under NDFWM is free of laser jitter because all interfering beams are derived from a single source. Results of NDFWM OPC in Rhodamine 6G doped boric acid glass films are presented in Table 5.1 and those for Fluorescein doped film in Table ??. Time periods of the triangular voltage form used in to drive the peizo-mirror are listed in the second column. The actual probe frequency shift which is twice the inverse of the time-period is listed in the third column. The minimum values of the OPC signal during upshift and downshift of the probe frequency averaged over typically ten to and fro motions of the peizomirror are listed in the 4^{th} and 5^{th} columns. The corresponding values for the maximum of the OPC signal similarly averaged are given in 6^{th} and 7^{th} columns. The last two columns give the modulation depth defined as

$$\text{Depth of Modulation} = \text{Max. OPC signal} - \text{Min. OPC signal} \tag{5.19}$$

$$V_{(mod)} = V_{(max)} - V_{(min)} \tag{5.20}$$

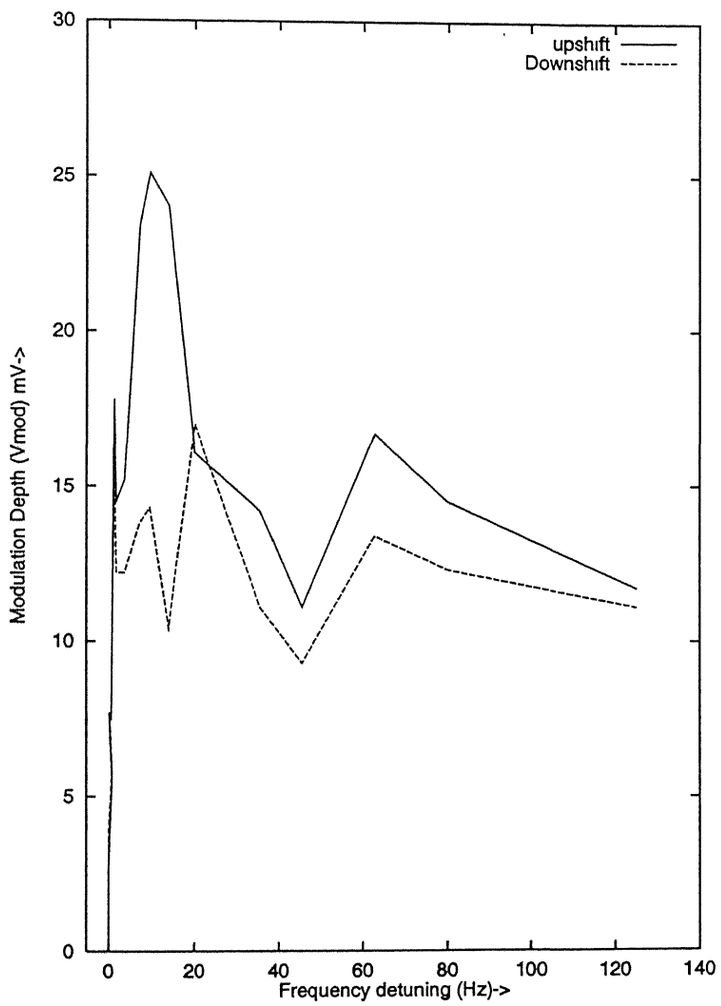

Figure 5.6: R6G doped BAG: Depth of modulation of NDFWM OPC signal with probe-frequency detuning

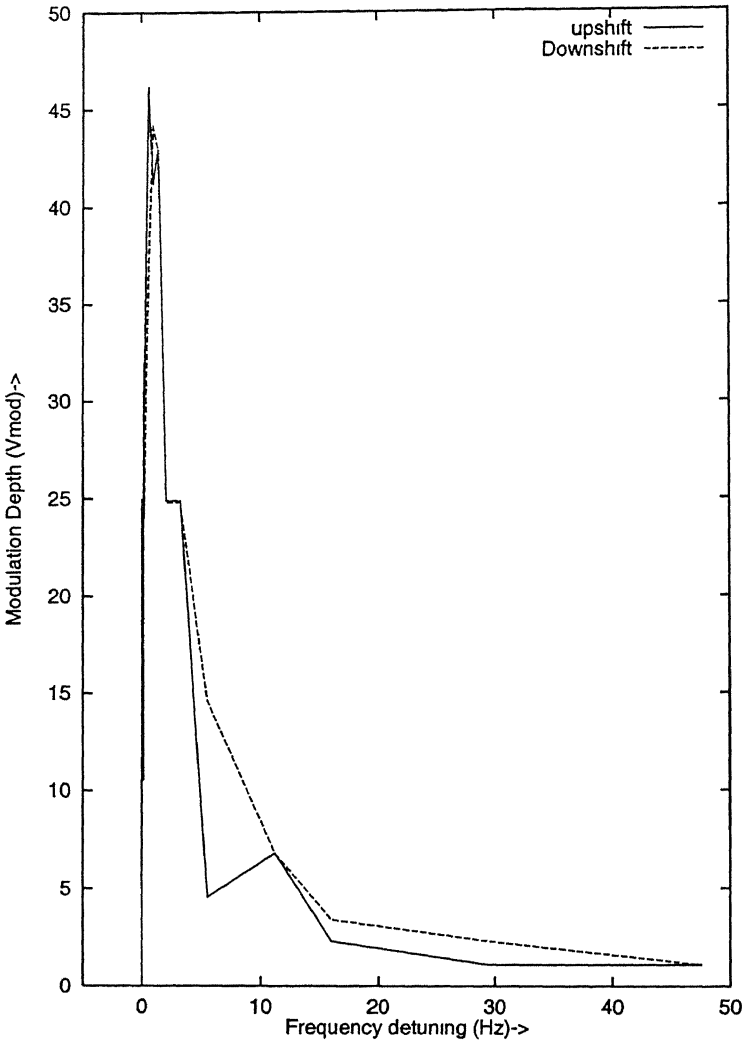

Figure 5.7: Fluorescein doped BAG: Depth of modulation of NDFWM OPC signal with probe frequency detuning

during up-shift and down-shift as a function of the time period of the peizo-drive voltage. The change in the depth of modulation with shift (positive and negative) in the probe frequency is plotted in Fig.5 6 and Fig.5 7. Fig.5 6 refers to R6G doped films and Fig.5.7 to Fluorescein doped films. There is a lot of scatter in the data giving a rather erratic variation. However grossly speaking, the modulation depth first increases with the frequency shift, reaching a maximum value around 10 Hz and then falls with further increase in the shift of the probe-frequency. This is an expected behaviour For small changes in the probe frequency the degradation of the OPC signal and hence the depth of modulation remains small. Both will increase as the frequency shift increases from zero value. At these low frequencies, sufficient time is available for the maximum and the minimum values of the OPC signal to be realized. As the probe frequency shift is increased further, the material response time comes into play. Enough time is not available to reach the minimum and the maximum values in a cycle which slows down the increase in the depth of modulation. At a particular value in the neighbourhood of 10 Hz the depth of modulation reaches a maximum value and then decreases with further increase in the shift of the probe frequency.

We now investigate the degradation of the OPC signal with shift in the probe frequency. Values of the minimum signal listed in columns four and five actually correspond to the OPC signal with shifted probe frequency. An entry in these columns correspond to the OPC signal when the peizomirror reaches a steady velocity. This is the time when the frequency shift corresponding to a given setting of the period of the triangular waveform is realized. Any increase in the OPC signal during the cycle indicates the decrease in the mirror velocity and hence decrease in the shift of the probe frequency. This decrease in OPC signal with shift in the probe frequency is quite systematic, though certain amount of scatter persists in this data as well. We have plotted in Fig.5.8 the NDFWM OPC signal identified with the entries in the 4^{th} and 5^{th} columns of table 5.1, with the shift in the frequency of the probe beam for the R6G doped films. The corresponding variation for the Fluorescein doped film is shown in Fig.5.9. Certain degree of asymmetry exists in the data for the up-shifted and the down-shifted probe frequencies. However Figures5.8,fig5x7 clearly bring out the systematics of the variation in the NDFWM OPC signal - a decrease in the signal with increasing shift (positive and negative) of the probe frequency. The OPC signal can be observed over a very narrow range of shift in the probe frequency. This behaviour is akin to a narrow band optical filter. Lorentzian fits based on Marquardt-Levenberg algorithm were attempted to the observed profiles. Because of the asymmetry in the data for the upshift and the downshift of the probe frequency as mentioned earlier, the peak position of the fitted profile is some-what off-centered with respect to the "zero" detuned frequency. Andrei *et.al.*[10] also observed such a shift which they attributed to unequal intensities of the pump beams. This shift for Rhodamine 6G is about -0.48Hz The

full width at half maximum for this sample is 13.4Hz The results for the fluorescein doped boric acid glass films are qualitatively similar to those of R6G doped films. The difference lies in the frequency response which is much narrower for Fluorescein doped film as compared to the frequency response of the R6G doped films. In the language of the optical filter, the Fluorescein doped BAG films have much narrower bandwidth. We notice from the table ?? that the OPC signal falls rapidly with the frequency shift of the probe beam. The modulation depth plotted on Fig.(5.7). shows a similar frequency dependence. The FWHM in this case is of the order of 1 Hz. the shift in the peak frequency from zero values is quite small(-0.02Hz) for Fluorescein films.

5.4.1 Interpretation of Results

We can apply the three level model developed by Rand *et.al.* to thin films of Rhodamine 6G and Fluorescein doped BAG films provided we neglect $T_1 \rightarrow T_2$ transitions. This may not be fully justified because some other studies[21] have shown the existence of these transition in these systems. Further the assumption of optically thin sample used in their derivation may not be justified in our samples with $\alpha_0 L = 0.27$ for the Rhodamine 6G films and $\alpha_0 L = 0.6$ for the Fluorescein doped films. Overlooking these complications we could still attempt to apply this model to systems of our interest. In these samples, the repopulation of the ground state due to the $T_1 \rightarrow S_0$ transition is the dominant process of ground state relaxation. Under this assumption, the decay time T_1 of the metastable T_1 of the lowest triplet state can be obtained from

$$T_1 = \frac{1}{\pi(FWHM)} \tag{5.21}$$

where FWHM is the fullwidth at half maximum as found in the preceeding section. This gives $T_1 = 24$ msecs for the Rhodamine6G doped films and $T_1 = 318$ msec for the Fluorescein doped films. Although the precise values of T_1 are not known because of the glassy nature of the host but the above values do fall in the correct range. But one must appreciate that it is not a measurement in the time domain. It is actually a measurement in the frequency domain giving the frequency profile of $T_1 \rightarrow S_0$ transition. All line broadening effects have essentially been eliminated in this technique based on NDFWM. While comparing our results in the frequency domain with those obtained in the temporal domain, it should be kept in mind that our measured line-widths may have significant power broadening. More detailed intensity dependent experiments need to be performed to get the absolute widths of the $T_1 \rightarrow S_0$ transitions.

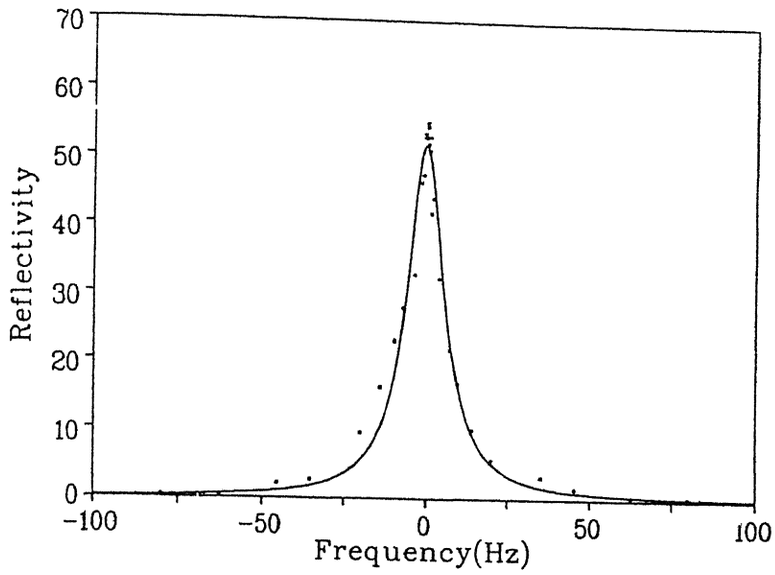

Figure 5.8: R6G doped BAG: NDFWM OPC signal versus detuning of probe frequency

It is noteworthy to mention that in an inhomogeneous system of dye doped in boric acid glass where the normal absorption spectrum for the $S_0 \rightarrow S_1$ transition is rather broad with a bandwidth of the order of 20 nm, one can still obtain extremely narrow resonances (of the order of few hertz) using this NDFWM technique eliminating the broadening effects due to the inhomogeneity of the medium. The estimates from this frequency domain experiment for the lifetimes of the excited state is about 24 msec and 318 msec for R6G and Fluorescein respectively. These values are fairly close to the values obtained from lifetime studies for these systems.

5.5 Conclusions

Using the technique of nearly degenerate Four Wave mixing in R6G doped BAG and Fluorescein doped BAG we are able to record line-profiles approaching the natural line-width of the transitions. The FWHM for Rhodamine and Fluorescein doped films are 13 4 Hz and 1 Hz respectively are indeed quite small. The spectrum obtained in the frequency domain is very clean and is devoid of any instrument broadening mechanisms. It is also free of laser jitter This is the first time such a measurement has been done on this kind of system, to our knowledge. Our experimental arrangement is much simpler than the one used by Rand*et.al* on $Cr^+ : YAlO_3$.

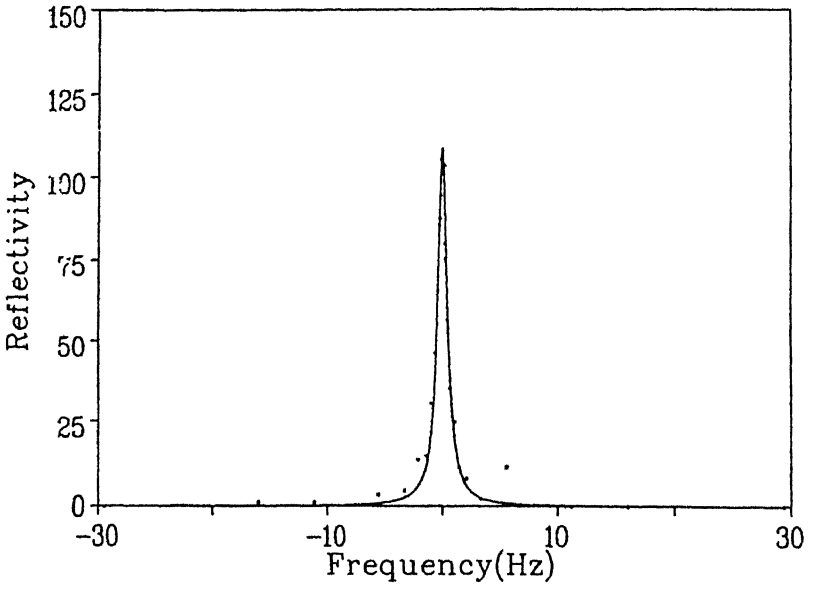

Figure 5.9: Fluorescein doped BAG: NDFWM OPC signal versus detuning of probe frequency

References

[1] S.C.Rand *Lasers, Spectroscopy and New Ideas -A Tribute to A.L.Schawlow (Ed W.M.Yen and M.D.Levenson*, **54**, (1985),266

[2] G.Ravindra Kumar *et.al., Optics Communications* , **73** , (1989), 81

[3] H.Fujiwara and K. Nakagama,*Opt Commun* , **55**, (1985), 386

[4] H.Fujiwara and K Nakagama,*Opt Commun* , **66**, (1988), 307

[5] Raj, R.K. *et.al. Phys. Rev. Lett.*,**44**,(1980), 1251

[6] Bloch, D.M., *et.al., Optics Communication*, **37**, (1981), 183

[7] MacDonald K.R *et.al.P R L*, **55**, (1985), 821

[8] Duncan G. Steel and S.C.Rand *P R L*, **55**, (1985), 2285

[9] Y.R.Shen *The Principles of Nonlinear Optics*, John Wiley,New York, (1984), 48

[10] Andrei G.S. and David Simkin, *Optics Letters*, **22**, (1997), 673

[11] Fisher R. A.(Ed), *Optical Phase Conjugation*, Academic Press Inc, New York (U.S.A), (1983).

[12] T.Todorov *et.al.,Opt. Quant. Elect.*, **13**, (1981), 209

[13] Y.Silberberg and I Bar Joseph,*Optics Communication* , **39**, (1981), 265

[14] M.A.Kramer *et.al.,J.Lumin*, **31-32**, (1984),782

[15] M.A.Kramer *et.al.,Phy. Rev A* , **34**, (1986),2026

[16] Y. Silberberg and I Bar Joseph,*IEEE J of Quant Elect.* , **QE-17**, (1981),1967

[17] S. Miyanaga, *et.al. ,Opt letters*, **13**, (1988), 1044

[18] K.P.B.Moosaad *et.al.*,*Pramana -J. of Physics* , **31**, (1988),281

[19] V.N.Blaschuk *et.al* ,*Sov J. Quant Elect* , **10**, (1980),356

[20] G.Martin , L K Lam,*Optics Letters* , **5**, (1980), 185

[21] K.Divakara Rao,*Ph.D. Thesis, I.I.T. Kanpur*, (1994)

[22] M.A.Kramer, W.R Tompkin and R.W.Boyd, *Phys. Rev. A*,**34**, (1986), 2026

Chapter 6

Effect Of Structural Modification On The Third Order Nonlinearity in Tetraphenylporphyrin Doped in Boric Acid Glass

Various nonlinear optical processes are being exploited for optoelectronic and photonic device applications. It often happens that the available nonlinear materials do not meet the requirements of a specific application. The need has been felt to attempt structural changes to achieve the desired characteristics of a nonlinear optical material. It is therefore desirable to understand the relationship between the molecular structure of a medium and its non-linear properties. Organic materials are best suited for these investigations

Structural changes in organic systems can lead to changes in the speeds and strengths of the optical nonlinearities. In this chapter we study the effect of structural changes on the third order nonlinearity. We have chosen for these studies, the planar molecule Tetraphenyl Porphyrin as the base on which various structural modifications were carried out. Chemically substituted porphyrin derivatives S_2TPP, TPP$(NO_2)_4$ and BrTPP were investigated (Fig.6.1). We chose the first order diffracted signal in the self-diffraction geometry to characterise the optical nonlinearity of these systems. The results of the structural changes are interpreted qualitatively in terms of their effect on the availability and delocalisation of π electrons.

6.1 Introduction

The optoelectronic and photonic applications make use of various nonlinear optical processes. For instance, the third order nonlinear optical phenomenon of optically induced changes in the refractive index of a medium is fundamental to optical switching, optical computing and host of other applications. Currently ferroelectric inorganic crystals are used in fabricating passive and active photonic devices. However they suffer from slow optical switching times. Organic materials with excellent non-linear optical properties are much more promising. Organic materials are of major interest because of their relatively low cost, ease of fabrication and integration into devices, tailorability which allows one to fine tune the chemical structure and properties for a given nonlinear application. Further, these materials have high laser damage thresholds, low dielectric constants, fast nonlinear response times. Then off- resonance nonlinear optical susceptiblities are comparable to or may exceed those of the ferro-electric inorganic crystals This has resulted in an interdisciplinary effort directed towards the basic understanding and exploitation of these non-linear systems.[5, 39, 40, 27].

The non-linear behaviour of organic molecules results primarily from π conjugation in these molecules. The third order susceptibility increases dramatically with π electron delocalisation. Correlations between the third order susceptibility and the electronic conjugation length have been established on many conjugated polymers[1]. However, these polymers have linear chain structures and the π electron density is delocalised and transferred only in one dimension i.e. along the longitudinal axis of the chain (say the x-axis). In this case, the major contribution comes from γ_{xxxx} (second order hyperpolarisability). Thus, only one tensor component contributes to the isotropically averaged susceptibility. When the dimensionality of the π electron system is expanded from linear to 2-dimensions as in the case of macrocycles or 3-dimensions as in fullerenes, the hyperpolarisation tensor will have several non-zero components.

Two dimensional macrocyclic systems such as porphyrins and pthalocyanines with large polarisable $\pi-$ electron cloud offer advantages in architectural flexibility, ease of fabrication and tailoring. It is possible to incorporate different kinds of metal ions in these systems. These two dimensional metallo-macrocycles offer additional features that can be used to optimise the nonlinear response. In addition to $\pi - \pi^*$ transitions of the conjugated system, the charge transfer transitions from ligand to metal (LMCT) and metal to ligand(MLCT) as well as the metal to metal transitions provide enhanced possibilities for tailoring of optical susceptibilities. One can vary the sizes and oxidation states of the metal ions and the nature of the axial ligands. A number of modifications can also be made in these macrocycles by introducing different substituents at the peripheral sites of the phenyl ring. This architectural flexibility is very helpful in optimising the nonlinear optical properties. These macrocycles exhibit electronic

transitions in the visible region (Q bands between 500 and 700 nm) and in the near UV (B or Soret bands between 350 and 450 nm)region[3, 17]. They possess large absorption cross-sections (typically $10^{-17}cm^2$) which are helpful in observing nonlinear effects at low light power levels Both Q and B bands are sensitive to factors such as the nature of the metal ions,oxidation state, substituents, environment of the molecule and so on Thus these hold the promise of vast improvement in their optical non-linearities by way of molecular engineering. This requires an understanding of the structure-nonlinearity relationship.

Porphyrins, a condensed product of four pyrrole rings connected to each other by methine groups has high π electron density and extended delocalisation. A variety of nonlinear effects have been observed and used to characterise these molecules. Guha *et.al.*[8] have used nanosecond and picosecond laser pulses to measure the third order optical nonlinearities of two metallotetrabenzoporphyrins and a platinum poly-ene dissolved in tetrathydrofuran by the use of direct intensity dependent total transmission of pulses as well as optical Kerr gate technique. Rao *et.al.*[9] established that the nonlinearity is predominantly electronic in origin. For this purpose, they measured the third order nonlinear optical susceptibility of tetrabenzoporphyrins in solution with tetrahydrofuran at 532 nm using degenerate four wave mixing with picosecond lasers. They also attempted to correlate the effect of substituents on $\chi^{(3)}$ for a series of tetrabenzoporphyrins possessing electron donating as well as electron withdrawing substituents. The results indicate that compounds having strong electron donating substituents exhibit higher nonlinearity. Using Z-scan technique, Kandaswamy *et.al.*[30] measured the third-order nonlinear optical susceptibility of T,3,4,BCEMPP doped in boric acid glass at different argon-ion laser wavelengths and at 784 nm using 60 fs pulses from a Ti:sapphire laser. They explained[4] the relationship between the substituted derivatives of H_2TPP and their corresponding hyperpolarisabilities on the basis of electronic interaction between the external substituents and the porphyrin core.

We note that the porphyrin system is an interesting system to undertake the study of substituent effect on the optical nonlinearity. It is drawing considerable attention in recent years and the studies reported so far on two dimensional porphyrins and their derivatives are still in infancy.

We have chosen the planar molecule TPPH (5,10,15,20 Tetraphenyl porphyrin) as a base molecule for our study of the effect of various substituents on the third order optical nonlinearity. Molecular structure of TPPH is shown in Fig.6.1. The structures of various derivatives of TPPH which have been investigated by us also shown in this figure. The TPPH and its derivatives were synthesised in the chemistry laboratory of our Institute.

We study the third order nonlinearity of these molecules doped in the boric acid glass in a self-diffraction experiment. We describe briefly the process of self-diffraction which we have

used to characterise the third order nonlinearity.

6.2 Self-Diffraction

Self-diffraction is a process whereby two interfering beams get diffracted from their own grating The diffracted signal which is essentially a new wave generated in the medium carries the information on the strength of the optical nonlinearity. Its origin is due to the nonlinear response of the medium to the incident light. In self-diffraction[2, 38, 11] we have two coherent pump beams of equal intensities interfering in the medium. The spatial light modulation created due to the interference between the input beams in turn creates spatial modulation of the populations of the ground and the excited states thereby creating a population grating. The pump beams thus write a grating in the medium. These writing beams in turn get diffracted and this process of generation of new diffracted waves is called self-diffraction. The efficiency of the diffracted signal defined as the ratio of the self diffracted signal of order n to the incident intensity (I_0) depends upon the material parameters. For the two beams of equal intensity[38] say '$I_0^+ = I_0^- = I_0$' crossing at an angle of 2θ the diffracted (say 'n^{th} order') signal is generated with an efficiency.

$$\eta_n = \frac{I_n}{I_0} = \left|\frac{\omega\chi_{NL}l}{2n_0c}\right|^2 \mathrm{Sinc}^2\left(\frac{\pi l}{l_n}\right)|C_n + C_{n+1}|^2 \tag{6.1}$$

where (6.2)

$$C_n = \left[\frac{\sqrt{(1+S_0)^2 - S_1^2} - 1 - S_0}{S_1^{|n|}\sqrt{(1+S_0)^2 - S_1^2}}\right]^{|n|}$$

are the Fourier coefficients and l is the thickness of the absorber. Saturation parameter S_0 and S_1 are defined as

$$S_0 = \frac{I_0^+ + I_0^-}{I_s} \tag{6.3}$$

$$S_1 = \frac{2\sqrt{I_0^+ + I_0^-}}{I_s}.$$

I_s is the saturation intensity, l_n is the coherence length of nth order given by

$$l_n = \frac{2\pi}{\beta_0 - \beta_n} \tag{6.4}$$

with

$$\beta_n = \left(\frac{\omega n_0}{c}\right)\left[1 - (2n+1)^2 sin^2\theta\right]^{\frac{1}{2}}$$

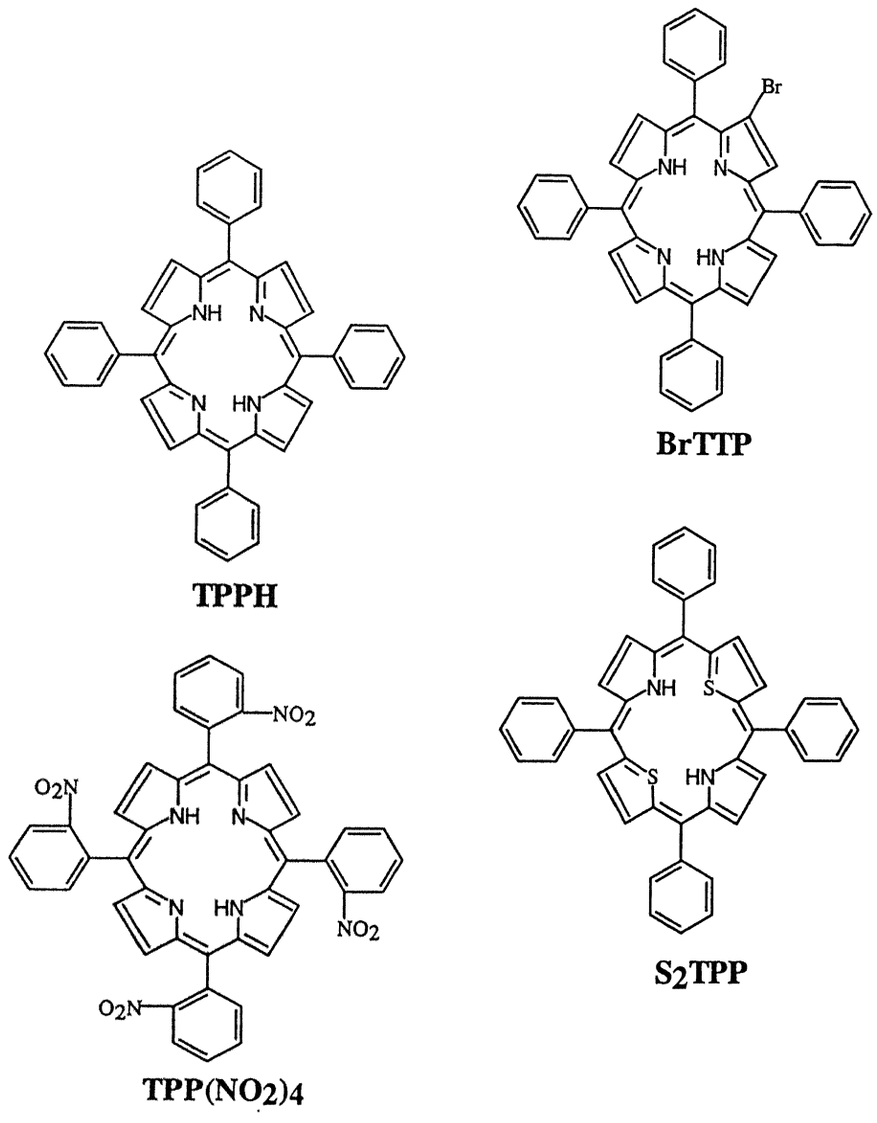

Figure 6.1: Molecular Structure of Tetraphenylporphyrin and its derivatives

ω is the frequency of the incident radiation and n_0 is the refractive index of the host in our case the boric acid glass, χ_{NL} is a parameter describing the non-linearity.

The first order diffracted signal (n=+1) may be associated with the third order nonlinear susceptibility. However, it contains some contribution from the 5th order component of the susceptibility. Neglecting this, the first order diffracted signal gets related to the forward four wave mixing process. We use the measured diffraction efficiency for n=+1 diffraction to characterise the strength of the non-linearity in our experiments on TPPH and its derivatives. We next describe the experimental setup used for these studies

6.3 Experimental Setup

The experimental setup used for self-diffraction studies is shown in Fig.6.2. The entire optical setup is mounted on an NRC vibration isolation table. The Argon ion laser beam is split into two by a 50:50 beam-splitter and with the help of the steering mirrors the two beams intersect at an angle 2θ in the sample giving rise to self-diffraction. The polarizers $P_1 - P_3$ were used to ensure that the light falling on the sample has the same linear polarization. The diffracted signals were measured at a large distance from the sample to reduce the background noise. The steady state signal was measured by the silicon photodiode Si-2386K. The output from the photodiode was fed to a Keithley picoammeter for quantitative measurement and to a storage scope (Kikusui DSS 6521) to monitor the signal level. Normally the pump beams were kept at 80mW each at an angle of $2\theta = 1.82^0$. The pump beam spot diameter was about 3.8mm on the sample. The crossing angle was kept low as the self diffraction process is efficient at low angles only.

We have carried out two studies on these samples. We have investigated concentration dependence of the third order non-linearity in TPPH samples with TPPH concentrations of $2.5 \times 10^{-5}M$, $1 \times 10^{-4}M$, and$5 \times 10^{-4}M$ in BAG films prepared for these studies. The non-linear signal for these samples was measured at 457.9 nm, 476.5 nm, 488.0 nm 496.5 nm, 501nm and 514.5nm lines of the Argon-ion laser. In another study, nonlinear signal was measured for porphyrin derivatives S_2TPP, TPP$(NO_2)_4$, BrTPP with 2.5×10^{-5} molar concentration in BAG film. For the later studies, the Argon line of 457.9 nm was used to measure the first order self-diffracted signal as this was the closest line to the absorption linecenter. The S_2TPP soret band is somewhat red-shifted and overlaps with several lines of the argon ion laser. The nonlinear signal in this case was measured at 457.9nm, 476.5nm and 488nm.

The sample of BAG film doped with the porphyrin derivatives are prepared by the same

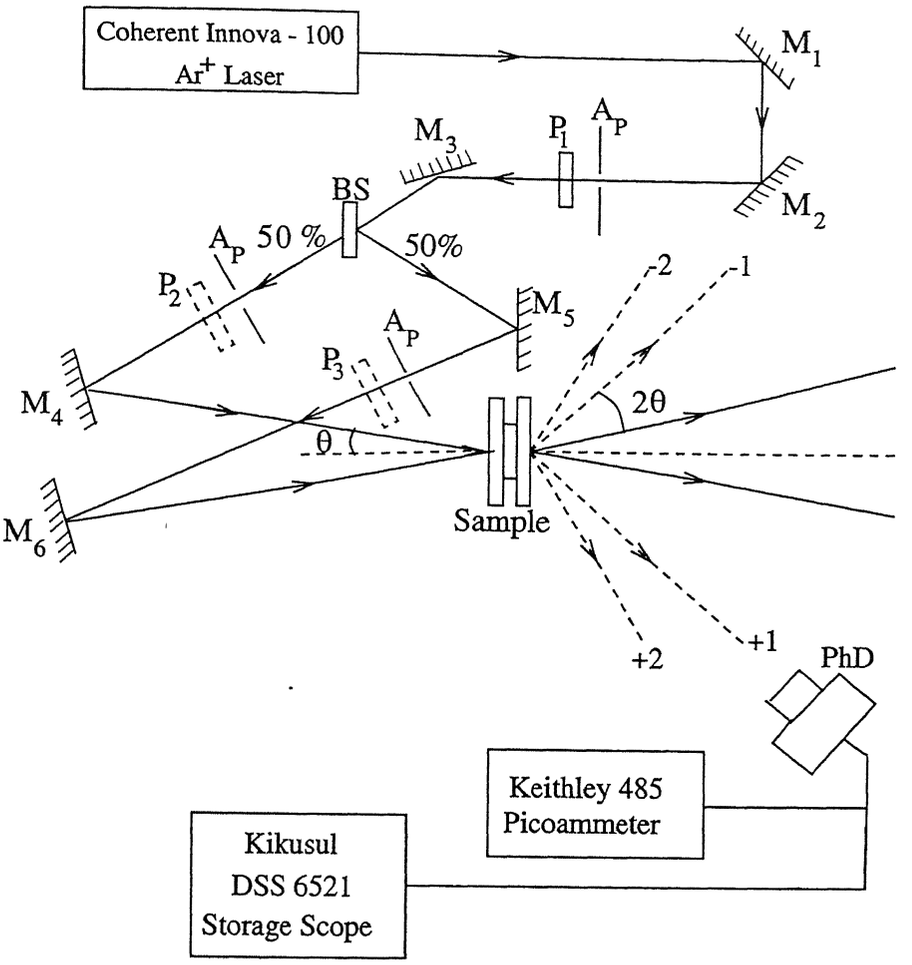

Figure 6.2: Experimental setup for self-diffraction studies.

procedure as mentioned in chapter 3. The porphyrin and its derivatives are mixed with the boric acid glass in the required proportion.

6.4 TPPH

We have chosen the planar molecule TPPH (5,10,15,20 Tetraphenyl porphyrin) as the molecule on which various structural modifications were carried out[7]. TPPH is a molecule consisting of four pyrrole rings in one plane (Fig.6.3). The 11 double bonds with 22 π electrons in the core are always delocalised. However the phenyl rings present at the mesopositions are perpendicular to the porphyrin plane. The πelectron density of the porphyrin rings also extends into these phenyl rings. The high π electron density of electrons coupled with extended delocalisation is responsible for the large optical nonlinearities observed in these systems.

First we look at the absorption spectrum of TPPH. The absorption spectra (of all samples

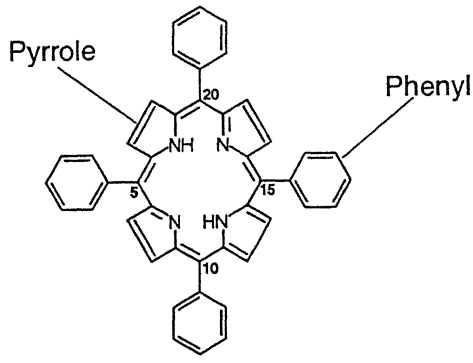

TPPH

Figure 6.3: Molecular Structure of Tetraphenylporphyrin and its derivatives

Table 6.1: Peak Positions and FWHM of Q and B bands of TPPH doped in boric acid glass films.

Molar Concentration	Soret(B) Bands		Q Bands	
	Peak position(nm)	FWHM (nm)	Peak position(nm)	FWHM (nm)
2.5×10^{-5}	437.0 nm	26nm	666.0 nm	37nm
1×10^{-4}	433.0 nm	37nm	666.5 nm	45nm
2.5×10^{-4}	424.5nm	69nm	664 nm	55 nm
5×10^{-4}	426.5nm	—*	688.5m	—*

* Since the spectra could not recorded beyond the scale shown in the figure, therefore it was not possible to estimate this quantities.

used in this study) were recorded on the Shimadzu UV-Visible Spectrophotometer model 160. Undoped films of the boric acid glass were used for the reference beam. However because of the nonuniformity of the thickness of these films and in the absence of direct method to estimate the thickness of our films it is difficult to calculate the absolute absorbance of our samples.

The $S_0 - S_1$ absorption band of thin films of planar porphyrin doped in boric acid glass (BAG) host peaks around 437 nm (Fig.6.4). This is the Soret or the 'B' band. For the nonlinear studies, the 457.9 nm line of an Argon ion laser lying in the far wings of this band has been used. The other band in the deep red region of the absorption spectrum is the Q band and it peaks around 666.0nm.

Absorption spectra of samples of various molar concentration of TPPH doped in BAG were recorded. They are reproduced in Fig.6.4 to Fig.6.7 as the molar concentration of TPPH increases from 2.5×10^{-5} to 5×10^{-4}. Some dramatic changes in the absorption spectrum

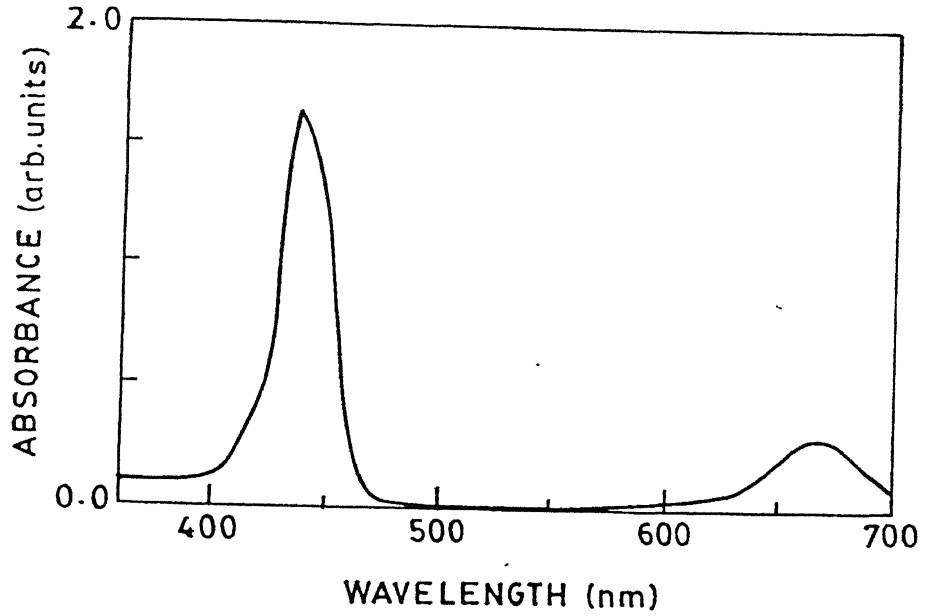

Figure 6.4: Absorption Spectrum of 2.5×10^{-5} M concentration TPPH doped in boric acid glass

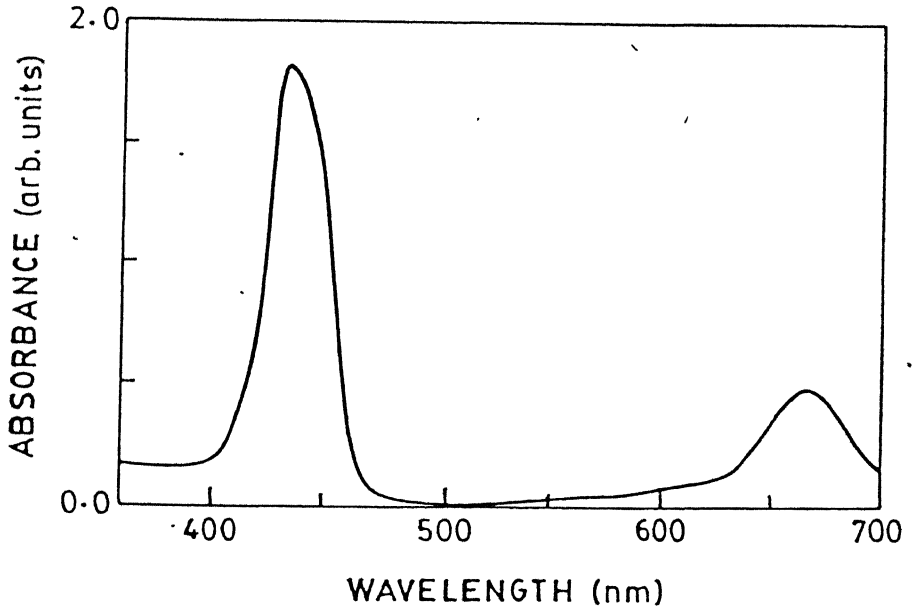

Figure 6.5: Absorption Spectrum of 1×10^{-4} M concentration TPPH doped in boric acid glass

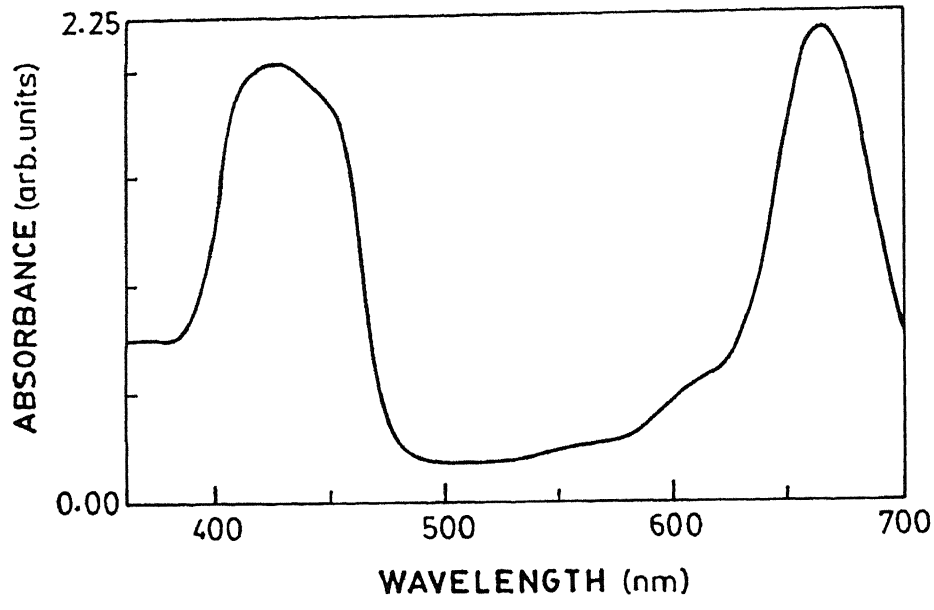

Figure 6.6: Absorption Spectrum of 2.5×10^{-4} M concentration TPPH doped in boric acid glass

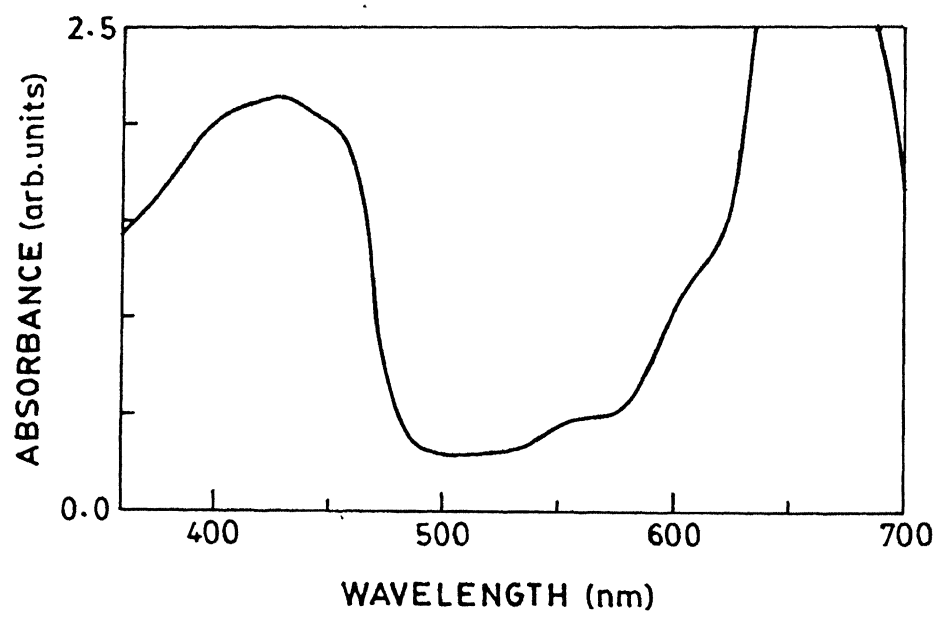

Figure 6.7: Absorption Spectrum of 5×10^{-4} M concentration TPPH doped in boric acid glass

appear. For the change in the molar concentration from 2.5×10^{-5} to 1×10^{-4}, there is only a slight increase in the overall absorption for the peaks in the blue (B band) and the red(Q band) regions with hardly any change in the overall profile of the spectrum (Fig.6.4, 6.5). It may also be mentioned that the increase in the absorption in the 1×10^{-4} sample as compared to the absorption in the 2.5×10^{-5} (Fig.6.4) molar sample (Fig.6.5) may not be entirely due to the increase in the concentration because of the uncertainty in the thickness of the films We, however believe the film thickness change may not account for more than 20%.

As the molar concentration is further increased to 2.5×10^{-4}M (Fig.6.6) the peak absorbance in the blue region goes up with an overall broadening of the profile which has become asymmetric in shape. There is also substantial change in the red region (Q band) as well. In fact the absorption peak in the Q band has increased many folds and the absorbance in the Q band is now greater than that in the Soret band or the B band. Further, significant absorption can be noticed in the spectral region between the Q band and the B bands. As the concentration is increased to 5×10^{-4}M there is a further increase in the absorbance in the two bands and there is substantial overall increase of absorbance in the entire profile of the spectrum. Table(6.1) gives the peak positions and the FWHM of the Soret and the Q bands in TPPH. We will comment on these changes later in this chapter.

6.4.1 Diffraction Efficiency of TPPH

Diffracted signal for the n=+1 order of diffraction in the self diffraction experiment described earlier was measured for various concentrations of TPPH in boric acid glass films at several lines of the Argon ion laser. The diffraction efficiency obtained from these measurements are presented in table6.2. These experiments were carried out with 80 mW of input power except in case of 488nm for which the input power was around 96 mW. Maximum diffraction efficiency of about 0.2% occurs at 457.9nm for the sample with 2.5×10^{-5}M concentration of TPPH. Further, this table shows that the diffraction efficiency decreases at all wavelengths as the concentration is increased from 2.5×10^{-5}M to 1×10^{4}M. There is, however, substantial recovery in efficiency when the concentration is further increased to 5×10^{-4}M. The wavelengths dependence of diffraction efficiency is shown in Fig.6.8. For low concentrations (2.5×10^{-5}M and 1×10^{-4}M) samples, the diffraction efficiency rapidly decreases as the wavelength of the laser line is shifted away from the linecenter. There is a partial recovery in the efficiency as the B band is approached. However for the higher (5×10^{-4}M) concentration samples the situation is quite different. The 457.9nm laser line, being very close to the line center of the soret band is almost completely absorbed at this concentration. Likewise, the self diffracted signal is also totally absorbed at this wavelength. However, as we move away from the line center, the self

diffracted signal can be observed. In fact, the diffraction efficiency at this concentration is nearly two orders of magnitudes higher than at the intermediate concentration 1×10^{-4}M for the corresponding wavelengths.

6.4.2 Discussion of Results

Fig.6.4 and 6.5 clearly show that the absorption increases as the concentration of TPPH in the boric acid glass film is increased. This is also reflected in tab6.1, where we find a steady increase in the width of the absorption bands with concentration. But what is not obvious from these figures and the table is whether the optical density of these samples increases linearly or non-linearly with concentration. This question cannot be settled conclusively because we are not in a position to ascertain thickness of these films. However, we are confident that the uncertainty in film thickness is not large enough to come in the way of interpretation of our results. When the concentration is initially raised from 2.5×10^{-5}M to1×10^{-4}M i.e. by a factor four, the ratio of FWHM of the soret band goes up a factor of 1.4. But when the concentration is increased from 1×10^{-4}M to 2.5×10^{-4}M (ratio of only 2.5), the ratio of FWHM of the same bands increases by a factor of 1.9. Such a difference cannot be accounted by uncertainty in film thickness because the films for different concentrations were prepared under more or less identical conditions. We believe that there is a tendency for cluster formation or polymerisation which sets in at fairly low TPPH concentrations but becomes prominent at around 1×10^{-4} molar concentration of TPPH. This is further supported by the fact that at low concentrations we see only the soret and the B bands in the blue and near the red regions with practically no absorption in the spectral region in between. With increased concentration, the absorption can be seen in the intermediate region as well. This also explains why fairly strong non-linear signal can be seen at the higher concentration 5×10^{-4}M for those laser lines which have no overlap with the soret or the Q bands but lie in the intermediate spectral region (Fig.6.7). In the lower concentration samples, the non-linear signal is at least two orders of magnitude weaker at these wavelengths. It is interesting to point that in the higher concentration sample, the non-linear signal is more or less independent of wavelength of the laser line. This may be due to the fact that close to the soret band, the signal is weakened by increased re-absorption in the concentrated sample. The absorption profile of the soret bands falls rather steeply (after Figs.6.6), 6.7) at the this concentration and consequently gradual changes in the nonlinear signal are not seen as at lower concentration. In the intermediate spectral region (between the soret and Q bands), the absorption is more or less uniform giving rise to essentially constant nonlinear signal in this region. At this stage we do not have a proper explanation for the partial recovery of the non-linear signal at 501nm and 514.5nm laser lines, in samples of low concentration.

Table 6.2: First order Self-Diffraction efficiency for TPPH doped in BAG at various Ar^+ ion wavelengths for different molar concentration

Wavelength	Diffraction Efficiency for n=+1 order at concentration of		
	2.5×10^{-5}M	1×10^{-4}M	5×10^{-4}M
457.9nm	2.1×10^{-3}	1.4×10^{-3}	Absorbing
476.5nm	4.7×10^{-5}	3×10^{-5}	2.8×10^{-4}
488.0nm	1.3×10^{-5}	9.5×10^{-6}	2.5×10^{-4}
496.5nm	9.3×10^{-6}	4.2×10^{-6}	1.5×10^{-4}
501nm	1.2×10^{-5}	8.4×10^{-6}	1.4×10^{-4}
514.5nm	1.1×10^{-5}	7.4×10^{-6}	1.2×10^{-4}

It may be due to the onset of polymerisation process or it may actually correspond to phase grating away from the linecenter. More work is needed to understand this peculiar feature of the non-linear signal. It may however be mentioned that the onset of polymerisation can extend very substantially the spectral bandwidth for non-linear optical application in these systems.

6.4.3 Saturation Characteristics

To establish that the optical nonlinearity in TPPH is due to the saturation of absorption we measured the transmittance of the laser beam through films of TPPH doped in BAG as a function of the beam intensity. The experimental setup used was the same as that used for similar experiments mentioned in chapter 3. The transmission experiment was done with the 457.9nm line of the Ar^+ ion laser (Fig.6.9). The transmission curve starts showing signs of nonlinearity around 5 mW of the incident power. As the incident power is increased further the transmittance increases, thereby establishing that the optical nonlinearity could be due to the saturation of the absorption coefficient.

6.5 TPPH Derivatives

TPPH possesses the inner core called the pyrrole ring. The pyrrole ring is planar and provides the bulk of π electrons which are delocalised. The outer rings are phenyl rings. It is generally assumed that the phenyl rings are delinked from the pyrrole rings. At best the two may be connected loosely. The four phenyl rings are not linked with each other and lie in the plane perpendicular to the plane of the pyrrole ring. The π electrons in the phenyl rings with limited delocalisation may not significantly contribute towards the molecular polarization or the

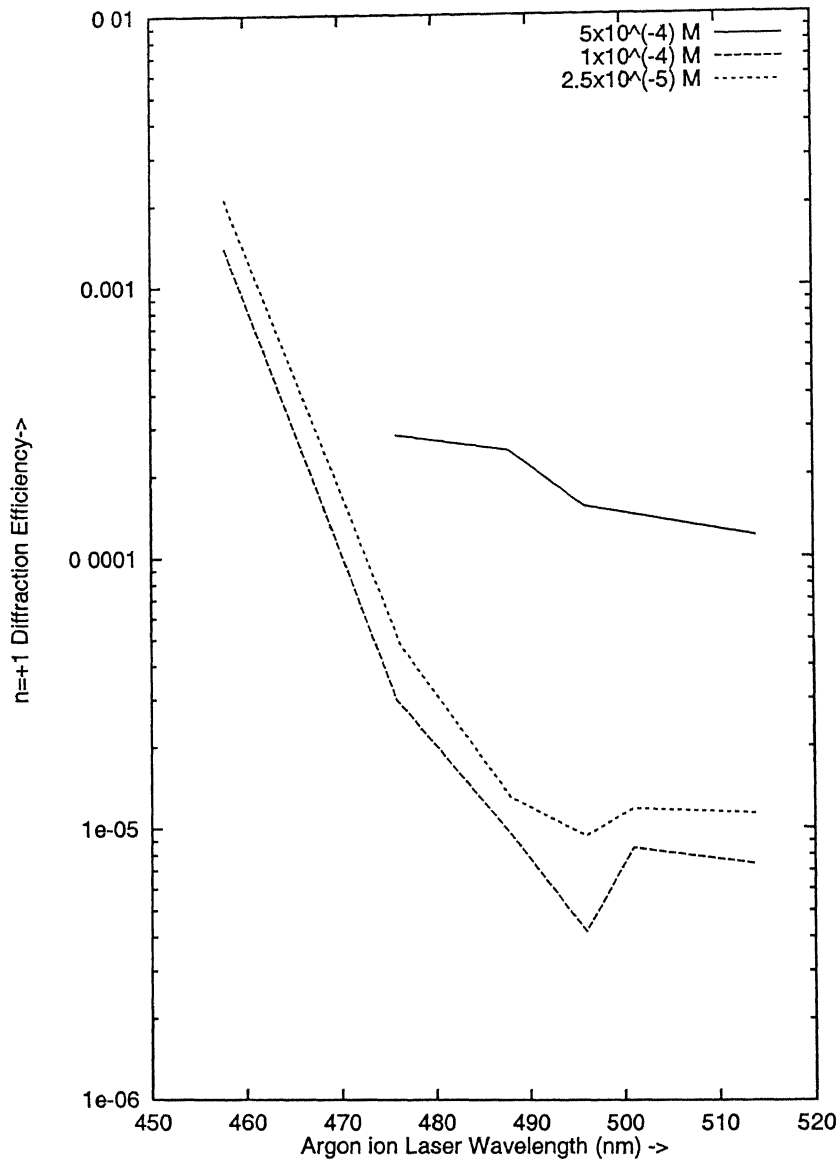

Figure 6.8: Self-diffracted signal (n=+1 order) from various concentration of TPPH doped in BAG at Argon ion laser wavelengths. The lines are drawn between the experimental points to show the trends.

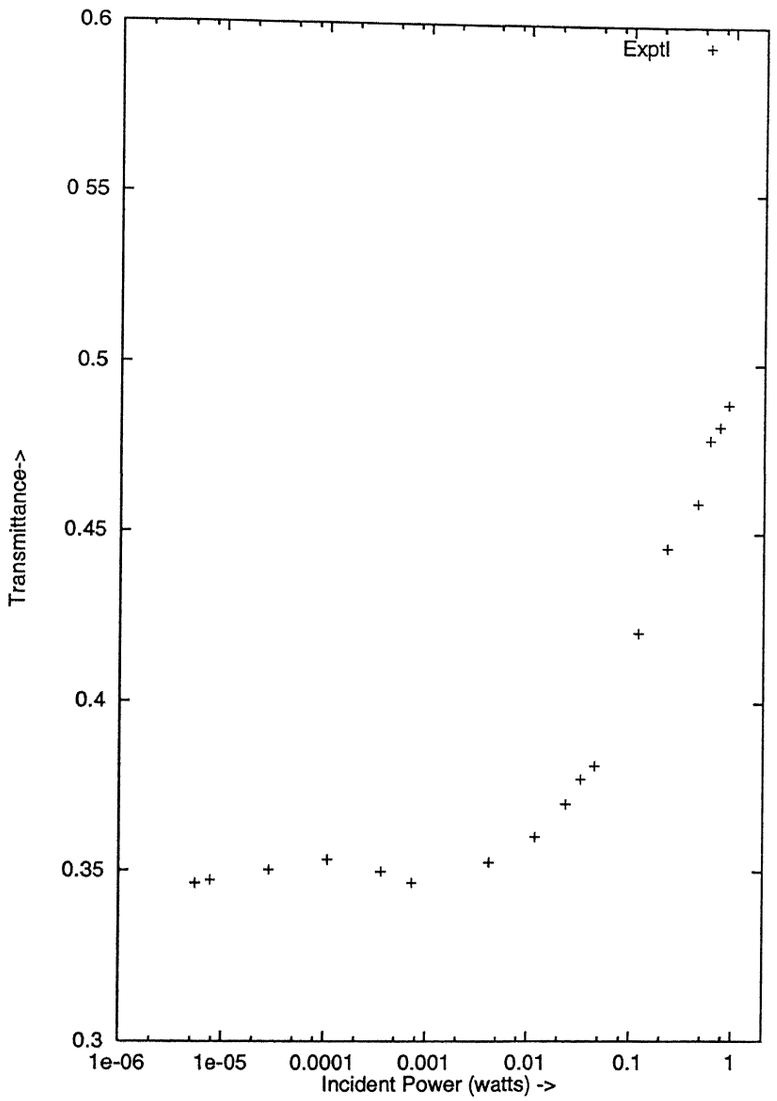

Figure 6.9: Saturation Characteristics of TPPH doped in BAG (2.5×10^{-5} M)

non-linearity. It is generally assumed that the phenyl rings are delinked from the pyrrole rings. At best the two may be connected loosely. If it is so then any modification on the phenyl ring should leave the non-linear signal more or less unaffected. If on the other hand the phenyl rings are in some-way linked to the pyrrole rings, and the pyrrole rings contribute significantly to the non-linear signal, the modification of the phenyl rings may affect overall π conjugation process and one may see changes in the non-linear signal where the phenyl rings are modified This is one of the hypothesis we wanted to test. Further any modifications of the core would certainly affect π- conjugation and hence the nonlinear signal

The phenyl ring modification was affected by introducing NO_2 molecules. This derivative is listed as $TPP(NO_2)_4$ The NO_2 being electron withdrawing is expected to reduce the electron availability in the phenyl rings. Two core modified derivatives were investigated by us for their non-linear optical behaviour. One involved bromine, substituting at the β carbon(shown in the figure 6.1) positions of the pyrrole rings. This derivatives is named as BrTPP. Bromine is a heavy atom and also an electron withdrawing group. Since it is placed at the β position, it directly affects the π conjugation of the porphyrin ring. The second core modified derivative is the S_2TPP in which two of the nitrogen of the TPPH molecule in the pyrrole ring are substituted with sulphur atoms. We first study the effect of these modifications on the absorption spectra before moving onto the nonlinear studies.

Absorption spectra of TPPH and its three derivatives, all with $2.5 \times 10^{-5}M$ concentration are shown in Fig.6.10. Spectra for these compounds are shown together to facilitate easy comparison. All compounds except S_2TPP show two banded spectra in the spectral range of investigation. Table(6.3) shows the peak position, the FWHM and the shifts in the positions of various bands.

BrTPP has red shifted spectrum of the Soret band by about 5 nm whereas the Q band has also undergone red shift of nearly the same amount. In $TPP(NO_2)_4$ the soret band is blue shifted by 6nm and the Q band is also blue-shifted by 35nm. There is red shift for S_2TPP's soret band by 30nm and its Q band seems to be either pushed out of the visible spectrum or has been washed away. The S_2TPP soret band overlaps very well with the spectral lines of the Argon ion laser.

The low power absorption constant $\alpha_0 L$ for different Ar^+ ion laser wavelengths are tabulated in table6.4.

We notice that whereas the base molecule TPPH has significant absorption only at 457.9nm laser line, the derivatives have substantial absorption at the other laser lines as well. It is interesting to point out that despite the blue shift in $TPP(NO_2)_4$, its Q band shows substantial

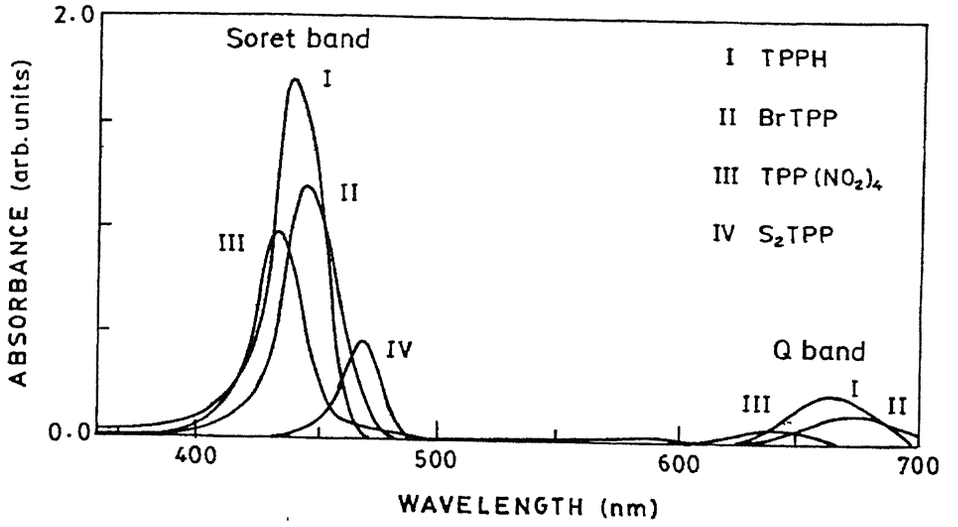

Figure 6.10: Absorption Spectrum of 2.5×10^{-5} M concentration porphyrin and its derivatives doped in boric acid glass

Table 6.3: Peak positions of soret and the Q bands of TPPH and its derivatives ($2.5 \times 10^{-5} M$ concentration) doped in boric acid glass [Fig.6.10]

Soret (B) Bands			
Sample	Peak Position (nm)	FWHM (B band) (nm)	Shift of B band w.r.t TPPH (nm)
TPPH	437.0	26	
S_2TPP	467.0	20	30(red)
BrTPP	442.0	26	5(red)
$TPP(NO_2)_4$	431.0	23	6(blue)
Q Bands			
Sample	Peak Position (nm)	FWHM (Q band) (nm)	Shift of Q band w.r.t TPPH(nm)
TPPH	666.0	37	-
S_2TPP	not seen		-
BrTPP	672	37	6(red)
$TPP(NO_2)_4$	637	33	29(blue)

Table 6.4: $\alpha_0 L$ values of thin films of boric acid glass doped with TPPH and its derivatives(All samples had 2.5×10^{-5} M concentration)

Doping	$\alpha_0 L$ at			
	514.5nm	488nm	476.5nm	457.9nm
TPPH	0.04	0.056	0.08	0.54
S_2TPP	0.1	0.21	0.62	0.63
BrTPP	0.08	0.15	0.33	2.01
$TPP(NO_2)_4$	0.31	0.35	0.38	0.55

Table 6.5: Table showing comparative diffraction efficiency (η) of n=+1 order of self-diffraction for different samples

Sample	λ(nm)	i/p power each beam	Diffraction Efficiency n=+1 order
TPPH	457.9nm	80mW	2.1×10^{-3}
BrTPP	457.9nm	80mW	1.4×10^{-4}
S_2TPP	457.9nm	80mW	5.8×10^{-6}
$TPP(NO_2)_4$	457.9nm	80mW	5.2×10^{-5}

absorption at all wavelengths. This is because the Q band has developed a flat tail on the longer wavelength side.

6.5.1 Diffraction efficiencies of TPPH and its derivatives

We have measured the first order self-diffracted signal for the four compounds at 457.9nm line of the Argon ion laser. All diffraction efficiencies at this wavelength are measured at 80 mW of input power of each beam. In the case of S_2TPP we have also measured the diffraction efficiencies at other wavelengths viz at 476.5nm and 488 nm. However at 488nm we measured the diffraction efficiency at 160 mW of input power of each beam because the signal at 80 mW beam power was quite weak. The results are tabulated in tables 6.5and 6.6. What we find in the table6.5 and 6.6 is that the diffraction efficiency is maximum for free base porphyrin TPPH and for the rest of them there is substantial decrease in the efficiency at 457.9 nm. At 457.9 nm S_2TPP is about two order of magnitudes less efficient than TPPH and BrTPP just an order of magnitude less efficient. Even with the absorption band well covered by the argon ion laser wavelengths the diffraction efficiencies of S_2TPP are at best comparable to TPPH at 476.5 nm and 488.0 nm.

Table 6.6: Table showing comparative diffraction efficiency (η) of n=+1 order of self-diffraction for different samples

Sample	λ(nm)	i/p power each beam	Diffraction Efficiency n=+1 order
TPPH	457.9nm	80mW	$2.1\text{x}10^{-3}$
S_2TPP	457.9nm	80mW	$5.9\text{x}10^{-6}$
TPPH	476.5nm	80mW	$1.3\text{x}10^{-5}$
S_2TPP	476.5nm	80mW	$9.5\text{x}10^{-6}$
TPPH	488nm	160mW	$6.9\ \text{x}10^{-6}$
S_2TPP	488nm	160mW	$5.8\text{x}10^{-6}$

6.5.2 Discussions

TPPH(tetraphenyl porphyrin) is a planar molecule with 22π electrons This results in high electron density and extended delocalisation which are responsible for the high nonlinearity observed in films doped with TPPH. The nonlinear optical signal in organic systems is due to the presence of the π electron cloud. The larger the π electron density, the greater will be the strength of the nonlinearity. Similarly extended delocalisation also generally increases the strength of the nonlinearity. BrTPP is obtained from TPPH by Br-substitution of the β-pyrrole carbon. Because of its position in the porphyrin, it is expected to modify π conjugation character of the porphyrin ring. In addition, being electron withdrawing bromine reduces the electron density. However the red shift of the absorption bands in both BrTPP and S_2TPP doped films suggests that the delocalisation has increased. Thus on the one hand, being an electron withdrawing group Br reduces the electron density but at the same time because it represents heavy atom substitution, the π delocalisation actually increases. The overall effect is that the non-linearity of BrTPP doped film has reduced as compared to that of TPPH doped film in BAG. Nitro groups in $TPP(NO_2)_4$ substitute for hydrogen atoms in the phenyl groups which occupy positions in a plane perpendicular to the plane of the porphyrin ring. This should not affect the π delocalisation. However the blue shift in the absorption spectrum suggests that the π delocalisation has decreased. Hence we are not sure at this stage whether the phenyl rings have undergone some distortion in the doping process so that the phenyl rings may no longer be perpendicular to the pyrrole rings. This will results in establishing link in the π clouds of the pyrrole and the phenyl rings.

The nitro groups being electron withdrawing groups, will also reduce the electron density. This may explain the reduction of the non-linear signal in $TPP(NO_2)_4$ doped films. Substituting two nitrogen atoms in the pyrrole ring by sulphur atoms provides an attractive core modification which changes the electronic environment of the porphyrin π-system. Being electron donor,

sulphur substitution in the core should increase the availability of electrons in the pyrrole ring. Further the optical bands are red-shifted indicating an increase in π delocalisation. This heavy core modification is thus expected to increase the intersystem crossing rate and should have led to higher nonlinearity or at least comparable nonlinearity with respect to TPPH. But the nonlinearity has actually decreased in this case as well. This may be explained if we assume that the heavy atom substitution may substantially distort the porphyrin core that it is no longer planar, thereby reducing the conjugation and resulting in lower electron density. This will result in reduced optical nonlinearity. If this hypothesis is correct, then it suggests that just by having an internal core modification which enhances the intersystem crossing rate the optical nonlinearity may not improve.

6.6 Conclusions

In conclusion we would like to mention that $2.5 \times 10^{-5}M$ film of TPPH doped in boric acid glass possess one of highest known diffraction efficiencies observed in similar systems. The efficiency for self-diffraction in the $+1$ order is a little over 0.2%. We have made no effort to optimise this value. At lower concentration (upto 1×10^{-4}), the diffraction efficiency is quite sensitive to the wavelength However, at somewhat higher concentrations the diffraction efficiency is nearly constant in the spectral range covered by the Argon ion laser. It may be possible to achieve reasonably high optical non-linearities in TPPH doped films over a broad spectral range. This may have to do with the onset of polymerisation in the films. We have also investigated the effect of introducing electron withdrawing and electron donating molecules in specific positions in the pyrrole and the phenyl rings of TPPH. We have not been able to observe any increase in diffraction efficiency as a result of these substitutions but the changes observed are at least qualitatively well understood. More work is needed for better understanding of these system.

References

[1] Paras. N.Prasad and D. J. Williams, *Introduction To Nonlinear Optical Effects in Molecules and Polymers* , (1991) John Wiley & Sons Inc New York.

[2] H. J. Eichler, *Laser Induced Dynamic Gratings*, (1986) Springer-Verlag, Berlin.

[3] M.Gouterman (ed by D.Dolphin), *The Porphyrins*,**Vol III**,(1978) Academic Press, New York.

[4] K. Kandaswamy *et.al.*, *Chem. Commun.*, , (1997), 1159

[5] J.L.Bredas *et.al.*, *Chem. Rev.*, **94**, (1994), 243

[6] M.Ravikanth *et.al.*, *Pre-print*

[7] Alok Sharan *et.al.*,*Proceedings of Workshop on Advanced Laser Spectroscopy, I.I.T Kanpur*,(1994).

[8] S.Guha, *et.al.*, *Optics Letters* , **17 (4)**, (1992),264.

[9] D.V.G.L.N.Rao *et.al.*, *Applied Physics Letter*, **58(12)**, (1991),1241.

[10] T.Sakaguchi *et.al.*, *Chem. Lett.*, , (1992), 281.

[11] G.Ravindra Kumar *et.al*, *J. Opt. Soc. Am .B*, **8(10)**, (1991), 2119.

[12] H. H. Jaffe, *J. of Chem. Phy.*, **20(2)**, (1952), 279.

[13] G. D. Dorough *et.al*, *J. A. C. S.*, **73**, (1951), 4315.

[14] A.T. Gradyuskho *et.al*, *Soviet Physics - Doklady*, **13(9)**, (1969),869.

[15] Daniel W. Thomas *et.al*, *J. A. C. S.*, **78** , (1956), 1335.

[16] Daniel W. Thomas *et.al*, *J. A. C. S.*, **78** , (1956), 1338.

[17] Martin Gouterman, *J. of Mol. Spect.*, **6**, (1961), 138.

[18] M. Meot-Ner *et.al*, *J.A.C.S.*, **97:18**, (1975), 5107.

[19] Alan D. Adler *et.al*, *J. polymer Sci.:Part C*, **29**, (1970),73.

[20] M. Meot-Ner *et.al*, *J.A.C.S.*, **94:13**, (1972), 4763.

[21] V.M.Albers *et.al*, *J. of Chem. Phy.*, **4**, (1936), 422.

[22] Daniel W.Thomas *et.al*, *Archives Of Biochem. & Biophy.*,**76**,(1958),287.

[23] Allen Stone *et.al*, *J.A.C.S*, **90(11)**, (1968),2735.

[24] K.N. Solovev *et.al*, *Opt. Spectrosk.*, **33**, (1972), 871.

[25] R.P.Pandian, *Ph.D Thesis (I.I.T. Kanpur*,(1993),66.

[26] Martin Gouterman, *J. of Chem. Phy.* , **30(5)**, (1959), 1139.

[27] B. I. Greene *et.al*, *Science* , **247**, (1990), 679.

[28] Ming-Tang Zhao *et.al*, *J. Phys. Chem.*, **93**, (1989),7916.

[29] Ming-Tang Zhao *et.al*, *J. of Chem. Phy.*, **89(9)**, (1988),5535.

[30] K.Kandaswamy *et.al*, *Appl. Phys. B*, **64**, (1997),479.

[31] Martin K. Casstevens *et.al*, *J. of Chem. Phy.*, **92(3)**,(1990),2019.

[32] J.Gordon Erdman *et.al*, ,**68**,(1946),1885.

[33] Lin X.-Q. Chen *et.al*, *Proc. SPIE*, **1852**, (1993),163.

[34] A Sastre *et.al*, *J. Phys. Chem. A*, **101**,(1997),9773.

[35] Martin Gouterman *et.al*, *J. of Mol. Spect.*, **53**, (1974), 88.

[36] Gary L. Wood *et.al*, *Optics Lett.*, **20(9)**, (1995),973 .

[37] C.Sauteret *et.al*, *Phys. Rev. Lett.*, **36**, (1976),956.

[38] H. L. Fragnito*et.al*, *J.O.S.A B* , **4**, (1987), 1309.

[39] D. S. Chemla and J. Zyss*Eds. Nonlinear Optical Properties of Organic Molecules and Crystals*,**Academic Press, Orlando**, (1987).

[40] H. M. Gibbs *Optical Bistability: Controlling Light with Light*,**Academic Press, Orlando**, (1985).

Chapter 7

Summary and Conclusions

In this thesis we have carried out nonlinear optical investigations in boric acid glass films doped with Rhodamine 6G, Fluorescein, Tetraphenyl porphyrin and its derivatives. The single beam transmission experiments reveal that the transmission never becomes 100% in these films at highest powers used in these experiments. The residual absorption is a strong indicator to the involvement of the triplet-triplet transitions in the non-linear process in these systems. The fine details of the transmission experiment can throw light on the relevance of various relaxation processes. It may also be possible to get information on the $T_1 \rightarrow T_2$ bands.

The energy transfer due to non-degenerate two wave mixing in Rhodamine 6G doped in boric acid glass has been studied. Zilio 's theory for the two beam coupling in saturable absorbers was extended to interpret the results of our two beam coupling experiments. It was found that unless care was used in comparing the theoretical and experimental results, quantitative agreement between the two was not possible. The basic parameters of the non-linear process such as the saturation intensity and the absorption coefficients of the $S_0 \rightarrow S_1$ and $T_1 \rightarrow T_2$ transition must be determined separately from the absorption studies. Only the quantities which are directly involved in the two beam coupling process such as the complex refractive index should be determined from the two beam coupling results. Good agreement between the experimental and theoretical results is possible if this care is exercised.

The probe beam, in the backward four wave mixing geometry to generate OPC signal, was detuned slightly with the help of the moving peizo mirror. This produced a nearly degenerate four wave mixing spectrum which was very clean and free of laser jitter. The spectrum obtained is also not limited by the instrument resolution. These NDFWM studies were carried on Rhodamine 6G and Fluorescein doped boric acid glass film. These studies yielded line-profiles of the optical transitions ($T_1 \rightarrow S_0$) which are lifetime limited. Some estimate was obtained on the lifetimes of the excited state after applying Lorentzian fits to the spectrum obtained. Since the intensity

dependences were not studied in great detail, an accurate estimation of the excited state lifetime was not possible due to power broadening effects. Narrow band spectrum like that of a narrow band optical filter could be seen in both the samples

In the study of the effect of structural modifications on the third order optical nonlinearity in tetraphenyl porphyrin(TPPH) doped in boric acid glass it was found that TPPH doped film possess one of the highest known diffraction efficiency (0.2%) in these systems. The diffraction process in low concentration film is quite sensitive to the wavelength of light used for these studies. However, heavily doped ($\sim 10^{-4}$M concentration films show reasonably uniform diffraction efficiencies over a broad spectrum extending from the blue to red regions of the visible spectrum This behaviour is related to the the onset of polymerisation in these films. Structural modifications in TPPH were carried out by introducing Bromine, NO_2 and Sulphur atoms in various locations within the molecules. Derivatives obtained on chemically substitution were S_2TPP, TPP$(NO_2)_4$ and BrTPP. These substituents have the effect of reducing the optical nonlinearity. S_2TPP though providing an attractive heavy core modification also results in reduced optical nonlinearity. This is because it also reduces the π conjugation and thereby decreasing the π electron density and eventually the optical nonlinearity. TPP$(NO_2)_4$ has electron withdrawing nitro groups on the phenyl rings. It reduces the electron density and thereby reducing the optical nonlinearity. These studies suggest some linkage behaviour between the phenyl and the pyrrole rings of TPPH.

7.1 Future Scope

The role of the fourth level in R6G dope in BAG has been conclusively established. The models incorporating the fourth level to explain the two beam coupling in saturable absorbers need to be developed. Also the model needs to bring out the dependence of the two beam coupling on the concentration.

The intensity dependent NDFWM studies reveal the extent of power broadening in the narrow band resonances recorded in R6G and Fluorescein doped films. With the kind of narrow band spectra obtained in R6G and Fluorescein doped in BAG one should be able to see the electro-magnetically induced transparency (EIT) effects in this sample clearly.

We have observed, not reported in this thesis, some instabilities in the high power transmission of TPPH doped in BAG. It will be interesting to see optical bistability kind of effects in these samples.

A131102

Date Slip

This book is to be returned on the date last stamped.